



POLITECNICO
MILANO 1863

SCUOLA DI INGEGNERIA INDUSTRIALE
E DELL'INFORMAZIONE

The light W-PIE neutron
spectrometer for soil moisture
measurements: design,
characterization and preliminary
measurements

MASTER OF SCIENCE IN
NUCLEAR ENGINEERING

Author: **Martina Artioli**

Student ID: 944012

Advisor: Prof. Marco Caresana

Co-advisors: Dott. ing. Andrea Cirillo

Academic Year: 2022-23

Abstract

Soil water content knowledge at the intermediate scale, which extends over areas of hectares and depths of ten of centimeters, is crucial to improve agricultural water management, nowadays affected by the impact of global climate change on the availability of water resources. Cosmic Ray Neutron Sensing is a nuclear technology which has the capability to estimate soil moisture in the intermediate scale, filling the gap left by other technologies between point scale measurement and large scale measurement. The working principle is the relation of the intensity of cosmic neutrons above ground, usually measured by neutron counters, and the amount of water content in the soil. In 2021, the W-PIE neutron spectrometer for soil moisture measurements was developed at Politecnico di Milano, introducing in the CRNS technique the potential major advantages of neutron spectrometers. The W-PIE has a 2 cm-thick layer of lead in the section detecting neutrons above 20 MeV which makes the system very heavy and therefore quite difficult to manage during its transport and installation. In this thesis work, a light version of the W-PIE coating structure was designed. The new instrument was characterized in laboratory activities, performing irradiations with an AmBe fast source, to investigate the instrument spectrometric capabilities. Finally, the light W-PIE was installed in a large park in the northern of Milano together with two classic small-scale soil moisture probe to perform preliminary measurements of soil water content. During all the laboratory and outdoor activities the light W-PIE performance were compared to the capabilities of its heavier counterpart. The spectrometric capabilities of the two devices in laboratory conditions were almost identical. In the outdoor activity, very limited precipitations occurred while measuring the light version of the instrument, which could not distinguish between statistical fluctuations and water content changes induced variations in the neutron flux. Therefore, its performance for soil moisture measurement requires further investigation.

Keywords: Cosmic ray neutron sensing, soil moisture, intermediate scale, neutron spectrometry

Abstract

La quantificazione dell'umidità del suolo su scala intermedia, caratterizzata da un'estensione in area dell'ordine degli ettari e profondità di decine di centimetri, è un obiettivo cruciale per l'ottimizzazione della gestione delle risorse di acqua nell'agricoltura, oggi influenzata dall'impatto del cambiamento climatico sulla disponibilità di risorse di acqua. Il metodo CRNS, dall'inglese Cosmic ray neutron sensing, è una tecnologia nucleare che ha scopo di stimare l'umidità del suolo proprio in scala intermedia, colmando il divario tra le misure puntuali e quelle a larga scala. Il principio di funzionamento della tecnologia sfrutta la relazione tra l'intensità dei neutroni cosmici sopra il terreno, solitamente misurata tramite contatori di neutroni, e il contenuto di acqua nel suolo. Nel 2021, è stato sviluppato al Politecnico di Milano lo spettrometro di neutroni W-PIE, introducendo nella tecnica CRNS i potenziali grandi vantaggi dell'utilizzo degli spettrometri rispetto ai contatori classicamente utilizzati. La struttura del W-PIE è caratterizzata da uno strato di piombo spesso 2 cm all'interno sezione adibita alla rilevazione di neutroni di energia maggiore di 20 MeV. Questa caratteristica rende il sistema molto pesante e di conseguenza difficile da gestire durante il trasporto e l'installazione. In questo lavoro di tesi è stata progettata la versione light dei rivestimenti del W-PIE. Il nuovo strumento è stato caratterizzato in attività di laboratorio effettuando degli irraggiamenti con una sorgente di neutroni veloce di AmBe, che hanno consentito di indagare le prestazioni spettrometriche dello strumento. Successivamente, il W-PIE light è stato installato in un parco molto esteso situato a nord della città di Milano, insieme a due sonde di umidità classiche di piccola scala, con lo scopo di effettuare delle misure preliminari di umidità del suolo. Durante tutte le attività, in laboratorio e esterne, le prestazioni del W-PIE light sono state confrontate con quelle della sua controparte più pesante. Le capacità spettrometriche dei due dispositivi verificate in laboratorio si sono dimostrate praticamente identiche. Nell'attività outdoor che ha riguardato il W-PIE light, le precipitazioni sono state minime e lo strumento non ha potuto distinguere le variazioni del contenuto di acqua nel suolo, indotte dalle variazioni di flusso, dalle fluttuazioni statistiche di misura. Per questo motivo, sono previste per il W-PIE light ulteriori verifiche.

Parole chiave: Cosmic ray neutron sensing, umidità del suolo, scala intermedia, spettrometria neutronica

Contents

Abstract	i
Abstract	iii
Contents	v
Introduction	1
1 State of the art of soil moisture measurements	5
1.1 The three forms of soil moisture	6
1.2 Point scale measurement techniques	6
1.2.1 Thermo-gravimetric method	6
1.2.2 Tensiometric method	7
1.2.3 Time Domain reflectometry	8
1.2.4 Frequency Domain Reflectometry	8
1.3 Large scale measurement techniques	9
1.3.1 Remote sensing	9
1.3.2 Ground Penetrating Radar	10
1.4 Soil moisture assessment by Nuclear techniques	10
1.4.1 Neutron Probe	11
1.4.2 Gamma Soil Moisture Sensor	14
1.4.3 Cosmic Ray Neutron Sensing	16
2 Problem statement and first WPIE design	29
2.1 Working principles of neutron detection and spectrometry	29
2.2 W-PIE first design	33
2.2.1 M800 thermal detector	33
2.2.2 WPIE moderating coatings	36
3 Analysis and Simulation Tools	39

3.1	MCNPX	39
3.2	Unfolding algorithm	42
3.2.1	GRAVEL	43
4	Realization	45
4.1	M800 MCNP model	45
4.2	Response Functions estimation	46
4.3	Starting point design	47
4.4	Considerations on response functions	48
4.5	Weight optimization implementation	49
4.6	Final design	56
5	Experimental measurements	61
5.1	Laboratory tests: AmBe source employed to assess L-WPIE neutron spec- trometric properties	61
5.1.1	Experimental setup	62
5.1.2	Spectrum reconstruction	62
5.1.3	W-PIE results	64
5.1.4	Light W-PIE results	67
5.1.5	Results discussion	72
5.1.6	Ambient dose equivalent rate estimation	73
5.2	Parco Nord campaigns: Cosmic rays measurment	74
5.2.1	Parco Nord Installation, Setup and Measurements acquisition	76
5.2.2	Results: Epithermal Flux variations	77
5.2.3	Soil Moisture Evaluation from the W-PIE and L-WPIE measured flux by means of the universal calibration function	79
5.3	Flux uncertainty evaluation procedure	84
6	Conclusions	87
	Bibliography	91
	A Appendix A	95
	List of Figures	99
	List of Tables	101

Introduction

Nowadays, the efficient quantification of soil water resources is an important task to be addressed for many different fields such as hydrology, agriculture and climate science. Although the volume of soil moisture is small compared to the other components of the hydrologic cycle, fluxes of water into and out of soils may be important in the exchange of matter and energy between the earth and the atmosphere [1]. Understanding energy and water fluxes is critical for making weather and seasonal prediction.

Soil acts as a storage system for the water entering the terrestrial environment as rain, and supports communities of flora and fauna, carrying nutrients for plant growth. Soil moisture is the main source of water for natural vegetation and agriculture and its status knowledge enables highly efficient irrigation eliminating the wasteful use of water and supporting water resource decision-makers.

The recent development of new nuclear techniques for measuring soil water content has the important potential to improve sustainable and climate-smart agricultural practices. In particular, the agricultural resource management may be supported by cosmic ray soil neutron sensors (CRNS). CRNS devices can monitor an area-averaged, of the order of hectares, soil water content preventing the need of installing a large number of point-scale sensors, which can be costly, labor intensive and which may not provide a well representative measurement. The basic principle exploited is that the intensity of natural neutrons above ground is inversely proportional to the amount of water present near the land surface.

The neutron flux measurable at the ground is the result of the neutrons generation occurring in the atmosphere upon the interaction of the charged particles flux coming from the cosmos with our planet atmosphere elements.

In general, nuclear techniques for soil moisture measurement were developed after the World War II with the *neutron probe*. This device is provided with an artificial neutron source acting as moisture probe and represented the first major technological advance in modern indirect soil moisture monitoring, especially for large sensing areas. CRNS devices developed in recent past years represent a big improvement, being non-invasive, able to

operate continuously and finally non-hazardous since they measure natural background radiation and don't make use of neutron artificial sources.

The CNRS method has gained particular importance since it fills the critical gap between point measurements, i.e., very small scale measurements (less than 1 m^2) and the large scale ones, reaching up to thousands of squared kilometer covered by satellite remote sensing. Remote sensing methods suffer from low spatial resolution and are able to provide only near-surface estimates of soil moisture. The sensing volume of CNRS instead extends over an area of hectares and a depth of tens of centimeters, therefore fitting a volume which is crucial for applications such as irrigation and farming. The knowledge of the soil moisture in this *intermediate* scale can be also useful to validate models employed in weather climate and hydrological forecast [2].

The CNRS method has been implemented in the COsmic-ray Soil Moisture Observing System (COSMOS) which counts around 500 soil water content monitoring stations, mainly placed in USA. To detect neutrons, each station is provided by three gas-filled neutron counters employing ^3He as sensitive volume. Helium-3 neutron detectors are largely sensitive to thermal neutrons, i.e. neutrons in equilibrium with the environment, having an energy of 0.025 eV at 20 °C, and can be sensitive to neutrons of higher energies when covered with proper moderating coatings. These *counters* can only counts the neutrons impinging on the detector thus giving information only on the intensity of the cosmic neutron flux and no information on the detected neutrons energy distribution.

^3He gas employed in the counters above mentioned is a rare helium isotope but yet largely employed in many applications such as national security, medicine, industry, science, and many others. Nowadays, the worldwide shortage of ^3He caused a considerable increase in the manufacturing costs of ^3He neutron counters [2].

Over the last year, an innovative ^3He -free neutron spectrometer performing CNRS measurements was developed at Politecnico di Milano, in Italy. A spectrometer is an instrument able to compute both the neutrons intensity and the neutrons energy distribution. The instrument is called WEDDING-PIE which is the short for Wide Energy Detector for Direct Investigation of Neutron spectrum at Ground level for Precise moIsture Evaluation. To detect neutrons of a wide range of energy, a proper moderating structure was design to coat the ^3He free neutron counter, made of several layers of different materials.

The W-PIE can detect neutrons in the energy range from 0.01 eV to 1 GeV The energy spectrum reconstruction, performed through an *unfolding* algorithm, allows an accurate evaluation of the epithermal neutron flux, i.e. the flux mainly employed as moisture probe in CNRS technique. Although the sensitivity of the ^3He -free spectrometer is less than the

one of the neutron counters currently employed, the information on the neutron energy distribution should improve the accuracy of the flux measurements and provide further information which can be exploited for the soil moisture measurement.

The W-PIE was successfully tested at Politecnico di Milano irradiating it with neutron sources and performing measurements of natural radiation [2]. In these activities, the W-PIE spectrometric capabilities showed satisfactory results, as well as the instrument sensitivity to cosmic neutrons.

The W-PIE can detect high energy neutrons, of energy above 20 MeV, thanks to a 2 centimeters thick layer of lead in the coating structure previously mentioned. The overall quantity of lead in the system makes it quite heavy, and therefore quite difficult to manage during its transport and installation. In this thesis work, a new lighter version of the W-PIE has been developed by designing a new coating structure with the dual purpose of lighten the overall structure and to maintain the spectrometric capabilities of the original heavier design. After the light W-PIE was manufactured, it was characterized by several irradiations carried out in Laboratory activities in Politecnico di Milano. Finally, the light W-PIE capabilities in performing soil moisture measurements were tested in an outdoor campaign which took place in a vast park in the northern of Milano and compared to its heavy counterpart.

1 | State of the art of soil moisture measurements

To provide context in which Cosmic-Ray Neutron Sensing technique is located, a general review of soil moisture monitoring is reported.

Soil moisture measurement techniques can be classified according to many different criteria. A preliminary distinction can be made between the "Classical methods" and the Modern measurements techniques [3]. The most important classical soil moisture technique is the Thermal-gravimetric method, which has been employed as the standard reference for determining soil moisture content over the past years. Although more elaborate and sophisticated soil moisture measurement equipment is being developed, the gravimetric method retains its importance since it is employed for the calibration of other methods. It is the only "direct" technique, i.e. the method directly weighting the water content.

Modern techniques employ electrical properties of the soil, soil moisture potential, infrared rays, and radioactive techniques such as neutron scattering, gamma attenuation and optical techniques. These methods are "indirect" techniques, i.e. measurements that require calibrations against other measurable variables that vary with soil moisture content [4]. They can be applied in laboratory, in situ or in both. Other criteria for classifying soil moisture measurement methods are for instance between destructive and non destructive techniques, or the possibility or not of scanning certain soil depths. Finally, soil moisture can be measured on different scales. Moisture measurements can be representative on a small scale, such as 1 m^2 or less, and they are called point-measurements. Some measurements instead, can represent an average value within a footprint.

Each classical or modern technique has its own advantages and limitations with respect to the specific application requirements, and none of these provides a holistic approach to soil moisture measurement. In this chapter, some of the most important techniques are described to give an overview based on the available literature. Then, soil moisture measurements techniques related to nuclear measurement are investigated to provide the context for the W-PIE study and optimization.

1.1. The three forms of soil moisture

Before discussing the large variety of types of soil moisture measurement, it is worth defining the three principal soil moisture forms. Indeed, assessing the applicability of the various techniques to soils with different features and the "types of moisture" that they can measure is still a debated point among researchers.

The first one is the *Gravitational moisture*, defined as the "free" moisture that can move through the soil, due to the force of gravity. It can be found in the macro-pores and its movement is quite rapid in well-drained soil. This moisture is not considered "available" moisture, since typically it drains out of the soil in 2-3 days after the rainfall.

Capillary moisture, instead, is the moisture present in the soil micro-pores which, thanks to cohesion and adhesion, is held within the soil against the force of gravity. Capillary moisture is the one responsible for all the all physico-chemico-mineralogical–biological interactions between the soil and the environment [3].

The last soil moisture form is the *Hygroscopic moisture*, which forms a very thin film around the surface of the soil particles. This kind of moisture is very difficult to remove since the soil particle surfaces are interested by very high forces of adhesion. Soils with higher surface area, such as clayey, retain a greater amount of hygroscopic moisture when compared to sand.

1.2. Point scale measurement techniques

In this section, the main small-scale soil moisture measurement techniques are reported. Information have been retrieved from several critical review articles [3], [5], [6].

1.2.1. Thermo-gravimetric method

The aim of the method is to measure the mass water content to determine the percentage moisture content, expressed as:

$$\text{Moisture Content} = \frac{(\text{weight of wet soil} - \text{weight of dry soil})}{\text{weight of dry soil}} \times 100 \quad (1.1)$$

The technique, also called oven-drying, consists in the removal from the field of a wet soil sample, about 100 g or less, and in its oven drying for 24 h at 105 °C. Then, the weight of the resulting dry soil is recorded. In this way, the percentage mass of water content can be determined by equation 1.1.

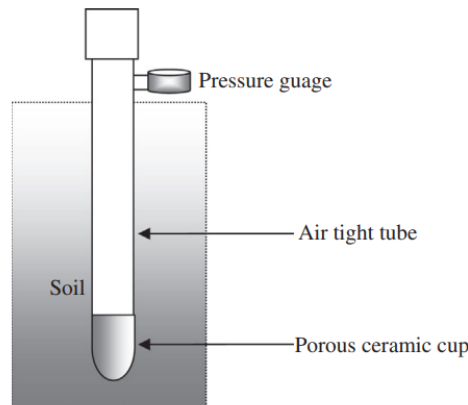


Figure 1.1: Schematic diagram of a tensiometer. Figure taken from [3]

The technique is quite time consuming, since, as previously mentioned, the response time is about 24 hours. However, this is not the only drawback: the method is indeed a destructive test, since the soil sample subjected to oven drying cannot be used for repetitive measurements, as the integrity of the soil structure is compromised by the thermal process. In addition, automatic control of this technique is not easy to be implemented.

The information given by the gravimetric method is very local and it gives no clue about an average value of the soil moisture in a certain area. An average estimation can be obtained by performing multiple measurements, which are needed due to the heterogeneous distribution of water in soil.

The advantages of the method are that it allows an easy to compute and accurate soil moisture estimate which does not depend on salinity and soil type. In account of this last features, thermal gravimetric method is considered the standard for all other soil moisture measurement techniques [3].

1.2.2. Tensiometric method

Tensiometers can directly measure the soil water potential, also called soil matric potential, which can be seen as the energy with which water is held by soil. It is equivalent to the energy that a plant has to overcome to extract water from the soil.

Figure 1.1 sketch a tensiometer consisting of a porous ceramic cup connected with a tight air tube, both filled with moisture. The system can be buried at any design depth in the soil. The moisture filling the cup is usually water.

The working principles is based on an exchange of water between the instrument and the soil: moisture inside the porous cup coming in contact with the soil tends to equilibrate

with the soil moisture through the pores of the ceramic cup. The loss of moisture from the tube causes a suction force that and a pressure drop in the tensiometer, indicated by the vacuum gauge at the top of the sealed tube.

The technique is non-destructive and cost effective, it can provide continuous reading and for long periods of time. However, there is a limited measurable pressure range from 0 to about 0.8- atm because of the vaporization of water at low pressure causing bubbles inside the tube. This range represents a small part of the entire range of available moisture [3].

1.2.3. Time Domain reflectometry

The Time Domain reflectometry (TDF) belongs to the "Dielectric techniques" and measures the volumetric water content by propagation of electromagnetic wave measurements. Propagation constants for electromagnetic waves in soil, such as velocity and attenuation, depend on soil properties, especially water content and electrical conductivity.

To determine the velocity of a EM wave in soil, very short electrical pulses are sent through a metallic 2 or 3-rod probe. From the travel time t and the length l of the probe which has been travelled along twice, the propagation velocity is calculated [ultimo] as $v = 2l/t$ [4]. The velocity of the pulse changes with the change in soil moisture content due to the relatively large dielectric value of water, and a lower velocity indicates a wetter soil. The pulse velocity in the probe is measured and correlated to the soil moisture [5].

The method is fast, non destructive and allows continuous measurement of the soil moisture, which is independent of soil texture, temperature and salt content. However, TDR probes are environment sensitive and measurements could be erroneous due to gaps between the soil and the probe [4].

1.2.4. Frequency Domain Reflectometry

Frequency Domain Reflectometry (RFD) belongs to the "Dielectric techniques", indeed it is quite similar to TDR and measures the volumetric soil water content. It is based on the measure of the variation in frequency of an electrical signal sent to the soil. The sensors are generally in the form of two or more parallel acting as capacitor terminals. Embedding the electrodes into the soil, the soil acts as dielectric medium. When an oscillating frequency is applied to the electrodes, the changes in the operating frequency are related to the capacitor dielectric, hence to soil water content.

The readout from the probe is not linear with water content and is influenced by soil type and soil temperature. Therefore, the technique requires soil specific calibration [5]. It is

sensitive to air gaps, soil salinity, temperature, bulk density [4].

1.3. Large scale measurement techniques

Large scale soil moisture refers to spatial support scales $> 1^2 m^2$ for a single sensor, or spatial extents $> 100^2 km^2$ for a sensor network [7]. Large scale techniques have advanced in recent years and may lead to an improved understanding of soil moisture and related processes.

Large scale measurements can be performed in two ways. The first one is to employ point measurement devices distributing them in a network covering a large scale. The second way is to design a single system capable of covering a large area.

1.3.1. Remote sensing

Remote sensing techniques measure soil surface moisture through the measurement of electromagnetic energy that has been either reflected or emitted from the soil surface. The intensity of this radiation with soil moisture varies depending on several soil properties, which can be quickly estimated.

Remote sensing based methods include the use of satellites, radar (microwaves) and other non-contact techniques. GPS signals path between the transmitting satellites and the receiving antenna can be employed. Two types of paths are possible for the GPS signal: a direct one from satellite to antenna and a multipath, reflected off the land surface [7]. The reflection coefficients depend on permittivity of the soil, surface roughness and elevation angle of the reflections. Therefore, reflected GPS signals can be used to estimate environmental parameters, among which soil moisture. Geometry of a multipath signal is sketched in Figure.

The most suitable part of the electromagnetic spectrum which can be used for quantitatively sensing soil moisture remotely is the lower microwave region, for several reasons. First of all, at lower frequencies, the atmosphere is less opaque, the vegetation biomass is more transparent and the effective emission profile is more representative of the soil below the surface skin layer [8].

Placing antennas at different height allow computing average soil moisture sensing different areas above a minimum of about $1 km^2$. The resolution of the method is low and the method is not suitable for applications like precision agriculture and irrigation. Another limit regards the sensing depth, around few centimeters.

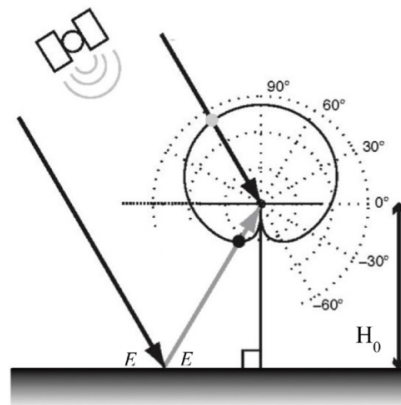


Figure 1.2: Schematic representation of the remote sensing technique. Figure taken from [7]

1.3.2. Ground Penetrating Radar

The Ground Penetrating Radar measurements are based on the transmission and reflection of electromagnetic wave in the soil. The transmitter antenna of the radar systems generates radio-waves reflected by the soil and then the receiver detects variations in the electrical properties of the sub-surface [4]. GPR is fast, non destructive, with high resolution. It can penetrate beyond the surface later and is capable of covering large areas, up to 500×500 m a day. However, the performance of GPR varies across soil types, many of which are radar opaque and dissipate radar energy, restricting its use [4].

1.4. Soil moisture assessment by Nuclear techniques

Three techniques involving nuclear processes can make assessment of soil moisture:

1. Neutron Probe
2. Gamma ray Spectroscopy technique
3. Cosmic Ray Neutron Sensing

Historically, the development of the first neutron probe after World War II represented the first major technological advance in modern soil moisture monitoring. The first literature study on the measurement of soil moisture based on neutron thermalization dates back to 1952, from former Iowa State College, now University [7]. The neutron probe remained the standard for indirect soil moisture measurements until the Electromagnetic methods were developed in Canada (1980) [7], leading the way to the development of many types of electromagnetic probes.

Soon after the first studies of the application of neutrons and gamma-ray techniques to soil moisture measurements, many benefits were found over other methods. In particular, the neutron method for measuring soil moisture evolved through the need in many types of studies to follow moisture changes in the soil without relying on destructive sampling [9].

Neutron Probe developed as small scale technique, whereas the much more modern Gamma ray Spectroscopy and Cosmic Ray Neutron Sensing techniques can be placed between point measurements and large scale measurements. They are capable of giving an average value of soil moisture in a field with dimensions of few hectares. Moreover, they do not make us of expensive and problematic, from a safety perspective, radioactive source.

The following sections describe and discuss the three methods.

1.4.1. Neutron Probe

A fast neutrons emitting source can be inserted into the soil as a depth moisture probe measuring the volumetric water content. A sketch of the system is shown in Figure 1.3. The neutrons emitted are slowed down as a result of elastic collisions with hydrogen nuclei. Eventually, neutrons are thermalized and few of them are backscattered towards a neutron counter, as shown in Figure, and detected. The number of slow neutrons detected is proportional to the concentration of the hydrogen nuclei, or water content in the soil [9]. The moisture content of the soil may be obtained upon a proper calibration of the probe.

Depth moisture probe consists of:

- a fast neutrons source such as americium-beryllium or radium-beryllium
- a thermal neutron detector such as $^{10}\text{BF}_3$, ^3He and scintillation detectors
- a preamplifier and a cable connecting the system to the associated electronics for counts readout

Figure 1.4 depict a simplified sketch of the whole system.

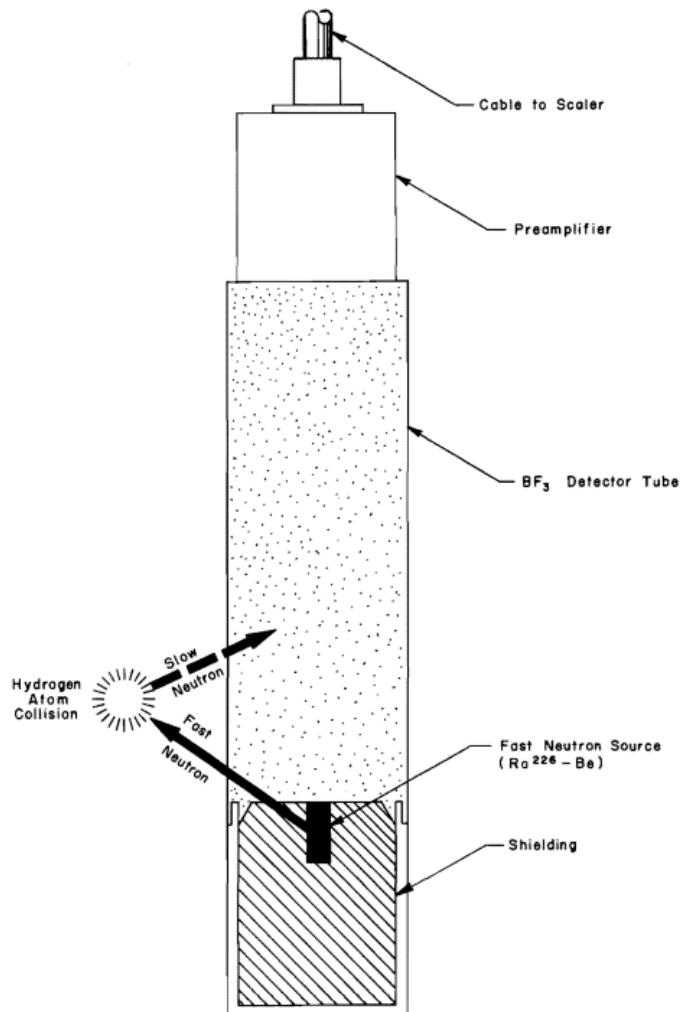


Figure 1.3: Depth moisture probe. Figure taken from [9].

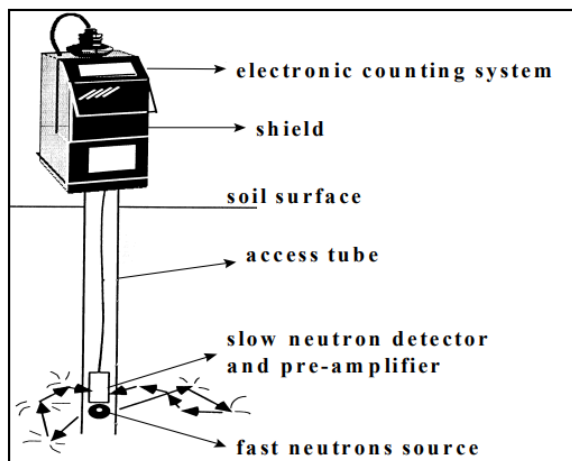


Figure 1.4: Depth neutron probe in working position. Figure taken from [1].

The system is stored in a shield providing radiological safety during transportation and facilitating a proper handling of the source. An access tube must be installed before lowering the probe to the desired depth. When testing is completed the probe is drawn into the shield avoiding user exposure.

Different depths can be investigated with the soil moisture neutron probe multiple times without perturbing the soil.

The alpha emitter of the source mixture emits alpha particles which bombard beryllium nuclei in form of fine powder generating fast neutrons up to 14 MeV with a mean energy of about 4.5 MeV. Most alpha emitters also emit gamma radiation which is shielded by lead when the probe is in the protective shield. The probe shielding also prevents users from fast neutrons exposure thanks to materials high in hydrogen content, such as paraffin and polyethylene.

Neutrons and gamma rays are highly penetrating, and when the probe is operating they penetrate the source capsule. The source of a small dimension can be approximated by a point source, emitting fast neutrons which travel radially outward from the source. Neutrons collide with atoms of the surrounding material undergoing several reactions, the predominant one being elastic scattering. A series of elastic collisions slow down the neutrons until their kinetic energy approaches the average kinetic energy of the moderating atoms as determined by the ambient temperature [9] (about 0.025 eV for ambient temperature). A thermalized neutron has no definite velocity direction with respect to the source and moves in a random fashion throughout the medium [9]. The element which is most effective in slowing down neutrons is hydrogen, contained in the soil mainly in soil water. Organic matter in soil contains hydrogen too, but this contribution to neutrons

scattering is usually negligible.

Most of all the neutron interactions occur in an effective space zone. The effective radius of this sphere of influence can be computed with various formulas taking into account the nature of the source and the water volume content in the soil. The volume, which decreases with increasing presence of water, represents a sensing volume over which the soil moisture estimation can be performed. This entails the reduction of the influence of small-scale variability in the soil, the sensitivity to soil disturbance due to installation and the number of measurements needed.

Fast neutrons emitted which thermalize and are backscattered into the detector can be counted and this measure can be correlated to the water content in the soil. Clearly, an important requirement for a successful soil moisture measurement is proper calibration, which may take into account the presence in the soil of elements which can scatter neutrons and in general other phenomena occurring alternatively to water hydrogen scattering.

Drawbacks of soil moisture neutron probe may be the cost of the instrumentation, radiation hazard, and issues regarding soil specific calibration, depth resolution and measurement of soil water near the surface.

1.4.2. Gamma Soil Moisture Sensor

The gamma-rays emitted by the soil can be exploited to determine the soil moisture content. Natural radionuclides emit radiation which is attenuated by moisture in the soil. The amount of moisture present in the soil can be inferred by the measured flux of gamma photons. Spectral analysis is needed since the flux seen by the sensor is also influenced by variations in atmospheric radon concentrations [10]. This last component can be filtered out by spectroscopy.

The technique measures radiation emitted by a large volume of soil and can be used to determine the average soil moisture concentration of this volume [10].

The radio-elements present in traces in the ground belong to the decay chains of ^{238}U , ^{232}Th and ^{40}Th . Several gamma rays are emitted along the decay chains and each chain has an expected gamma spectrum, as can be seen in Figure 1.5.

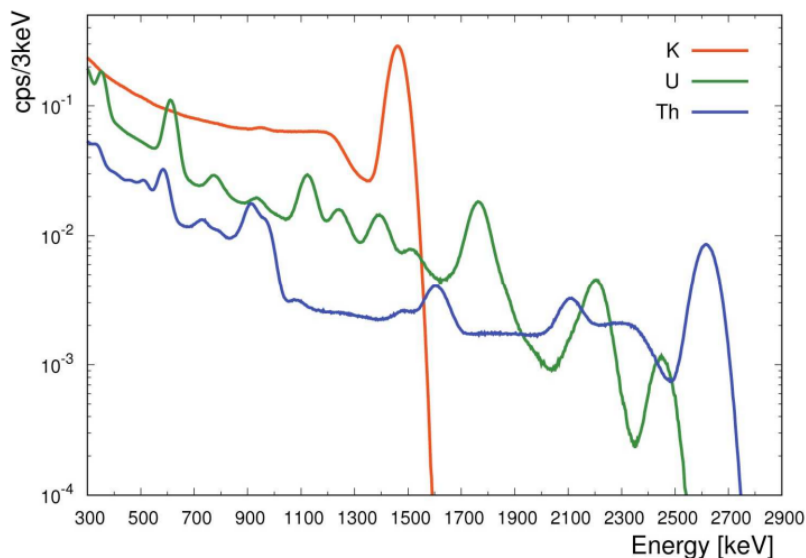


Figure 1.5: Fundamental spectra obtained with Monte Carlo simulations referred to a dry soil with uniform radionuclide concentration. Figure taken from [11]

The measured gamma spectrum is affected by the gamma radiation interaction with soil constituent elements and soil water. As water has 1.11 times as many electrons per gram compared to most soils, water is 1.11 times as effective in attenuating gamma-radiation compared to typical soils [12].

The measured gamma spectrum can be considered sensitive to soil moisture variation assuming the source of the radiation and the soil composition constant in time.

Theoretical study of the counts detectable for selected photopeaks performed by Grasty [12] investigates the relation between the counts and the water mass w in dry soil, determined by proper calibrations and knowing soil composition.

The vertical and horizontal sensing limits of the gamma ray spectroscopy technique were studied by Feng et al. [13], The results were that a weighted average soil moisture in an area inside a radius of some tens of meters and in the depth of some tens of centimeters can be measured. The average is weighted because the amount of contribution changes if it comes from the nearest ground (higher contribution) or from a greater distance.

In 2018 in Italy a system using the gamma ray spectroscopy technique for measuring soil moisture was implemented. The detector employed for gamma detection was a NaI scintillator of one litre coupled with a photomultiplier tube and the photopeak considered was the one of ^{40}K . Experiments were carried out for several months in a permanent station installed.

Results were in agreement with simulations and direct measurements. However, radius and sensing depth for soil moisture assessment were limited to 25 m and about 30 cm respectively, leaving a gap in between the meter scale and the large scale.

1.4.3. Cosmic Ray Neutron Sensing

Area-average soil moisture can be measured in the field using cosmic-ray neutron background radiation, whose intensity in the air above the land surface depends primarily on soil moisture [7]. Cosmic-ray probes employed in the Cosmic Ray Neutron Sensing (CRNS) technique can integrate soil moisture of areas of hectares and a varying depth from 0.1 to 0.6 m [14] depending on soil water content. Measurements on this scale can be reached with point measurement devices only installing large networks of devices.

CNRS systems developed recently and can be applicable to a number of disciplines including agronomy, atmospheric science and ecology. In general, CNRS is suitable for those applications taking advantage of a quite large footprint providing spatial representativeness and of a non-invasive sensor which prevents disturbing the hydrologic properties of the soil being measured.

In this section, the several aspects involved in the CNRS technique are described, starting from the natural neutron source. Then the physical principle of the method, i.e. fast neutron thermalization, is treated to explain the CNRS system working principle. Finally, existing correlations between the volumetric soil moisture and the neutron measured flux are reviewed and reported.

CNRS natural radiation neutron source

CNRS employs the cosmic rays natural radiation as a neutron source, preventing the costs and hazard issues related to the neutron artificial source adopted in depth neutron probes. Cosmic ray neutrons, as a natural component of Earth's radiation environment, are ever present at the land surface.

Actually *cosmic* neutrons are only a byproduct of chain reactions initiated at the top of the atmosphere by cosmic rays [14]. The so called *primary* rays are mainly highly energetic protons and charged nuclei originated from the Sun in our galaxy and from distant galaxies. About 99% are atoms bare nuclei, and 1% are solitary electrons. Among the bare nuclei, 90% are hydrogen nuclei, i.e. protons, 9% alpha particles and 1% are heavier elements.

The primary cosmic radiation, which is modulated by solar activity manifesting cycles of a

few tens of years, is influenced by the galactic, the interplanetary, the magnetospheric and the geomagnetic magnetic fields while approaching the Earth [15]. Cosmic rays particles may pass the magnetic fields and reach the atmosphere, depending on their momentum and on their cutoff rigidity [16].

In penetrating the Earth atmosphere, primary cosmic radiation is subject to interactions with atoms and molecules constituting the air. The composition of the radiation field changes as it propagates through the atmosphere. The incident hadrons undergo strong interactions when colliding with nuclei in the atmosphere such as nitrogen and oxygen, producing showers of particles, mainly pions. The strong interactions spallation fragments continue to propagate and interact successively producing more particles along their trajectories.

Energetic primary protons undergo about 12 interactions along a vertical trajectory down to sea level. Indeed, they have an interaction mean free path of about 80 g/cm^2 [15] versus the atmosphere depth of about 1020 g/cm^2 . They make energetic collisions with atmospheric target nuclei which get highly excited and evaporate mainly alpha particles and nucleons.

The majority of heavy nuclei, instead, are fragmented in the first interaction occurring at higher altitudes than for protons, because of their much larger interaction cross section and correspondingly shorter interaction mean free path. In practice, a heavy nucleus does not penetrate down to sea level.

Neutrons belong to the *secondary cosmic-ray* particles, resulting from interactions of primaries with nuclei of air constituents. They can be originated from different processes. The evaporation process occurs when nuclei of the atmosphere are left in excited states after the interaction with the impinging particles. In the de-excitation process, some protons and neutrons can evaporate in an isotropic process, with energies around 1 MeV. These fast neutrons have an isotropic angular distribution and can be easily moderated by hydrogen atoms.

When primary protons and heavier atoms split the atmospheric nuclei into particles, high energy neutrons in the order of 100 MeV may be produced in this fragmentation process. High energy neutrons are also produced in charge exchange reactions, i.e. when a proton in a target nucleus is exchanged for a neutron in the projectile nucleus, or vice-versa.

Primary and secondary particles generate particle cascades penetrating the atmosphere and eventually reaching the ground level. Figure 1.6 sketch a cascade phenomenon: a primary cosmic ray particle interacts with the nucleus of an atmospheric constituent at a high altitude, leading to a hadron cascade. In subsequent collisions of low energy

secondary particles with atmospheric target nuclei, nuclear excitation and evaporation of nuclei may occur. Unstable particles are subject to decay or interaction, and electrons and photons undergo bremsstrahlung and pair production, respectively.

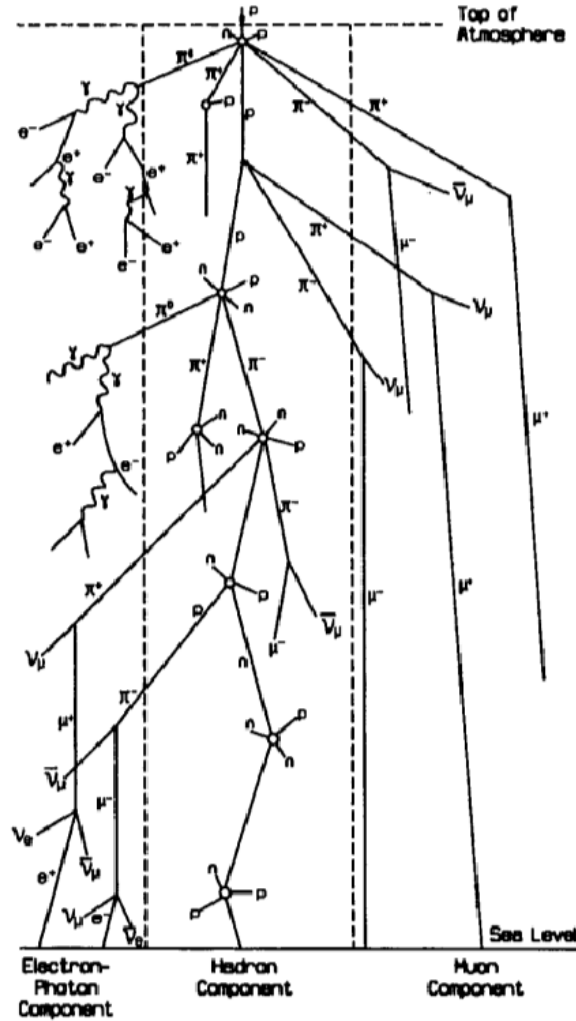


Figure 1.6: The three component of the cascade shower. Figure taken from [17]

As previously mentioned, high energy neutrons of the order of 100 MeV are generated within hadron cascades. These neutrons may reach the sea level and be measured. The production of these high energy neutrons is directly related to the primary impinging rays. This means that solar activity, affecting primary radiation fluence as previously mentioned, affects the fluence rate of high energy neutrons. This aspect must be taken into consideration when measuring soil moisture through cosmic neutron radiation detection.

The high energy neutrons impinging on soil elements may lead to strong reactions leaving the target nuclei in an excited state. The consequent de-excitation entails the evapora-

tion of neutrons. The evaporated neutrons have energy around 1 MeV and are emitted isotropically. These fast neutrons are efficiently slowed down by light elements in soil and populate the ground level with lower energies, i.e. epithermal and thermal energies. The thermal component cannot be found at higher altitudes.

Eventually, the ground level is populated by neutrons of different energies. The cosmic neutron energy spectrum has the shape shown in Figure 1.7 can be conventionally divided into four regions:

1. The High Energy region, which includes the neutrons generated by primary particle radiations in the upper layers of the atmosphere. The peak energy is around 100 MeV.
2. The Fast region, which includes the neutrons generated by evaporation after the interaction of the high energy neutrons with air and soil molecules. The peak energy is around 1 MeV. Neutrons in this region are also called evaporation neutrons.
3. The Epithermal region includes the neutrons which are slowed down to energies between 0.5 eV and 0.5 MeV.
4. The Thermal region has a peak around 10 meV and includes neutrons in equilibrium with the surroundings.

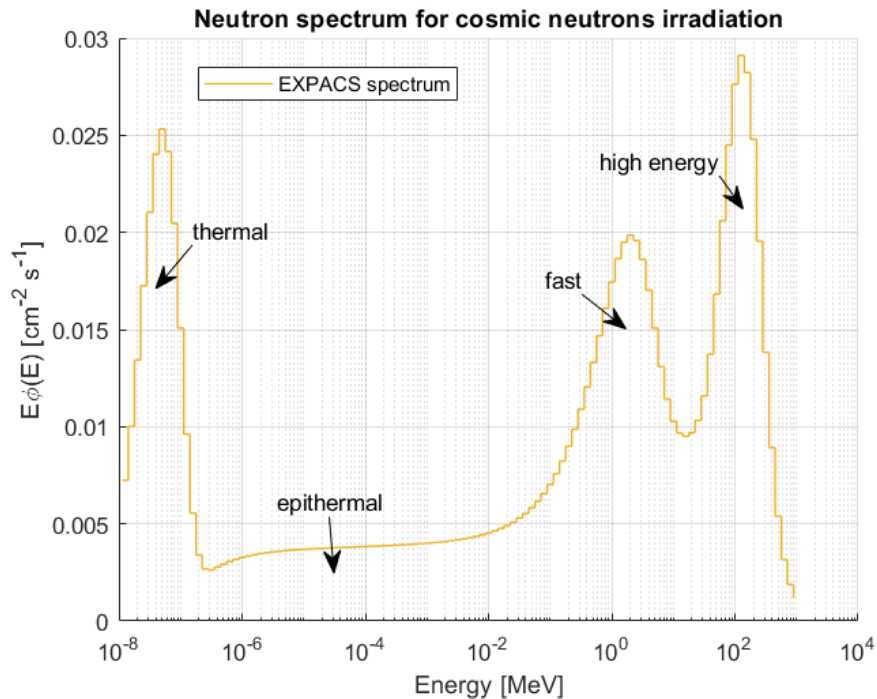


Figure 1.7: Neutron spectrum simulated by EXPACS at ground level plotted as neutron fluence rate per energy bin

EXPACS stands for Excel-based Program for calculating Atmospheric Cosmic-ray Spectrum and is available on IAEA website. It is based on a set of analytical functions developed by Sato and Niita [18] with the purpose of reproducing the cosmic neutron spectrum.

The shape of the neutron energy spectrum above the ground is qualitatively the one in Figure 1.7. The actual magnitude of the spectrum depends mainly on the altitude, whereas its actual shape is mostly dominated by the environmental hydrogen content [19]. The hydrogen-sensitive region of the cosmic ray neutron spectrum lies in the epithermal to fast range. As previously said, neutrons of such energy mainly interacts with matter losing kinetic energy. The physical process involved in this phenomenon is neutron elastic scattering, i.e. a collision between the projectile neutron and a target atom in which the total energy is preserved. The main findings of the slowing-down theory are reported in the following section.

CNRS physical basic principles

Hydrogen is the most effective element in moderating neutrons, i.e. in slowing down them. For this reason, the content of water, which is the main hydrogen pool in soil, can be correlated to the amount of neutrons that are slowed down. It is the same principle used by neutron probe (1.4.1), but instead of employing an artificial source of fast neutrons, such as AmBe, the natural radiation is exploited.

The good moderating properties of hydrogen are due to its high scattering cross section σ and to its low mass, nearly equal to that of neutron.

The elastic scattering cross section essentially quantifies the probability of a neutron to interact with an atom via elastic scattering, which is the predominant interaction between epithermal or fast neutrons and light nuclei, with $A < 25$. The values expressed in barns ($1 \text{ barn} = 10^{-24} \text{ cm}^2$) can be compared in Figure 1.8, where the cross sections of the most abundant elements on earth are plotted.

The rate of energy loss per interaction in the elastic scattering theory is described by the quantity ξ , the mean logarithmic reduction of the neutron energy E per collision [20]:

$$\xi := \ln \frac{E_0}{E} = 1 + \frac{(A-1)^2}{2A} \ln \left(\frac{A-1}{A+1} \right) \approx \frac{2}{A+1} \quad (1.2)$$

where E_0 is the neutron energy previous to the collision, E the neutron energy after the single collision, and A is the atomic mass number of the target element.

ξ is related to a quantity called *lethargy* and in particular it is the average change in

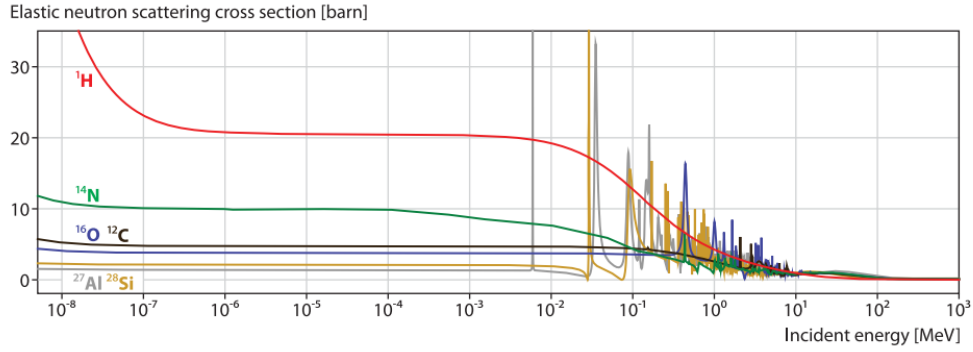


Figure 1.8: Comparison of elastic neutron cross sections of hydrogen (red), nitrogen (green), oxygen (blue), carbon (black), silicon (orange), and aluminium (grey) for kinetic energies between 5 meV and 1 GeV. Figure taken from [16]

lethargy per collision. Considering the lethargy u necessary to slow down a neutron of energy E_0 down to energy E_1 , the number of collisions is:

$$n_{col} = \frac{u}{\xi}, \quad \text{where} \quad u = \ln \frac{E_0}{E_1} \quad (1.3)$$

The lethargy ξ depending on the mass number A according to equation 1.2 is a property of the material decreasing with increasing A . The average number of collisions necessary to slow down neutrons down to a certain energy can be estimated by relations of eq. 1.3. Being the hydrogen the element with $A = 1$, it is the element which slows down neutrons more efficiently, i.e. with less average number of collisions with respect to all other elements. This aspect can be observed in Table 1.1, where the ξ values and the average number of collisions to thermalize neutrons (energy ~ 0.025 eV) are reported for some elements.

Element	Log. energy decrement ξ	Avg. no. collisions n_{col}
^1H	1	18
^{12}C	0.1577	111
^{14}N	0.1363	128
^{16}O	0.1199	145
^{27}Al	0.0723	242
^{28}Si	0.0697	251

Table 1.1: Slowing down of neutrons from 1 MeV to thermal energies by interaction with different isotopes.

For an inhomogeneous medium, an effective $\bar{\xi}$ can be computed weighting the single collision average lethargy of the medium constituting elements i for the elastic cross section:

$$\bar{\xi} = \frac{\sum_i \sigma_i}{\sum_i \sigma_i \xi_i} \quad (1.4)$$

As can be seen from Table 1.1, hydrogen is by far the most effective moderator among the typical soil constituents. This means that an increase in soil water content leads to an enhancement of the moderating properties of soil. Another beneficial consequence of the differences in moderating properties is that an estimation of water content measuring moderated neutrons is expected to be almost independent on soil composition. In any case, the soil composition fixed contribution is taken into account in the calibration process.

The neutrons that have been thermalized in the soil carry soil moisture information. The total spectrum seen at ground level is the result of several contributions, which can be seen in Figure 1.9. The first (white line) is the direct spectrum, i.e. the spectrum of the incoming neutrons impinging from air to ground. This contribution includes neutrons making all the high energy peak and part of the fast peak, i.e. those neutrons generated from evaporation in air. The incoming neutrons contribution to the spectrum is not affected by soil moisture. The second contribution (purple line) is given by the back-scattered part of the spectrum, i.e. the one produced in the ground and emerging at the surface after having been slowed down. This contribution includes albedo neutrons coming from the evaporation after the excitation of soil nuclei, and it is the principal component of the fast peak. Neutrons coming from the ground contribute to the totality of the thermal peak and the greatest part of the epithermal component, thanks to the thermalization occurring in the soil, principally due to the presence of water molecules.

In the end, the presence of soil leads to the increase of the evaporation peak and to the formation of the epithermal and thermal component, as shown in Figure 1.9. The water content influences the number of neutrons coming from the soil that have been slowed down. This effect is well visible mainly in the epithermal region, but also present in the fast one. This effect can be observed in Figure 1.10. The high sensitivity to hydrogen of neutrons in the epithermal-to-fast range ($1-10^5$ eV) makes neutron detectors efficient suitable probes for measuring the environmental water content.

For an inhomogeneous medium, an effective $\bar{\xi}$ can be computed weighting the single collision average lethargy of the medium constituting elements i for the elastic cross section:

$$\bar{\xi} = \frac{\sum_i \sigma_i}{\sum_i \sigma_i \xi_i} \quad (1.5)$$

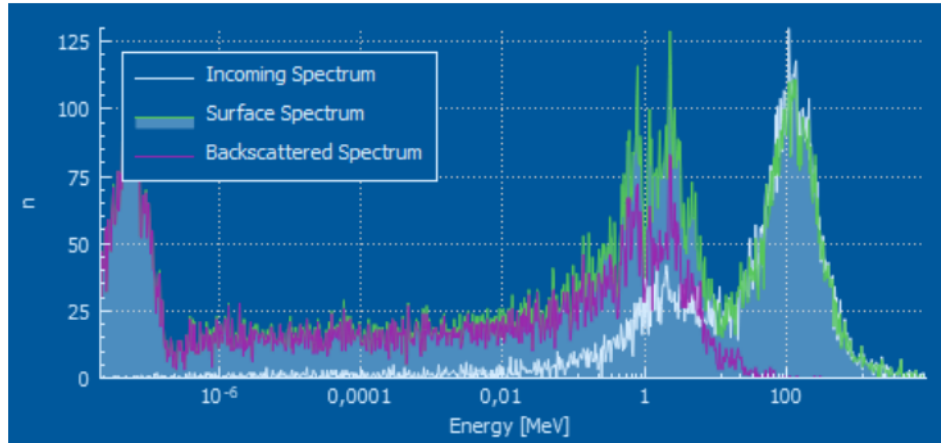


Figure 1.9: Cosmic-ray neutron spectrum above ground simulated by URANOS with a water content of 0.2 g out of 1 g of soil [21].

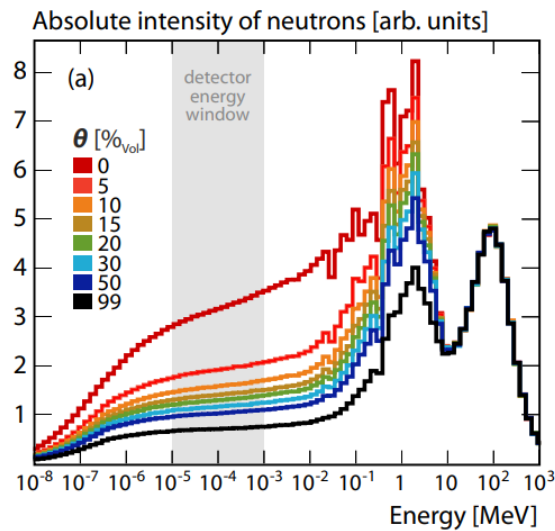


Figure 1.10: The effect of water content in soil (θ) on the cosmic neutrons energy spectrum [16]. Dry soils show greater fluxes in the epithermal ($10^{-6} - 10^{-1} \text{ MeV}$) and fast ($10^{-1} - 20 \text{ MeV}$) energy ranges.

The number of collision in a typical ground medium can be derived by the relation $n_{col}^- = u/\bar{\xi}$. For a macroscopic medium, the macroscopic cross section $\Sigma = \rho\sigma$ can be considered, where ρ is the density of the material. A typical ground medium can be described by a macroscopic cross section Σ^{soil} plus a fraction w of added water Σ^{water} [20]:

$$n_{col}^{ground} = u \frac{\Sigma^{soil} + w\Sigma^{water}}{\Sigma^{soil}\xi^{soil} + w\Sigma^{water}\xi^{water}} \quad (1.6)$$

Since the neutron epithermal-to-fast flux is proportional to n_{col} , i.e. the number of scatterings required for thermalization, the above ground neutron intensity is inversely proportional to the water fraction w :

$$\phi_{epith-to-fast}(H_2O) \propto n_{col}^{ground} \propto (\Sigma^{soil}\xi^{soil} + w\Sigma^{water}\xi^{water})^{-1} \quad (1.7)$$

This hyperbolic relationship is the base of the conventional correlations between neutron cosmic flux and soil moisture employed, reported in the following section.

Correlations between neutron cosmic flux and soil moisture

The cosmic-ray probe provides a measurement on the cosmic-ray neutron intensity. The measured intensity must then be converted to soil moisture through a calibration function.

Several studies attempted to investigate the relation between the neutron intensity in air above the land surface and soil moisture. That intensity is influenced not only by soil moisture but also by hydrogen in other pools, such as soil lattice water, water vapor, and biomass. Desilets et al. [22] presented a theoretical calibration function derived from nuclear physics theory:

$$\theta(N) = \frac{0.0808}{\frac{N}{N_0} - 0.372} - 0.0115 \quad (1.8)$$

where θ is the volumetric water content (m^3m^{-3}), N is the neutron counting rate normalized to a reference atmospheric pressure and solar activity level and N_0 is the counting rate over dry soil under the same reference conditions. The equation requires at least one independent estimate of *area-average* soil moisture to define the free-parameter N_0 . In principle, the method is computationally simple, requiring only one calibration parameter. However, it requires intensive soil sampling to adequately estimate this calibration parameter. Indeed, analysis of 35 different COSMOS site calibration datasets was performed by Franz et al. in [23] showing the significant variability of N_0 from time to time and in time within the same site, due to the presence of other time-varying sources of hydrogen [23] which are not took into account in eq. 1.8. Franz et al. derived an univer-

sal calibration function that can be used in environments which are problematic from the point of view of the local sampling calibration. The equation was developed in a simplified but general framework taking into account all hydrogen sources that may be present [23], among which lattice water. Therefore, the soil water content is estimated on the basis of measurements of neutron intensity in combination with other measurable hydrogen pools without the need of a site-specific calibration using in situ soil moisture methods.

The information required to perform the necessary neutron intensity corrections is some ancillary data on location and some physical parameters, such as surface pressure and air temperature. Further specific details can be found in [23].

In the end, Zedra et al. in [1] suggest the three calibration options to be followed in cosmic-ray soil moisture measurement. The first one is to collect a large number of samples within the footprint to obtain an area-average soil moisture, to includes all factors affecting the measurement, which in fact have to be included in the calibration parameter N_0 of equation 1.8. This is also called the N_0 method [24]. Whenever soil moisture measurements are not available, soil samples have to be collected to be analysed chemically, in particular to investigate the lattice water content. These analyses allows a construction of a local calibration function which contains soil-chemistry corrections. The last option, when none of the previous can be implemented, is to use the universal calibration function of Franz et al. [23], which already embeds the hydrogen contribution of all the reservoirs and does not require additional corrections. The shape of the universal calibration function, as well as the shape of the local one, is hyperbolic and determined by nuclear physics calculations. In these calculations the fast neutron density at the equilibrium is the result of a balance equation between neutrons generated by a source and neutrons slowed down in moderation. The equation is computed assuming that only hydrogen can moderate neutrons. This is a reasonable approximation, according on the previous considerations on the greatest hydrogen importance in moderation. In particular, the approximation is good for water content greatest than 3%. Performing Monte Carlo simulations, the coefficient a_0 , a_1 and a_2 of the following equation can be determined independently on the type of soil:

$$\theta \left[\frac{g_{water}}{g_{soil}} \right] = \frac{a_0}{\phi/\phi_0 - a_1} - a_2 \quad (1.9)$$

ϕ is the neutron flux measured, and ϕ_0 is the calibration parameter, i.e. the measured flux corresponding to a known value of θ . As can be noted, the main difference with respect to equation 1.8 is the substitution of the neutron count rate with the neutron flux.

Footprint characteristics of the technique

The identification of the footprint for a soil moisture method is crucial to understand the area probed by the instrument and therefore the applicability of the technique for various scenarios. The footprint depends on the area in which the carrier of the soil moisture information, i.e. neutrons coming from the soil which have been thermalized, is detected.

In case of a centrally located neutron sensor detecting neutrons isotropically, a circular footprint area can be assumed, i.e. $A = \pi r^2$ [16], where r is defined as the Euclidean distance between the point of detection and the point of neutron's first contact with the ground.

Actually, since r depends on the neutron initial energy and on the number of collisions [16], the upper limit of r can be very high, of the order of 1 km. However, it is necessary to look at the radius within which most of the detected neutrons have probed the ground. A quantile definition can be stated, considering that high quantile value will include long range neutrons regardless of how often they have actually probed the soil.

As reported by [16], Zedra and al. [25] legitimate the use of the 86% quantile R_{86} , studying the problem adopting a simple diffusion model for neutrons and performing Monte Carlo simulations estimating the detected neutron intensity (W_r) for increasing radial distances. The footprint can therefore be assumed the circular area $A = \pi R_{86}^2$, where R_{86} is the solution of the equation:

$$\int_0^{R_{86}} W_r dr = 0.86 \int_0^{\infty} W_r dr \quad (1.10)$$

The quantity on the right-hand side is the 86% of the total number of neutrons detected, i.e. the 86% of the number of neutrons that have been detected which have originated within a radius approaching infinity. The same quantity can be expressed by the integral on the left-hand side, which integrates the neutron intensity up to a limit radius, R_{86} : the area πR_{86}^2 around the central detector is the area within which the 86% of the signal is generated. The solution R_{86} and therefore the footprint $A = \pi R_{86}^2$ is assumed to be the area over which the detected signal is well representative.

Figure 1.11 shows that when the water content increases in the soil, the footprint above defined is reduced, due to the greater moderation of fast neutrons.

Similar considerations can be adopted for the penetration depth, i.e. the thickness of the probed soil layer. Theoretical studies were performed [16] using URANOS simulations to investigate the penetration depth D_{86} on the radial distance from the sensor for a range of water contents.

Looking at Figure 1.11 reporting the behaviour for radial footprint and penetration depth, it follows that the technique has the potential to probe soil moisture for areas of tens of hectometers and for depths of tens of centimeters.

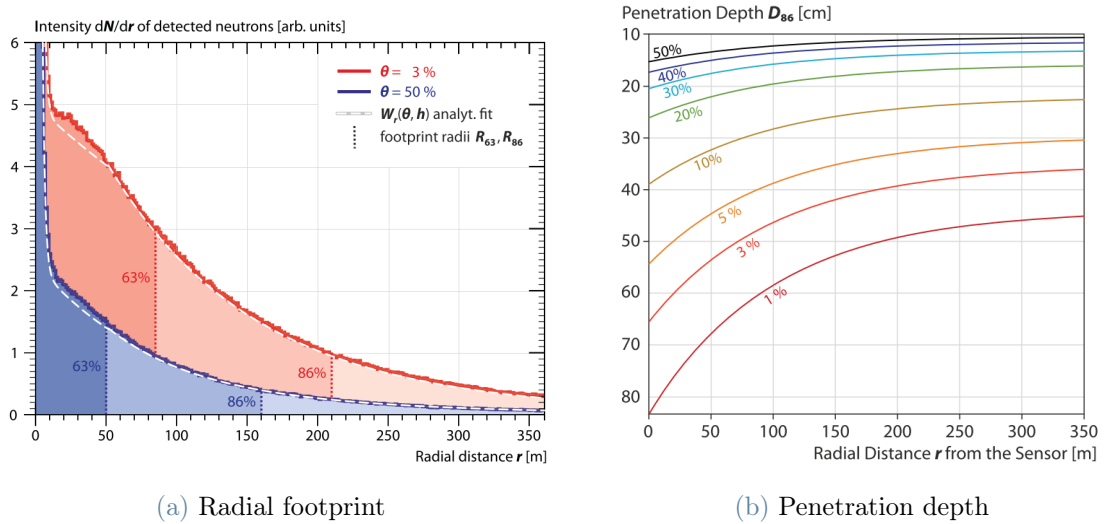


Figure 1.11: (a): Detected neutron intensity over distance r between origin and detection for two soil water contents. R_{86} ranges from 160 to 210 m for wet and dry soils respectively. (b): Dependency of the penetration depth on radial distance r to the sensor for a range of soil water content. Penetration ranges from 15 to 65 cm.

Improving Cosmic-Ray Neutron Sensing with neutron spectrometry

It is evident that fast and epithermal neutrons are strongly affected by soil moisture (Figure 1.10). Indeed, they are the main particles used for assessing the water content in a field with the CNRS technique [26].

The CRNS method has been successfully employed in USA and in Germany, reaching good soil moisture sensitivity. The instruments employed in CRNS measurements are counters, in particular ^3He proportional counters and large scale Boron-lined proportional counters. Those instruments are optimized for thermal neutrons detection, and to maximize their sensitivity to epithermal neutrons, they are covered with moderator layers which slow down them before they are being detected. However, counters can provide only numerical information of the flux of cosmic neutrons in the epithermal range but cannot reconstruct the whole spectrum [26] and cannot clearly separate the four energy region (thermal, epithermal, fast and high energy, Figure 1.7). The proportional counters suffer therefore by non-negligible contamination from fast and, more importantly, thermal neutrons [2].

There are several reasons explaining why epithermal neutrons measurement are more suitable to measure the water content in soil and why the fast and thermal components can represent a contamination. The fast component, also called evaporation component, is made by neutrons coming both from the evaporation of the soil and of the air element. This means that a fast neutron that has been generated in air and that has not actually interacted with the soil, does not carry any useful information on the water content on the land. For this reason, the fast flux would require a different calibration function with respect to the epithermal one. The thermal part of the spectrum instead, is highly affected by the environmental chemical composition and slightly affected by soil moisture. This means that a universal calibration function independent on the soil composition would not be suitable for estimating water content from a signal highly influenced by the soil chemistry.

In conclusion, a cosmic neutron spectrometer results particularly useful for CRNS purpose. It allows a clear separation of the four energy regions, with the possibility to isolate the epithermal neutron flux. In addition, thanks to the spectrometric information, further aspects may be investigated. In particular, the high energy neutrons spectrum allows an accurate correction for the oscillation of the incoming primary neutron flux explained in Section 1.4.3). During the last years, a cosmic neutron spectrometer was developed at Politecnico di Milano. The instrument is presented in the next chapter.

2 | Problem statement and first WPIE design

The aim of this study is to design a new coating system for the existing W-PIE neutron spectrometer developed at Politecnico di Milano in 2021 [2] to produce an instrument which is lighter than the current one, and thus easier to be transported and to be installed. In particular, the presence of a quite thick slab of lead in the High Energy section results in a heavy system which is difficult to manage. At the same time, the spectrometric capabilities of the instrument, assessed for the current W-PIE in previous work [2], should be maintained as much as possible to ensure its operation as accurate soil moisture probe.

In this chapter the general working principles of neutron detection and spectrometry is briefly explained. Then, the structure and the components of the current W-PIE neutron spectrometer are illustrated to describe the new design starting point and to clarify the need for a new coating.

2.1. Working principles of neutron detection and spectrometry

Neutrons can be detected in matter through indirect methods, i.e. through the interaction with various nuclei causing the emission of one or more charged particles that produce detectable electrical signals. The main interactions with matter for neutron detection are:

- the scattering process, through which the neutron transfers to a nucleus some of its kinetic energy. The recoiling nucleus can ionize the material surrounding the point of interaction;
- the neutron capture reaction, the products of which can initiate the detection process;

The scattering mechanism is efficient for neutrons interacting with light nuclei, in particular hydrogen and helium are light enough for practical detectors. The impinging neutrons

must be fast enough so that the scattering process gives sufficient energy to generate an electric pulse. This is the reason why this mechanism can't be employed to detect thermal neutrons. Some nuclear reactions can require a minimum amount of energy to take place, but most of captures occur at thermal energies. Detectors exploiting thermal reactions are thus usually surrounded by moderating materials when they have to be used for fast neutron detection. In this way, the incident fast neutron is thermalized in the moderator and eventually detected by the thermal neutron detector in the center.

Elements which can be employed for neutron detection by means of nuclear reaction are elements such as He-3, Li-6, B-10 characterised by high absorption cross section for thermal neutrons. The energy released by the reactions with these nuclei is definitely greater than the original one of the of the thermal neutrons impinging on the target (25 meV vs around 1 MeV). The signal produced is related to the energy released after the neutron absorption by the target. This energy, manifested as kinetic energy of reactions products, can generate a detectable signal by ionizing a proportional gas or by producing scintillation. In this way the signal can be collected and processed. However, the information on the impinging neutron energy is lost. This makes impossible the estimation of the incident neutron energy.

To make epithermal and fast neutrons efficiently interact with absorbing materials, they are first slowed down inside a moderating material, such as high density polyethylene (HDPE). This is the material employed in the Bonner spheres, the most used devices employed to determine the energy spectrum of a neutron field. A bonner sphere is based on a thermal detector (usually an He-3 proportional counter) surrounded by sphere of HPDE [27]. The sphere shape allows to obtain a detector isotropic response to neutrons. The radius of the sphere determines the detector sensitivity to non-thermal neutrons. The range of energy covered employing HPDE in any case cannot overcome 20 MeV, because at this energy the $\sigma_{el,scatt}$ drops to zero, i.e. the moderation is no more efficient and the absorption in the detector becomes less likely. Actually, to moderate neutrons above 20 MeV employing polyethylene only, impractical or not releasable sphere radius would be needed.

Employing more spheres of different radii, each sphere has a sensitivity peaked at a particular neutron energy. From the measured readings of a set of spheres, information can be derived about the spectrum of the neutron field in which the measurements are made. The derivation of the spectrum is not simple and requires the knowledge of the so called "Response function" $R_i(E)$ relative to the i -th sphere. If the i -th sphere has a response function $R_i(E)$ and is exposed in a neutron field with a spectral fluence $\phi(E)$,

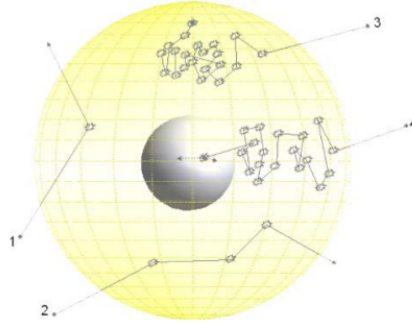


Figure 2.1: Moderating sphere with a thermal neutron detector in the center. Impinging neutron can be back scattered (1), scattered outside the moderator-detector system (2), moderated and then absorbed in polyethylene (3), moderated and finally absorbed in thermal detector.

then the sphere reading M_i is obtained mathematically by *folding* $R_i(E)$ with $\phi(E)$, i.e:

$$M_i = \int R_i(E)\phi(E)dE \quad (2.1)$$

where the integral extends over the range of neutron energies present in the field. There are two approaches to determine the response $R(E)$: experimental calibration in monoenergetic neutron fields and neutron transport calculations. Experimental determination has several limits, while a theoretical determination of $R(E)$ can be performed by means of Monte Carlo simulations. However, Monte Carlo calculations may be quite inaccurate and therefore require some validation through experimental data. For this reason, a common approach is to calculate the response function with simulations and then perform some experimental models to check the accuracy of the results. The document ISO-8529 suggests various neutron fields to perform calibration, including thermal fields, source fields and monoenergetic fields. The last option is probably the best one, having a well-defined energy. However, monoenergetic neutron fields can be generated, by nuclear reactions, in the range 10 keV-20 MeV. Above an energy of 20 MeV, "quasi-monoenergetic" neutron field can be generated in very few facilities in the world. For energies below 10 keV, except for thermal neutrons, it is practically impossible to perform experimental measurements to validate the Monte Carlo results.

Using data on the response functions, measurements with a Bonner Sphere set in a unknown field allow information on $\phi(E)$ to be extracted.

Neutron spectra are usually represented as an array ϕ where element ϕ_j is the fluence in the energy group j extending from energy E_j to E_{j+1} and the measured reading is given

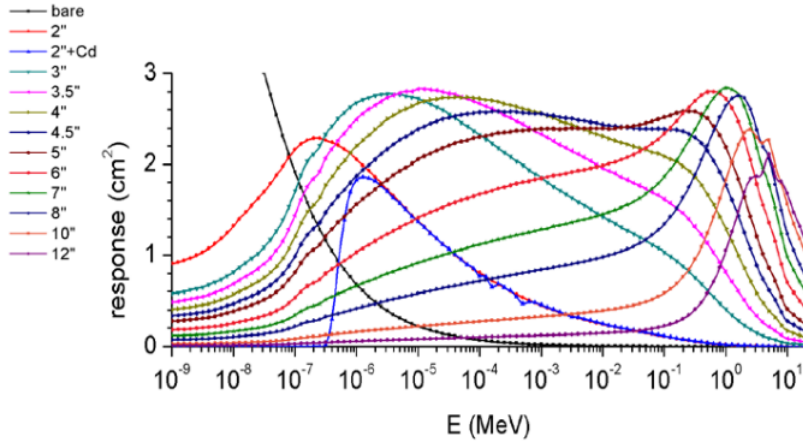


Figure 2.2: Response functions relative to different bonner sphere diameters.

by:

$$M_i = \sum_{j=1}^n R_{ij} \phi_j \quad (2.2)$$

where R_{ij} represent $R_i(E)$ averaged over group j . The above equation is an approximation of equation 2.1. The degree of approximation decrease as the number of energy groups n increases. Supposing to have m spheres, the equation 2.2 represents a set of m linear equations. However, m is usually small, in the order of 10, while n is usually larger to avoid losing information on important spectrum features by broadings energy group. The problem is thus an ill-posed problem, usually approached with a mathematical algorithm called unfolding. Details on the algorithm can be found in chapter 3.

As previously mentioned, HPDE material cannot efficiently moderate neutrons with energy higher than 20 MeV. The issue is address by means of a lead layer: high energy neutrons react by fragmentation with lead inducing the evaporation of secondary neutrons at lower energy (around 1 MeV) that can instead be thermalized and measured. The bonner spheres provided with lead are called "extended-range". These spheres also contain a layer of cadmium to shield thermal neutrons. Inevitably, the presence of lead significantly increase the weight of the system.

To measure the flux and energy spectrum of cosmic-ray induced neutrons the extended-energy Bonner sphere spectrometer are employed. An example are the measurements made at several locations across the United States with a multisphere spectrometer by Gordon and al.[28]. The spheres and the helium detector employed were 14 collecting data across an energy range from 1 meV to about 10 GeV. Figure 2.3 shows the 14 element-Bonner sphere spectrometer on the roof of the IBM T.J. Watson Research Center in



Figure 2.3: Bonner sphere used by Gordon et al. [28]

Yorktown Heights, in New York.

2.2. W-PIE first design

The W-PIE spectrometer for soil moisture measurements is an innovative spectrometer designed in 2020 based on a He-3-free neutron detector, detecting neutrons in the energy range from 0.01 eV to 1 GeV [2]. The reconstruction of the energy spectrum, allowing an accurate evaluation of the epithermal neutron flux at ground level, is performed thanks to the system illustrated in Figure 2.4.

The system is composed by a M800 thermal neutron detector manufactured by Arktis divided in four regions, each covered with different coatings. The coating structure was designed to maximize the detector sensitivity to neutrons in a certain energy range. In the following, the M800 thermal detector is described, as well as the moderators structure.

2.2.1. M800 thermal detector

The neutron detector ARKTIS M800 (ARKTIS Radiation Detectors, Switzerland) consists of a ^4He filled aluminium tube and is based on the gaseous scintillation principle [29].

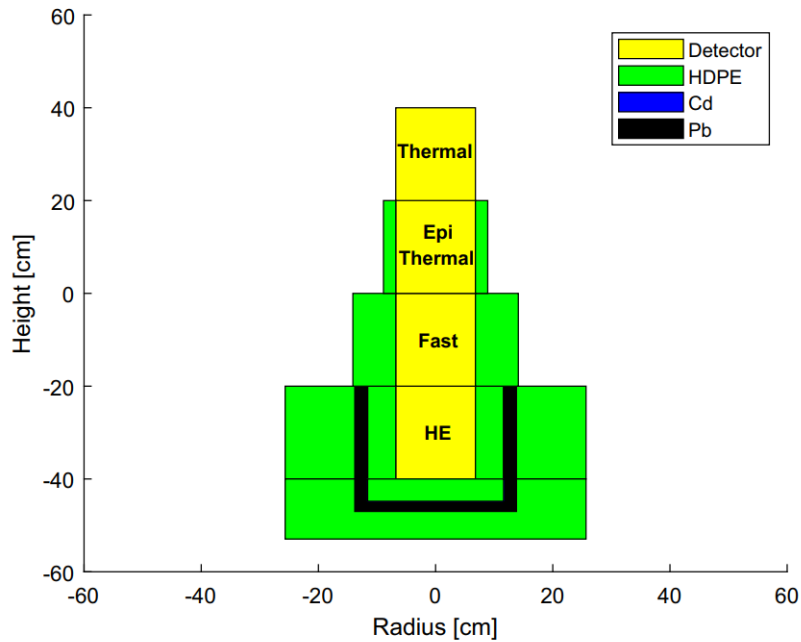


Figure 2.4: First W-PIE structure showing the detector and the coatings allowing neutron spectrometry. Figure taken from [2].



Figure 2.5: The ARKTIS M800 neutron detector. Figure taken from ARKTIS M800 sheet.

The detector is 91.62 cm long and 14.4 cm in diameter and it is partitioned in eight independent sectors. The neutron sensitive material is a large area ${}^6\text{Li}$ -impregnated polymer: lithium captures a neutron and emits high-energy α particles causing the gas scintillation. Light is then collected by 24 SiPM (Silicon Photomultiplier), i.e. 3 for each sector.

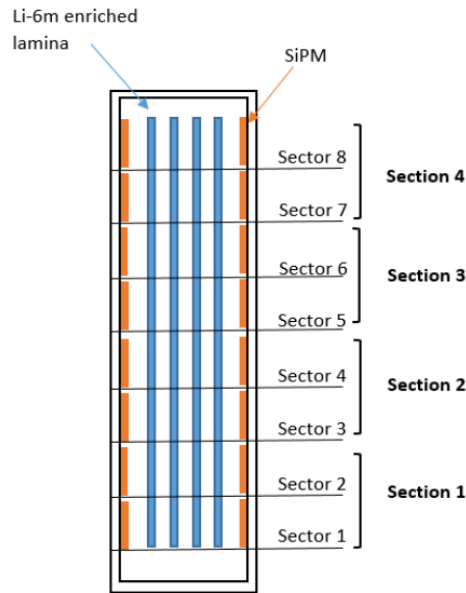
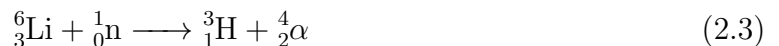


Figure 2.6: M800 scheme: the enumeration and the orientation of the section refers to the convention employed. Figure taken from [21].

Figure 2.6 shows the sensitive volume and the SiPM schematic structure, as well as the division in sectors and section adopted hereafter.

When a thermal neutron reaches ${}^6\text{Li}$ inside the detector, the occurring reaction is:



where the reaction products tritium and alpha particles ionize helium atoms. These excited atoms de-excite by emitting photons, giving rise to scintillation phenomenon. The photons produced are detected by the SiPM and the signal is processed by the electronics simultaneously. The three SiPMs of each sector operate in coincidence, i.e. an event is recorded only if at least two out of three detect a signal. Analog-to-digital conversion is performed on board and the information is sent via Ethernet to a laptop, together with other detector information. The system is controlled and powered by a single Power over Ethernet (PoE) cable. Further details on the detector working principle and on the output produced can be found in [29].

A cut on the amplitude of the acquired signal must be set to remove noise and to address the gamma rejection issue. The low density and the low Z value of ${}^4\text{He}$ makes unlikely respectively the reaction event and, in case the event occurs, a photoelectric reaction. A large energy deposition of gamma rays in the detector is thus unlikely and a low cut is

set to eventually reject a low amplitude signal generated by a Compton interaction. The cut must be increased if a non negligible gamma flux is expected.

Studies on M800 detector [29] conducted to investigate whether this detector could be employed for radiometric surveillance of scrap metal, in particular to detect ^{241}Am orphan source, showed that the M800 in a moderating box is extremely sensible to any source of radiation, even the background due to cosmic radiation. Then, if properly coated, the M800 is able to build good statistics in relatively short times even for weak neutron fluxes such as cosmic neutron radiation.

2.2.2. WPIE moderating coatings

The detector was coated with moderators to realise a spectrometer. In particular, WPIE detector is divided into four regions (constituted by two adjacent sectors) and each of them is covered with different coatings to maximize its sensitivity to neutrons in a certain energy range [2].

The coatings aim is the one of the Bonner spheres: to make the thermal detector, the M800 in the W-PIE case, able to produce adequate output data to unfold the spectrum. Each count detected has to be related to the corresponding Response Function.

As previously mentioned, the M800 is divided into eight sectors each recording its own signal. The eight sectors are grouped into four sections: since each section coating is specifically designed to detect neutrons of certain energy in that region, they have different sensitivities to neutrons of different energies. In this way, counts coming from each section are related to a specific response along the spectrum and are mainly representative of a specific energy interval.

The eight sectors were grouped in four section to prevent the reduction in counting statistics that would have occurred by reducing each section sensitive volume, i.e. by having a small segment of the active volume dedicated to each section. Indeed, to make the spectrometer usable in CNRS, it is desirable to reach good statistics within an hour.

The energy interval of interest are the ones in Figure 2.7. In particular, each section focuses on the following energy intervals:

- Section 1: energies over 20 MeV, called High Energy (HE) region;
- Section 2: energies between 0.5 and 20 MeV, called Fast region;
- Section 3: energies between 10^{-6} MeV and 0.5 MeV, called Epithermal region;
- Section 4: energies up to 10^{-6} MeV, called Thermal region;

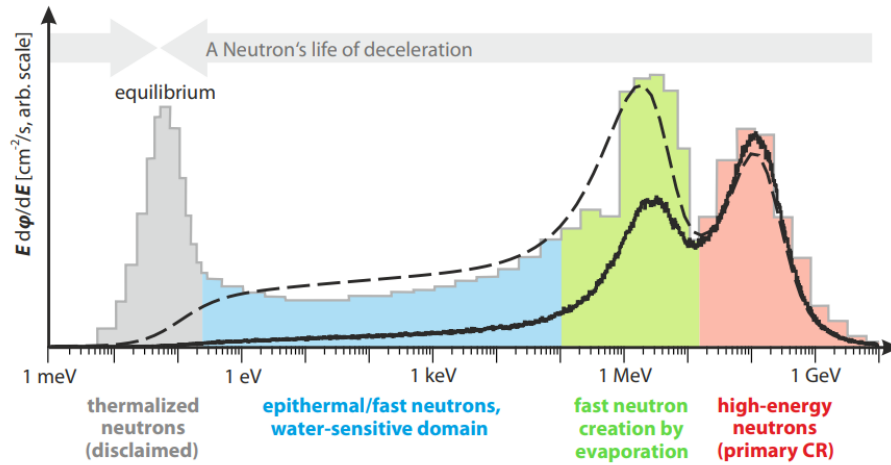


Figure 2.7: Cosmic neutrons energy spectrum, from [16]. The gray peak represents the energy distribution of thermal neutrons at equilibrium with the environment, the blue region represents the epithermal neutrons, the green peak includes the fast neutrons generated by evaporation, and the red peak is the distribution of high energy neutrons generated in the upper atmosphere

The WPIE moderating coatings for each section shown in Figure 2.4 were designed following the principles of the extended-range Bonner spheres explained in section 2.1. The moderators thicknesses were optimized with respect to the ideal properties of the response functions necessary to perform the neutron spectrum deconvolution.

The W-PIE structure is such that:

- the high energy region, i.e. the first section, is characterized by (from the inner to the outer part) 4.8 cm of HPDE, 0.2 cm of cadmium, 2 cm of lead and 5.9 cm of HPDE. Their aim is to extend the sensitivity to the high energy range, thanks to the fragmentation reaction of high energy neutrons with lead and to reduce the sensitivity of the section to thermal neutrons, thanks to the cadmium absorption of neutrons in thermal region.
- the fast region, i.e. the second section, is covered with a 7.2 cm layer of HPDE to slow down fast neutrons and finally detect them as thermal neutrons in the sensitive volume;
- the epithermal region, i.e. the third section, is covered with a 2-cm layer of HPDE, to slow down epithermal neutrons and finally detect them as thermal neutrons in the sensitive volume;

- the thermal region, i.e. the fourth section, is bare, to detect the originally thermal neutrons;

Of course cross-talk phenomenon is present, i.e. a neutron of a certain energy is moderated by the coating of a certain section and eventually captured in another. Cross-talk in W-PIE was investigated in the design process, considering the hypothesis to put absorbing layers between moderators sections. Simulations showed that the relevant effect was to reduce sensitivity, and eventually no absorber layer has been put.

Measurements were performed with the W-PIE design described above irradiating it with AmBe and Am sources, as well as with natural radiation [2]. These activities showed the instrument capability of performing reliable neutron spectrometry and the system sensitivity to cosmic neutrons. In particular, measurements of the natural radiation performed both at ground level and in an elevated position, showed that the detector counts roughly 0.6 cps (summing all regions) in these configuration [2].

However, the WPIE illustrated in Figure 2.4 has an overall weight of about 100 kg, about 90 of which due to the High Energy section, where lead is present. This fact makes the WPIE quite difficult to be transported and to be managed.

For this reason, the design described above was the starting point for the next optimization, taking into account the weight of the coating system, together with the important properties that the system response functions had to maintain in order to make the system suitable for a neutron spectrometry satisfactory for the soil moisture estimation purpose.

3 | Analysis and Simulation Tools

In the following sections, the tools and methods employed to perform the optimization of a new lighter coating design are reported. Monte Carlo simulations were performed to assess the response to neutrons of the region in which the detector is divided and to optimize the moderators' thicknesses to improve as much as possible the unfolding procedure. The code employed for Monte Carlo simulations was MCNPX ver 5.1 code, briefly described in the first section of this chapter. The spectrum unfolding procedure was performed by means of the GRAVEL algorithm, described in the second section.

3.1. MCNPX

MCNPX, standing for Monte Carlo N-Particle eXtended, is a general purpose Monte Carlo radiation transport code designed to track many particle types over broad ranges of energies [30]. The transport of particles such as neutrons, electrons, ions and photons, is simulated to occur through a three dimensional representation of materials defined in a solid geometry, bounded by several user-defined surfaces. Tabulated nuclear and atomic data and physical models are embedded in the code to simulate the physics at each particle collision occurring during the simulated transport process. The probability density functions of each event process are sampled using pseudo-random numbers to simulate the particle tracking through the defined geometry. MCNP contains numerous tallies such as average flux at a surface and flux averaged over a cell.

MCNP is employed in applications such as radiation protection and dosimetry, medical physics, radiation shielding and many others, providing a predictive capability that can replace expensive and experiments difficult to perform.

The basis of MCNP is the Monte Carlo method, which is very different from deterministic transport methods employing numerical methods to solve a set of differential equations. Monte Carlo "solves" a transport problem by simulating particle histories and not by solving an equation. Monte Carlo simulates individual particles and records some aspects, i.e. tallies, of their average behaviour. The average behaviour of particles in the physical

system is inferred (using the Central Limit Theorem) from the average behavior of the simulated particles.

Monte Carlo is thus particularly useful for complex problems that cannot be modeled by computer codes using deterministic methods. It theoretically duplicates a random walk process (such as the interaction of nuclear particles with matter). The individual probabilistic events composing a particle history from birth to death are simulated sequentially, while different particle histories can be simulated in parallel.

Various particles random walks example are shown in Figure 3.1.

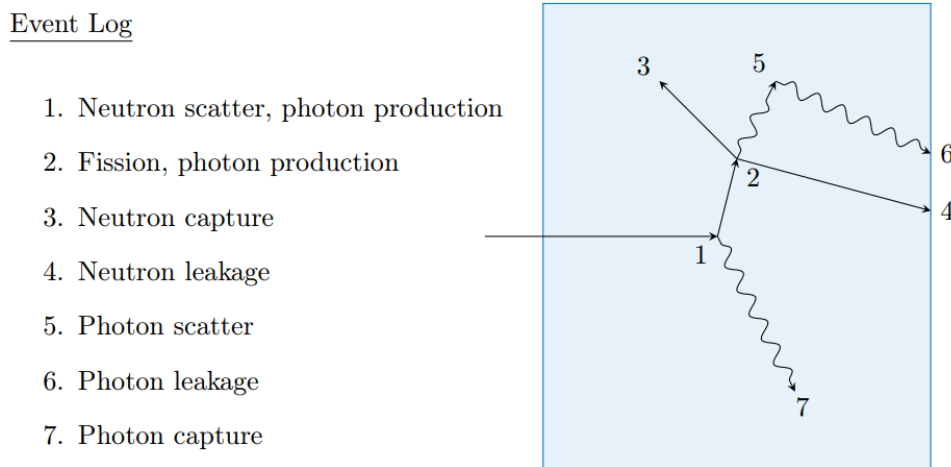


Figure 3.1: Various particle random walks relative to different physical events. Figure taken from [31].

The probability density functions from which the code samples to simulate events are determined by the physics of the process, the transport data and the materials involved. Several classes of data tables exist for the MCNP code, among which there are continuous-energy neutron interaction data. Neutron tables, as well as photonuclear tables, are isotopic in nature, i.e. each isotope requires its own table.

For most materials, there are many cross-section sets available because of multiple sources of evaluated data. An evaluated nuclear data set is produced by analyzing experimentally measured cross sections and combining those data with the predictions of nuclear model calculations, in an attempt to extract the most accurate interaction description [31].

The simulation space is composed by "volume cells" characterized by specific density and material, enclosed by defined surfaces. The user can define the materials to simulate, indicating each element present and its relative abundance.

The instructions needed to perform the simulations are contained in the text input file, consisting of a series of structured commands called "Cards". Each card consists of a series of keywords and data entries, separated by one or more blank spaces, and a card always starts on a new line [31]. A collection of multiple cards is referred to as a block, which can be optional or required, as shown in Figure 3.2.

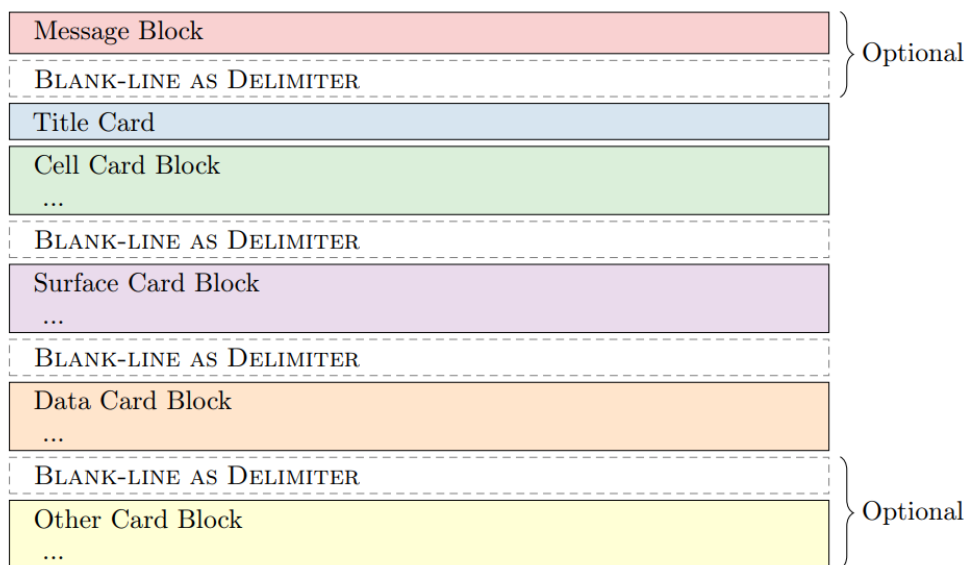


Figure 3.2: MCNP Input File Format

Figure 3.2: MCNP Input File Format. Data Cards include Tally and Material specifications. Figure taken from [31].

The required Cards are:

1. **Cell Cards:** cells are volumes, which must be enumerated, enclosed by the surfaces indicated in the surface cards. The cells materials and densities can be indicated, together with a complete specification of the geometry of the cell. Among the geometry specifications, a list of signed surfaces bounding the cells can be provided. The sign denotes the sense of the regions defined by the surfaces.
2. **Surface Cards:** surfaces must be enumerated and the surface type has to be indicated. A particular surface type (such as "px" for a plane normal to the x axis, or "s" for a sphere) has an equation, whose numerical coefficients must be provided in the required order. Simplified description can be employed to ease the surface implementation.
3. **Material Cards:** this cards specify both the isotopic composition of the materials

and the cross-section evaluations to be used in the cells. In particular, a "Nuclide Identification Number" (ZAID) is required, together with a "Nuclide Fraction", which may be provided as weight or atomic fractions, and which can be normalized or left unnormalized.

4. Tally Cards: the tally cards are used to specify the specific quantity to be inferred from the Monte Carlo calculation, such as current across a surface, flux at a point, etc.

Further details on MCNPX and the text input file can be found in [30].

Once the simulation run has been performed, an output file is generated in which all the important parameters of the simulation and tallies are present.

A relative error R accompanies the output tallies, defined to be one estimated standard deviation of the mean divided by the estimated mean, i.e. $R = S_{\bar{x}}/\bar{x}$. R is proportional to $1/\sqrt{N}$, where N is the number of histories. The Central Limit Theorem states that as N approaches infinity there is a 68% chance that the true result will be in the range $\bar{x}(1 \pm R)$ and 95% chance in the range $\bar{x}(1 \pm 2R)$, i.e. that it will be following a normal distribution. This confident statement only refers to the calculation of the Monte Carlo itself and not to the accuracy with respect to the *true physical* value. The quality of the Tally is considered "Generally reliable" if $R < 0.10$.

There are cases in which an important but unlikely particle path in phase space may not have been sampled in the problem, resulting in incorrect expected values and confidence interval statements. To try to inform the user about this behavior, MCNP computes a figure of merit (FOM) for one tally bin of each tally and prints the results at the end of the output. The FOM is defined as $FOM \equiv 1/(R^2T)$ where T is the computer time in minutes [31]. Since R^2 is proportional to $1/N$ and T is proportional to N , the FOM should be approximately constant as N increases. The FOM value must be examined to be sure that the tally behaves correctly.

3.2. Unfolding algorithm

An unfolding algorithm is a mathematical procedure allowing to rebuild the neutron spectrum from a vector of detected counts.

As described in the previous chapter, to make neutron spectrometry a set of Bonner spheres together with their response functions are generally employed. Each instrument of the set provides the counts acquired in a certain measurement time.

Assuming to have M Bonner spheres, each j-th sphere characterised by a specific response function $R_j(E)$, and that each sphere can be exposed to the same neutron flux $\phi(E)$, the M detected counts c_j can be expressed as:

$$c_j = \int R_j(E)\phi(E)dE \quad j = 1, 2, \dots, M \quad (3.1)$$

which is the Fredholm integral equation of the first type. Response functions can be theoretically computed by simulations in their discrete form, dividing the energy interval of interest in N energy bin. The discrete form of equation 3.1 is:

$$c_j = \sum_{k=1}^N R_j(E_k)\phi(E_k) \quad j = 1, 2, \dots, M \quad (3.2)$$

where k from 1 to N refers to the k-th energy bin.

Considering the vector of counts $\mathbf{c} = (c_1, c_2, \dots, c_M)$ and the fluxes for each energy bin $\boldsymbol{\phi} = (\phi_1, \phi_2, \dots, \phi_N)^T$ the problem can be seen in a compact way as:

$$\mathbf{c} = \mathbf{R}\boldsymbol{\phi} \quad (3.3)$$

where the size of \mathbf{c} is M, the size of $\boldsymbol{\phi}$ is N and the matrix \mathbf{R} has size $M \times N$.

To obtain the neutron spectrum $\boldsymbol{\phi}$, equation 3.3 need to be inverted. However, the task of determining the unknown $\boldsymbol{\phi}$ from the observable \mathbf{c} is an ill-conditioned problem. Indeed, usually the energy bins are more than 100 while the number of Bonner sphere usually used is around 10. Therefore, $N \gg M$ and the problem has N unknown and M equations. A procedure to unfold the spectrum is necessary.

The unfolding algorithm employed in this work is called GRAVEL and is described in the next section.

3.2.1. GRAVEL

The GRAVEL algorithm is an important algorithm developed by PTB Laboratory widely used in the field of energy spectrum unfolding. Among the available unfolding algorithms, GRAVEL is suggested for few-channel unfolding.

The algorithm is fed by the response matrix \mathbf{R} , the vector of counts \mathbf{c} , the vector of counts uncertainty $\boldsymbol{\sigma}$ and the *guess spectrum*. The more the number of Bonner spheres employed gets lower, the more the final reconstructed spectrum is affected by the initial guess spectrum.

The procedure is iterative, and considering the generic $K+1$ step and the K previous step, $\phi = (\phi_1, \phi_2, \dots, \phi_N)^T$ is computed as:

$$\phi_j^{K+1} = \phi_j^K \exp \left(\frac{\sum_i W_{ij}^K \ln \left(\frac{C_i}{\sum_{j'} R_{ij'} \phi_{j'}^K} \right)}{\sum_i W_{ij}^K} \right) \quad (3.4)$$

where W_{ij} is:

$$W_{ij}^K = \frac{R_{ij} \phi_j^K}{\sum_{j'} R_{ij'} \phi_{j'}^K} \frac{C_i^2}{\sigma_i^2} \quad (3.5)$$

At step $K = 1$, a first input spectrum ϕ^0 is needed when the iteration is started and it is called guess spectrum.

The criterion adopted to stop the iteration is the χ^2 per degree of freedom, χ^2/N . The value of χ^2 per degree of freedom is defined as:

$$\chi^2/N = \frac{1}{N} \sum_i \frac{\left(\sum_j R_{ij} \phi_j - C_i \right)^2}{\sigma_i^2} \quad (3.6)$$

Each solution with $\chi^2/N \approx 1$ should be considered as consistent.

In any case, if the χ^2 value is not lower than the χ_{target}^2 decided by the user, the process is repeated taking ϕ_{j+1} as new input spectrum.

4 | Realization

In this chapter, the procedures adopted to design the new light W-PIE are described.

4.1. M800 MCNP model

The theoretical Response Functions (RF) evaluation by means of the Monte Carlo simulation code MCNPX required the modeling of the W-PIE made by the detector and the coating models. The M800 thermal neutron detector model developed, investigated and validated in [21] was employed. The M800 was modeled by reproducing as close as possible the known features provided by manufacturers and by making some approximations, such as modeling SiPMs as single layer of silicon and leaving the electronics not modeled for lack of information.

Figure 4.1 shows the two vertical and horizontal cut of the model employed in Monte Carlo simulations.

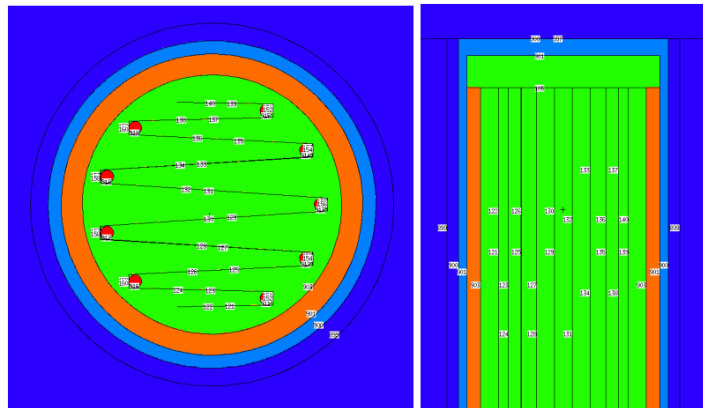


Figure 4.1: M800 MCNPX model vertical and horizontal cut. Blue: air, light blue and red: aluminium, orange: silicon, yellow: LiF, green: He. Figure taken from [21].

This M800 model coated with the moderators such as shown in Figure 4.3b was the starting point employed to perform a further coating optimization taking into account the overall weight.

4.2. Response Functions estimation

The Response Functions (RF) of the 4-channel W-PIE spectrometer were theoretically computed employing the MCNPX ver 6.2.0 code. They are the input of the GRAVEL unfolding algorithm, explained in section 3.2, implemented in Python. Thanks to the knowledge on the matrix \mathbf{R} containing the response functions for each region and on the measured counts per second \mathbf{N} , the algorithm can unfold the following equation:

$$\mathbf{N} = \mathbf{R}\phi \quad (4.1)$$

obtaining the spectrum ϕ , expressed as energy-binned neutron flux.

RF were evaluated simulating a planar source next to the detector, generating neutrons in a random points of the plane source, with a direction parallel to the x axis, according to the configuration of Figure 4.2. Neutrons energy were uniformly sampled from 110 discrete values in the range 10 meV to 1 GeV.

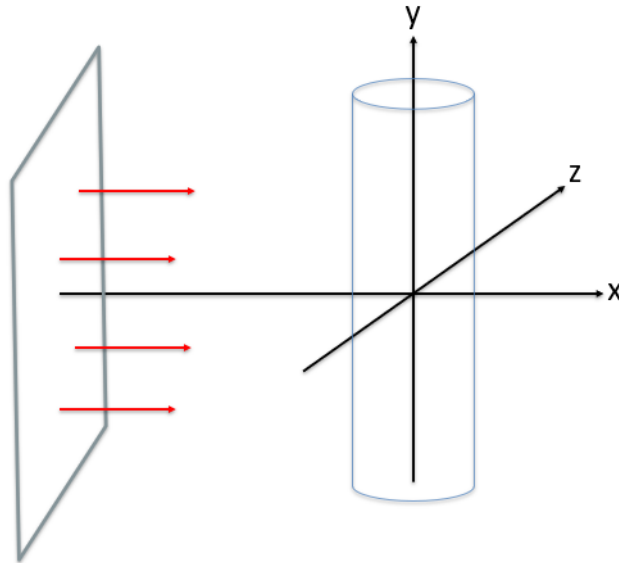


Figure 4.2: Planar source configuration used in simulations. The source generates an expanded and aligned neutron field with energy uniformly sampled from 110 discrete values in the range 10 meV-1GeV

To evaluate response functions, the W-PIE model and the planar source modeled as the one shown in Figure 4.2 were embedded in the simulation. For each section and for the i -th energy bin, with i from 1 to 110, the MCNP code estimates:

1. impinging neutron fluence averaged on the external surface of the detector
2. number of capture reactions that occurred in the sensitive volume

Then RF_i has been defined as the ratio of the number of capture reactions and the impinging neutron fluence, equal to the reaction rate divided by the impinging neutron flux:

$$RF_i = \frac{RR_i}{\phi_i} \quad (4.2)$$

In this way, RF for each energy bin can be plotted obtaining a plot such as the one in Figure 4.3a, showing the different sections responses to the different neutron energies.

4.3. Starting point design

The optimization procedure starting point is W-PIE described in Section 2.2. The specific dimensions are reported in table 4.1.

W-PIE first design (103.75 kg)		
Section 4	bare	-
Section 3	HPDE layer	2.0 cm
Section 2	HPDE layer	7.2 cm
Section 1	internal HPDE layer	4.8 cm
	Cd HPDE layer	0.2 cm
	Pb layer	2.0 cm
	external HPDE layer	5.9 cm

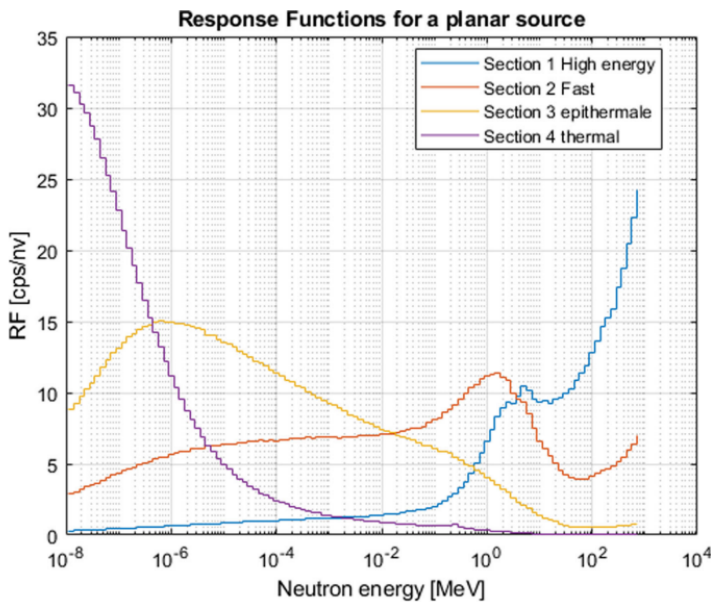
Table 4.1: Thicknesses of each coating layer for the starting W-PIE configuration. Thicknesses of the high energy section S1 refers both to lateral thicknesses and vertical thicknesses.

The overall system, i.e. the M800 detector covered with moderators, is the one shown in Figure 2.4.

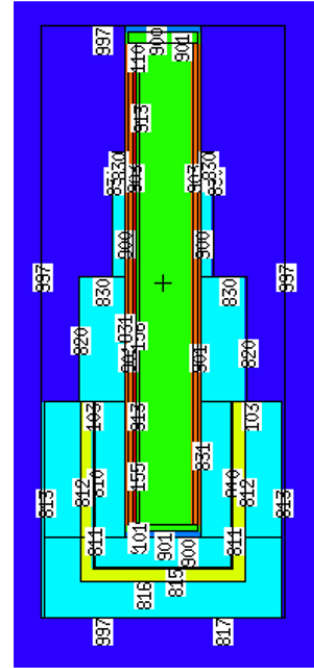
The optimization performed for the first W-PIE design in developing the figure of merit did not take into account of a factor for the weight. The instrument is thus quite heavy. In particular, due to the presence of lead, Section 1 alone weights about 90 kg. The overall weight reaches about 100 kg. Table reports more specifically these weights, computed

considering the following densities: 0.99 g/cm^3 for HPDE, 8.7 g/cm^3 for Cd and 11.34 g/cm^3 for lead.

The RF corresponding to W-PIE with coating thicknesses of table 4.1 are shown in Figure 4.3a, together with the MCNP-simulated detector.



(a) W-PIE Response Functions



(b) W-PIE MCNP model

Figure 4.3: a: W-PIE Response functions for the four sectors in case of an expanded and aligned neutron field. The ordinate axis shows the cps per unit flux ($\frac{cps}{nv}$) as a function of the neutron energy. Figure taken from [2]. b: MCNP model of the W-PIE

4.4. Considerations on response functions

The ideal response functions properties to perform spectrum unfolding are:

- at each energy at least two RFs must be non null
- the RFs shapes should be as different as possible from one another in the energy range of interest
- the RF values must be as high as possible to increase the count rate of the instrument
- all sections should reach good statistics at similar times. If the mean value of the RF of a section is very low compared to the other sections, this would result in a longer time necessary to reach good statistics.

The first and second requirements above should ease the unfolding procedure. The third and fourth ones are specifically needed for the W-PIE application in soil moisture monitoring, to measure rapid changes in soil moisture. Accordingly with the considerations above, the W-PIE Response Functions of Figure 4.3a have some desirable features to be maintained as much as possible. In particular, the response functions corresponding to each sections "dominate" their region of interest covering with a sufficiently high response energy ranges. Moreover, they show inverted trends in many points, and when this is not verified, response functions values are sufficiently distant.

4.5. Weight optimization implementation

The objectives to be addressed to optimize the W-PIE response functions, taking into account the RF ideal properties and the weight, are multiples and somehow conflicting. Indeed, the thicknesses of the coatings, to be reduced with the aim to reduce the overall system weight, are the ones ensuring the best RF shape for the W-PIE design. In particular, the High Energy section, which is the heaviest and most cumbersome section, provides a high response in that region, and a response much higher than the non null fast response.

In this perspective, it is necessary to reach a trade-off between the desirable RF shape and the coating weight. To embed together these multi-objectives, a figure of merit "f.o.m." was defined as combination of the following factors:

- p_1 = mean RF in the epithermal region
- p_2 = mean RF in the fast region
- p_3 = mean RF in the high energy region
- p_4 = mean difference between RF of the epithermal region and RF of the fast region
- p_5 = mean difference between RF of the fast region and RF of the high energy region
- p_6 = the total weight

While factors from p_1 to p_5 have to be as high as possible, on the contrary a low p_6 is desired. The above factors, and thus the figure of merit, are a function of the coating thicknesses, i.e:

- x_1 = thicknesses of HPDE layer in epithermal section
- x_2 = thicknesses of HPDE layer in fast section

- x_3 = thicknesses of internal HPDE layer in high energy section
- x_4 = thicknesses of Cd layer in high energy section
- x_5 = thicknesses of Pb layer in high energy section
- x_6 = thicknesses of external HPDE layer in high energy section

The figure of merit was defined as:

$$f.o.m.(x_1, \dots, x_6) = \sum_{i=1}^5 p_i - p_6 \quad (4.3)$$

In this way, all p_i have the same importance. The behaviour of the f.o.m. with respect to a chosen set of coating thicknesses values was investigated performing more than 1000 Monte Carlo simulations with MCNPX. Table 4.2 report the thicknesses domain in which simulations were performed.

Section	Layer	Dataset [cm]
S3	x_1 HPDE thickness	{2}
S2	x_2 HPDE thickness	{4, 4.5, 5, 5.5, 6, 6.5, 7}
S1	x_3 internal HPDE thickness	{2, 2.5, 3, 3.5, 4}
	x_4 Cd thickness	{0.2}
	x_5 Pb thickness	{1, 1.33, 1.66, 2}
	x_6 external HPDE thickness	{3, 3.5, 4, 4.5, 5, 5.5, 6, 6.5, 7}

Table 4.2: Domain of the inputs considered for each dataset. Thicknesses of the high energy section S1 refers both to lateral thicknesses and vertical thicknesses.

The total number of combinations is 1260. The simulations were performed with $5 \cdot 10^7$ number of particles allowing to reach a f.o.m. evaluation uncertainty of about 6%. Each MCNPX input file was generated by a Phyton script implemented for this purpose.

Each simulation consisted in the generation of the input file describing the W-PIE coating geometry corresponding to a combination of the values in Table 4.2. The simulated W-PIE is exposed to the expandend and aligned neutron field of generated by the planar source described in Figure 4.2.

Each output file provides the tallies necessary to estimate the response functions as in equation 4.2.

The f.o.m behaviour of equation 4.3 was investigated in MATLAB. From the response functions obtained from the simulations, the f.o.m was computed for each of the 1260 combination. The f.o.m. values were normalized with respect to the mean values, i.e. each objective p_i was divided by the mean value over all the simulation values.

The obtained f.o.m values were sorted and plotted to infer which was the coating designed that better performed with respect to the f.o.m.

The resulting "first-ranked" best coating design has the thicknesses of Table 4.3.

W-PIE optimized design 1 (60,21 kg)		
Section 4	bare	-
Section 3	HPDE layer	2.00 cm
Section 2	HPDE layer	7.00 cm
Section 1	internal HPDE layer	2.00 cm
	Cd HPDE layer	0.20 cm
	Pb layer	1.33 cm
	external HPDE layer	7.00 cm

Table 4.3: Thicknesses of each coating layer for the weight-optimized W-PIE configuration obtained maximizing f.o.m. of eq. 4.3. Thicknesses of the high energy section S1 refers both to lateral thicknesses and vertical thicknesses.

The overall weight of the moderating coating system in this way was reduced to about 60 kg, among which about 50 related to the High Energy section containing lead. The weight was greatly reduced with respect to the 100 kg of the design starting point.

The impact of the thicknesses modification on the response functions was analysed to understand whether such configuration was suitable according to the desirable response functions features. Response functions are shown in Figure 4.4.

The most evident effect is the fast and high energy response reduction across the fast and the high energy region. In particular, the fast and high energy response functions trends invert at higher energies with respect to the first design.

The second design considered, the "second ranked" was the same of the one in Table 4.3 part from the Pb layer in the high energy section, which is 1 cm in the second configuration. Results are shown in Table 4.4.

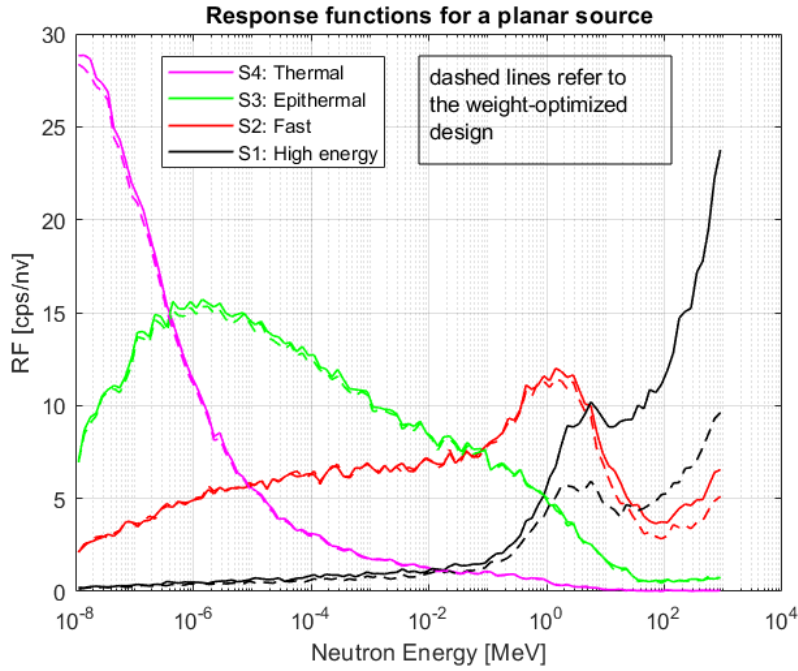


Figure 4.4: Comparison between starting Response functions vs weight optimized ones. High energy response is lowered about by a factor 2.

W-PIE optimized design 2 (52,96 kg)		
Section 4	bare	-
Section 3	HPDE layer	2.00 cm
Section 2	HPDE layer	7.00 cm
Section 1	internal HPDE layer	2.00 cm
	Cd HPDE layer	0.20 cm
	Pb layer	1.00 cm
	external HPDE layer	6.50 cm

Table 4.4: Thicknesses of each coating layer for the weight-optimized W-PIE configuration obtained maximizing f.o.m. of eq. 4.3

The result is of course a further reduction of the High Energy section weight. Response functions of the second weight-optimized design (1 cm of lead) remains quite unchanged with respect to the first optimized design (1.33 cm of lead) before 30 MeV, while above 30 MeV the responses are further reduced.

The figure of merit was modified to investigate the optimization result when assigning an

higher coefficient to the objective p_6 , i.e. the one related to the weight. The new f.o.m. is:

$$f.o.m.(x_1, \dots, x_6) = \sum_{i=1}^5 p_i - 2p_6 \quad (4.4)$$

The highest value of the f.o.m. of the above equation corresponded to the design describe in Table 4.5.

W-PIE optimized design 3 (50,75 kg)		
Section 4	bare	-
Section 3	HPDE layer	2.00 cm
Section 2	HPDE layer	7.00 cm
Section 1	internal HPDE layer	2.00 cm
	Cd HPDE layer	0.20 cm
	Pb layer	1.00 cm
	external HPDE layer	6.50 cm

Table 4.5: Thicknesses of each coating layer for the weight-optimized W-PIE configuration obtained maximizing f.o.m. of eq. 4.4

This last design includes a reduction of 0.50 cm for the external HPDE layer of the high energy section. In this case, the response functions remained the same, and visually no differences were detected.

To compare the high energy response functions at energies > 100 MeV of the various coating design taken into consideration, the respective RF were integrated. The resulting counts are reported in Table 4.6

Design	integral of cps/nvfor E > 100 Mev
starting (4.1)	340.45
optimized 1 (4.3)	147.34
optimized 2 (4.4)	121.40
optimized 3 (4.5)	120.09

Table 4.6: Integrated response functions for E > 100 MeV

To choose the final configuration, the expected cps for each section of each configurations

were computed considering an impinging cosmic flux $\phi = 0.0112 \text{ cm}^{-2}\text{s}^{-1}$ predicted in Milan by EXPACS. EXPACS allows estimating the predicted neutron fluence rate in a specific time and place in ideal conditions. Predictions of this software must be considered quite approximate. Results are shown in Table 4.7, also reporting the respective design weights.

Design	High Energy cps	Fast cps	Epithermal cps	Thermal cps	total weight [kg]
starting (4.1)	0.0661	0.0699	0.0701	0.0669	103.75
opt. 1 (4.3)	0.0335	0.0667	0.0694	0.0662	60.21
opt. 2 (4.4)	0.0305	0.0653	0.0695	0.0660	52.69
opt. 3 (4.5)	0.0316	0.0654	0.0691	0.0657	50.75

Table 4.7: Comparison of the expected cps in each section of each design for a cosmic flux source given by EXPACS. Weight-optimized design results in a reduction of the High Energy cps detected.

Results show that the High Energy section cps for the weight-optimized design are reduced of about a factor 2 with respect to the starting design of the W-PIE coating and in a substantial reduction of the overall weight.

Finally, the second weight-optimized design 4.4 was considered the best choice. It is the second-ranked design according to the optimization performed maximizing a figure of merit assigning the same importance to the ideal RF properties and to the total system weight. The Pb layer thickness of 1.00 cm instead of 1.33 cm was considered the most reasonable choice considering the specific manufacturing procedures adopted by the mechanical workshop, allowing to produce layer of a minimum thickness of 0.5 cm.

The design considered as the best one is shown in Figure 4.5, while Figure 4.6 shows its response functions.

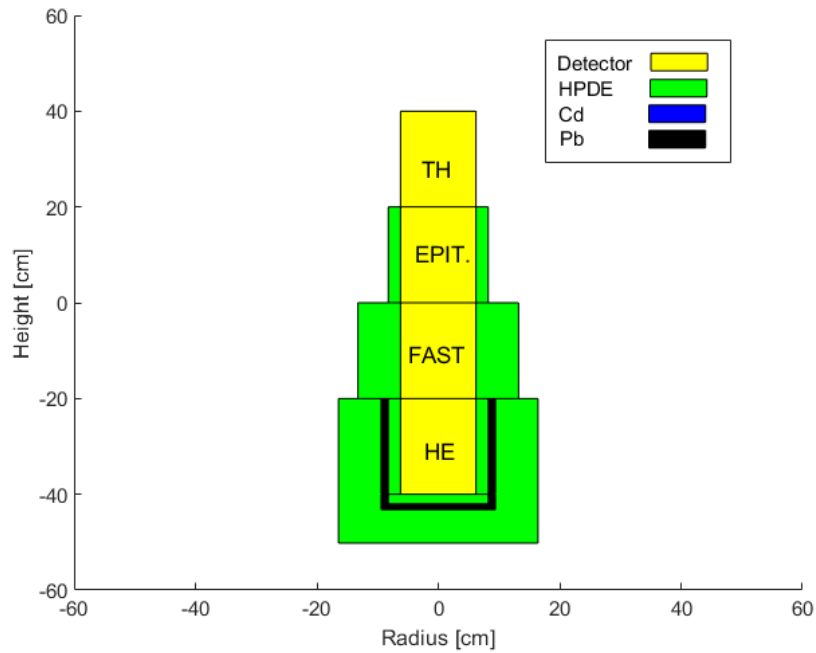


Figure 4.5: Sketch of the optimized design, i.e the one with thicknesses of Table 4.4. The Cd layer is too thin to be appreciated.

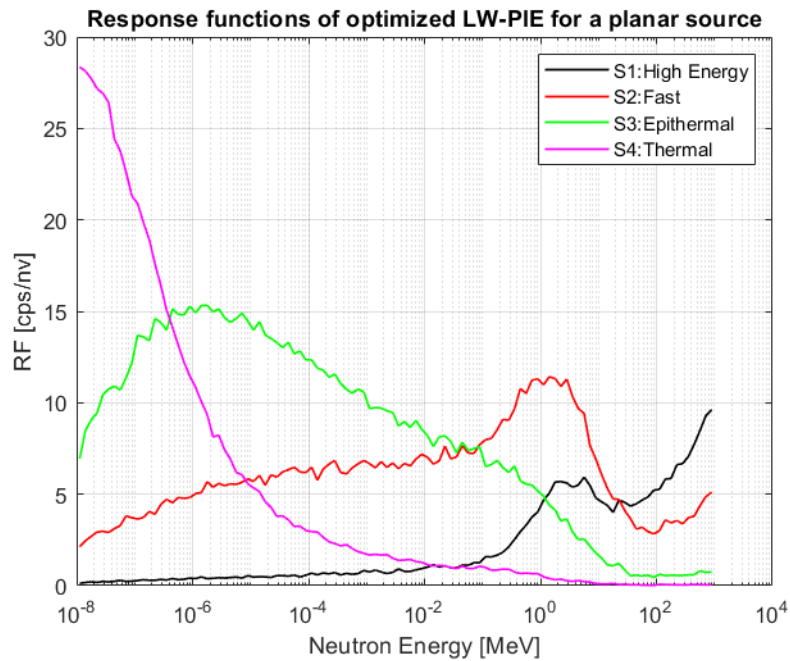


Figure 4.6: Optimized "light" W-PIE (LW-PIE) design response functions.

4.6. Final design

The very final "light" W-PIE design (L-WPIE) was determined taking some additional considerations. In particular, it was necessary to shorten the overall height of the L-WPIE system to make it fit on a proper case, planned for its transportation, which was already available on the market. A dedicated design of this case would have increased the cost and would have taken a longer period.

The following decisions were made:

- the thickness of the *base* external HPDE layer in the High Energy section was shortened to 3 cm, while the *lateral* external one was left unchanged, i.e. of 7 cm
- due to the presence of a valve on the bottom of the M800 detector of about 6 cm, the High Energy section moderators on the base were modified to have a central hole (concentric with respect to the cylinders base) with a diameter of about 5 cm. In this way the valve could be "embedded" in the moderators at the base. This was done to do not let the M800 exceed the required height previously mentioned. In the first W-PIE project there was a smaller hole, not centered but shifted towards the circumference of the cylinders base, designed for the Ethernet cable.
- the internal diameter where the M800 detector was supposed to be inserted was slightly increased, to insert the detector more easily in the coatings.

The decisions above were taken considering that the simulations to optimize the design were performed irradiating with a lateral source, therefore the contribution "from below" was considered negligible.

Finally, the LW-PIE manufactured sketch is shown in Figure 4.7 together with its computed Response Functions in Figure 4.8. Tables reported in Appendix A were created with the software AutoCad and delivered to the company "Officina Meccanica Finotti Sergio" for the coating realization. The LW-PIE of Figure 4.7 was tested in laboratory experimental activities described in the next chapter, showing satisfactory spectrometric capabilities with respect to a fast AmBe source.

However, the instrument testing in the first LW-PIE outdoor campaign showed that the cosmic spectrum reconstruction was pretty poor. The reconstructed spectrum behaviour suggests that a non-radial contribution, i.e. a contribution not considered in the simulations performed to compute the response functions, was underestimated.

This behaviour was not foreseen, since the irradiation contribution coming from right under the detector was expected to be much smaller than the contribution given by

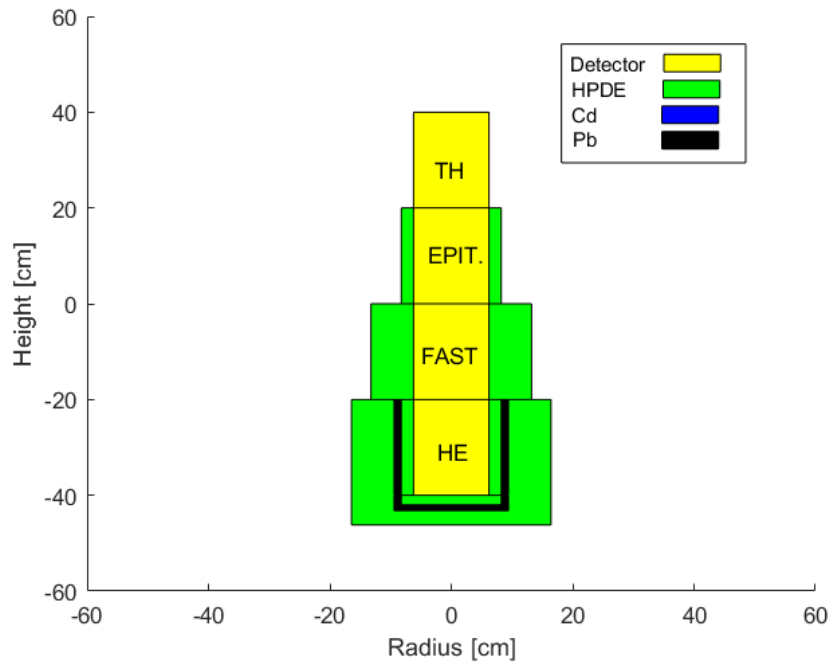


Figure 4.7: LW-PIE design manufactured by "Officina Finotti" company.

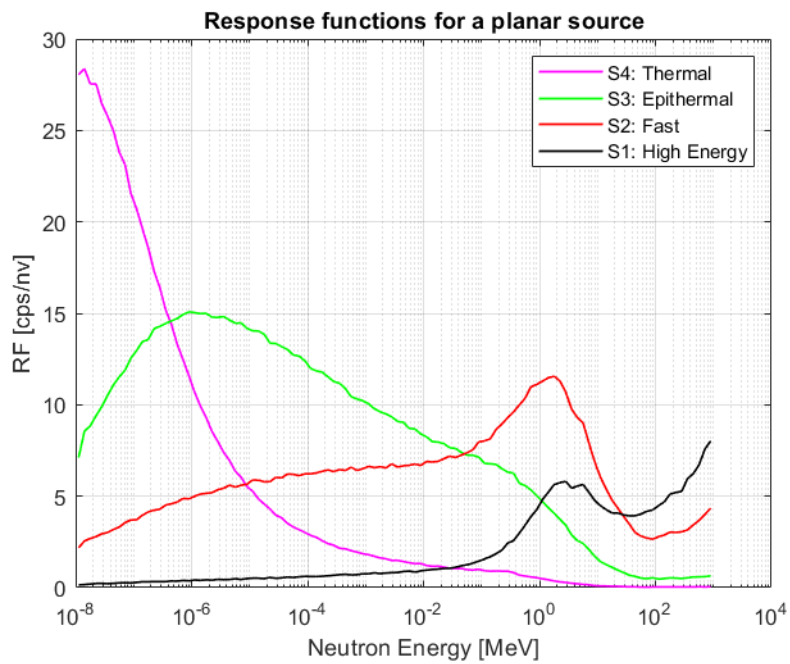


Figure 4.8: LW-PIE with the cut base response functions.

neutrons coming from the radial footprint, and therefore interacting with moderators in radial direction. Few centimeters of HPDE on the High Energy section base were not expected to make a significant difference on the cosmic neutron spectrometry.

To cope with this issue, a further HPDE layer of about 3 cm of thickness was commissioned to increase the thickness of the High energy base. The table of its design can be found in Appendix A. In addition, to improve the computation of the spectrum, the response functions were recalculated performing further MCNP simulations. The 'materials' file, providing materials information to the input of the simulation, was modified to change the cross section of the hydrogen, which is the constituent of the HPDE together with carbon. The cross section was changed from the monoatomic-hydrogen to the hydrogen-in-the-polyethylene one.

The new L-WPIE instrument is shown in Figure 4.9 and its response functions in Figure 4.10.

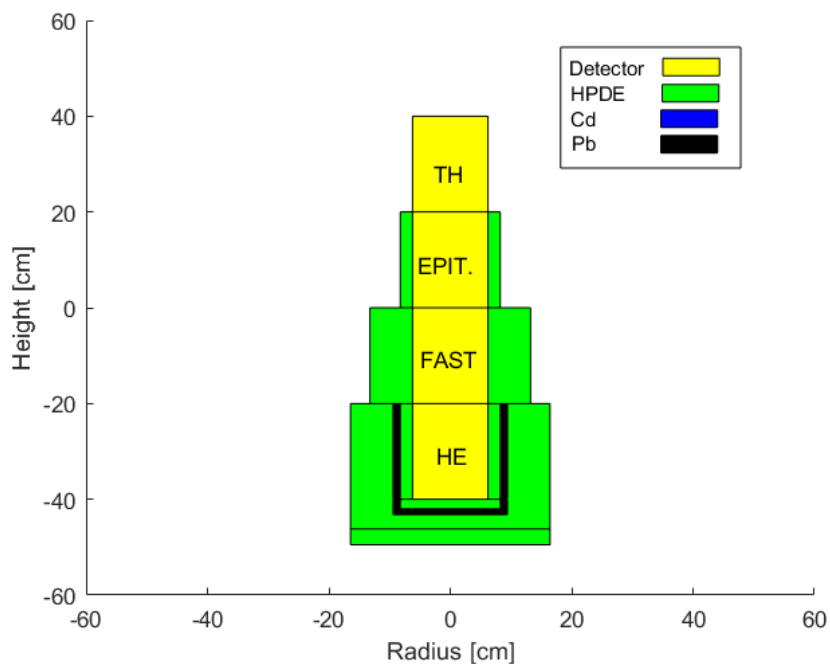


Figure 4.9: LW-PIE design manufactured by "Officina Finotti" company with the adjoint of a 3.3 thick polyethylene base.

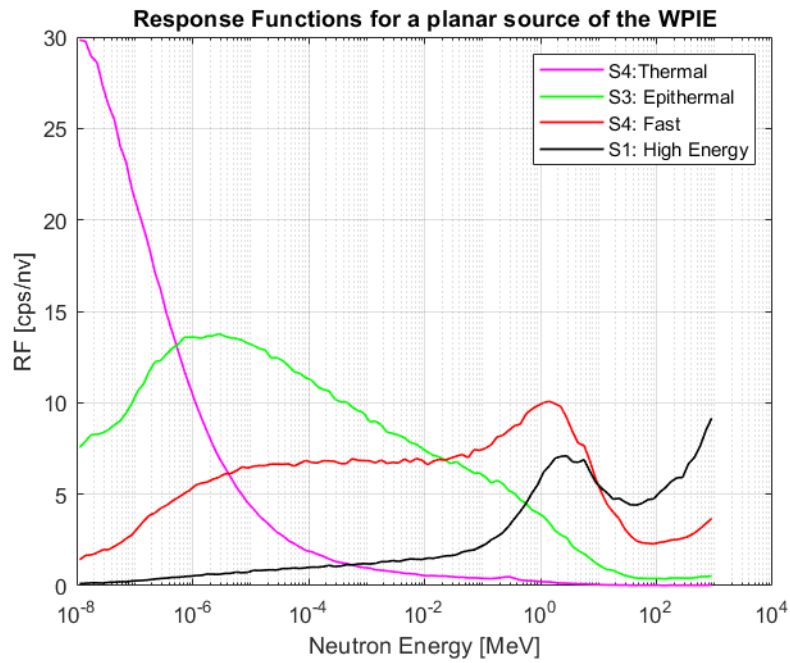


Figure 4.10: LW-PIE with the addition of a 3.3 thick polyethylene base. response functions.

5 | Experimental measurements

Experimental measurements consisted in two Laboratory sessions and three outdoor campaigns, carried out in different periods of the 2022/2023 year. The procedures and the findings are reported in the following sections. Section 5.1 describes the Laboratory measures, illustrating the set up and commenting the results. Section 5.2 describes and discuss the outdoor campaigns conducted with the M800 detector, employing three different coatings as moderator. Finally, in Section 5.3 is explained how the flux uncertainty is evaluated.

Cronologically, first the L-WPIE without the 3 cm polyethylene base was tested in Laboratory before its installation in Parco Nord. However as mentioned in the previous section, its spectrometric capabilities were not satisfactory and a 3 cm polyethylene base was added to improve them. The L-WPIE with the new base was then tested in Laboratory before its second installation in Parco Nord.

For the sake of clarity and to compare results, Laboratory measurements are described all at once in Section 5.1. For the same reason, Cosmic Neutron Rays measurements performed by M800 with the three different coatings are all discussed in Section 5.2.

In the following, W-PIE refers to the very first and heavy W-PIE design. L-WPIE refers to the lighter, optimized W-PIE coated with the final moderators, i.e. with the High Energy section having a total polyethylene base about 6 cm thick. Then, when describing the measurement results of the first L-WPIE version, i.e. the one with the High Energy section having a polyethylene base 3 cm thick, the specification "**without the addition of the 3 cm polyethylene base**" is included.

5.1. Laboratory tests: AmBe source employed to assess L-WPIE neutron spectrometric properties

5.1.1. Experimental setup

To assess properties and capabilities as neutron spectrometer of the M800 detector coated with moderators of different thicknesses, several measurements were performed, in the Secondary Standard Calibration Laboratory (LAT No.104) of the Department of Energy of Politecnico di Milano and in the Laboratory room of the same building.

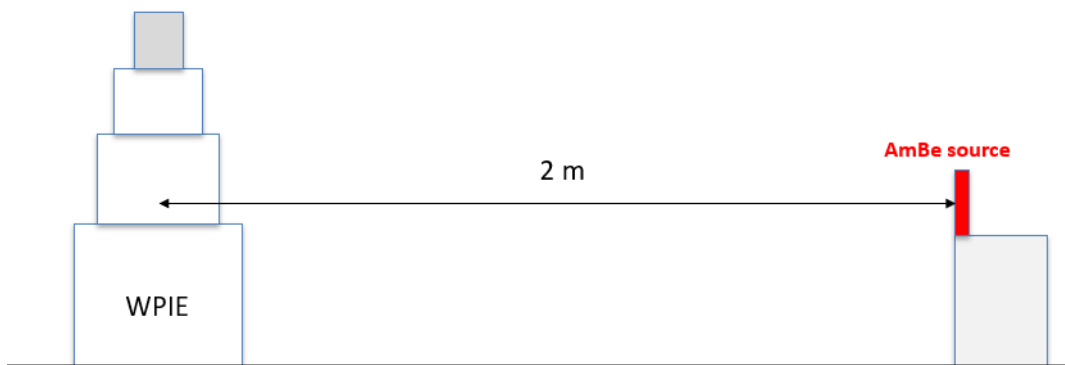
The W-PIE, the L-WPIE and the L-WPIE without the 3 cm polyethylene base were irradiated by an AmBe source, for 10 minutes, in two configurations: the expected vertical one, and an horizontal one, with the High Energy moderators base facing the source, as shown in Figure 5.1b. This was done in order to investigate the neutron spectrometer behaviour with a source positioned below its base.

Measurements were performed in rooms of rather small size with respect to the desirable one for measuring neutrons. In particular, if the measuring room is not optimized for such measurement, neutrons undergo several scattering on the air, on the materials and on the walls of the room, before being detected. Therefore, in these cases, the radiation field detected is a sum of a direct component coming from the source plus a scattered component, of lower energy. To perform a finer calibration, the lower energy component can be reduced with techniques such as the one of the shadow cone described in ISO 8529-2 [32]. The principle is to shade the detector from the source, in order to make a measurement which considers the scattered component only. Then, the total component can be measured, without the cone, and the direct component can be estimated from the difference between the two measurements.

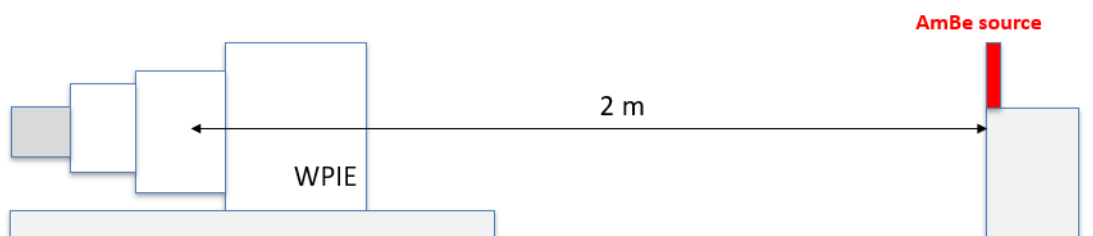
In this work, no scattering corrections were adopted, since the aim was to evaluate the spectrometer performance and there was no calibration purpose.

5.1.2. Spectrum reconstruction

The spectrum unfolding was performed by means of GRAVEL algorithm [33]. The four response functions corresponding to the sections, computed as explained in Chapter 4, are used as algorithm kernel. Two different spectra were employed as algorithm guess spectrum: the first one has a peak centered at the AmBe neutron emission energy, while the second one has a distribution corresponding to the Cf-252 neutron emission energy. This allowed us to investigate the unfolding algorithm capability to approach the real spectrum emitted by the source, even with less information associated with the guess spectrum.



(a) Vertical configuration



(b) Horizontal configuration

Figure 5.1: AmBe irradiation experimental setup. Picture not to scale

5.1.3. W-PIE results

The following W-PIE measurement were taken in the Laboratory room.

W-PIE in the vertical configuration

Table 5.1 shows experimental counts detected for each section. HE refers to High Energy section, FAST to Fast section, EPITH. to Epithermal section and TH to the un-moderated Thermal section.

Vertical W-PIE Counts

section	counts	cps	σ_{cps}
HE	1136	1.9061	0.0566
FAST	1598	2.6813	0.0671
EPITH	1165	1.9547	0.0573
TH	779	1.3071	0.0468

Table 5.1: Counts, counts per second and uncertainty after 10-minutes measurements

Figure 5.2 illustrates the resulting unfolded spectrum in the two guess spectrum case of AmBe and Cf-252. The AmBe emission is shown in red, expressed in arbitrary units for having a energy range reference in which the source emission falls.

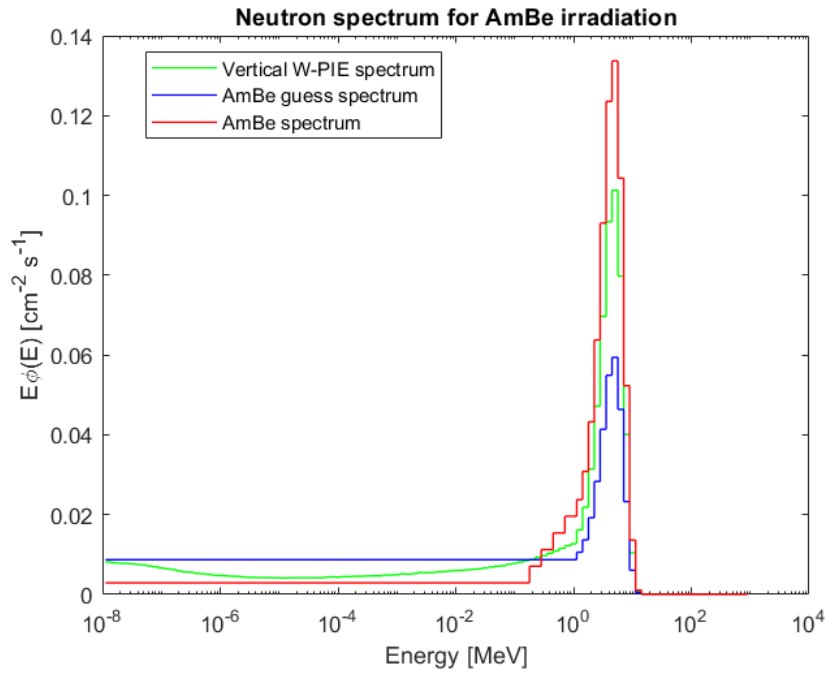
W-PIE in the horizontal configuration

Table 5.2 shows the counts detected positioning the spectrometer as in Figure 5.1b. Figure 5.3 shows the resulting spectrum, obtained by unfolding using AmBe spectrum as guess spectrum.

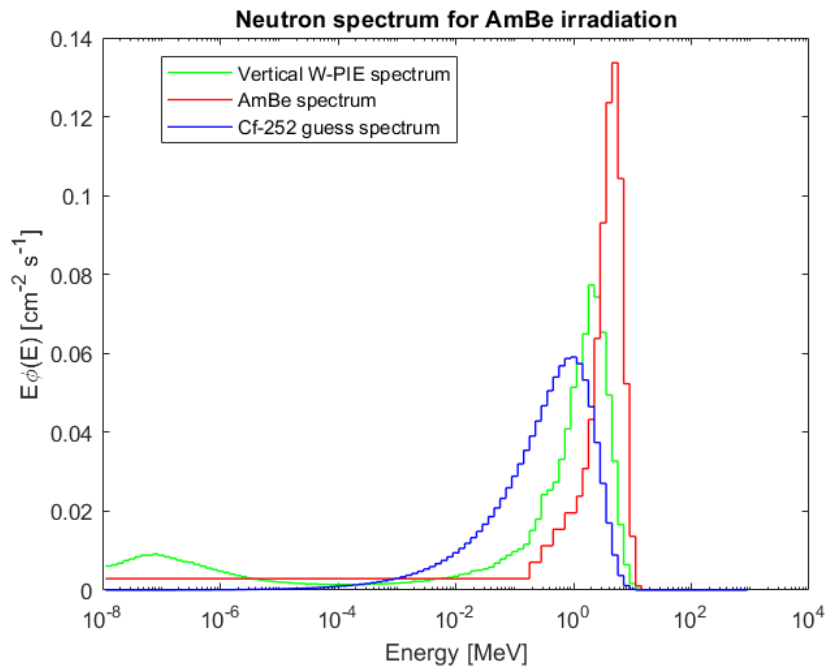
Horizontal W-PIE Counts

section	counts	cps	σ_{cps}
HE	695	1.1661	0.0442
FAST	659	1.1057	0.0431
EPITH	701	1.1762	0.0444
TH	605	1.0151	0.0413

Table 5.2: Counts, counts per second and uncertainty after 10-minutes measurements



(a) AmBe guess spectrum



(b) Cf-252 guess spectrum

Figure 5.2: Reconstructed spectrum (green) and guess spectrum (blue) for AmBe irradiation of the W-PIE in vertical configuration. Spectra are normalized for having unitary integral.

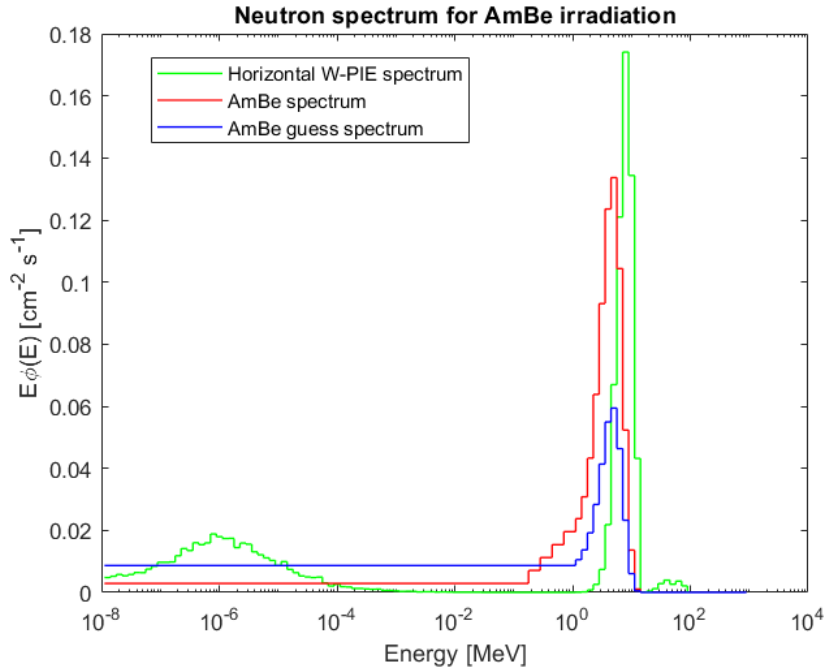


Figure 5.3: Reconstructed spectrum (green) and guess spectrum (blue) for AmBe irradiation of the W-PIE in horizontal configuration. Spectra are normalized for having unitary integral.

Comments on W-PIE measurements

By turning the W-PIE in the horizontal configuration, the counts per second decreased in all sections. This is due to the geometry of the set-up, which in fact shields the source. Moreover, the instrument has a cylindrical shape and this inevitably leads to an anisotropy between the radial and the axial directions. The aim was to investigate how much such anisotropy could affect the measurement. Looking at the spectrum of Figure 5.3, i.e. the one acquired in horizontal position, a small unphysical peak can be noted at about 100 MeV. Moreover, the AmBe peak energy is shifted towards higher energies. In any case, the principal emission is correctly identified in the range from 1 to 20 MeV, and a thermal component is detected.

It has to be noted that, as previously mentioned, the response functions adopted, composing the W-PIE kernel to unfold the spectrum, are the radial ones, i.e. the ones obtained with a simulation set-up as the one of Figure 4.2, corresponding to the W-PIE positioned vertically. In principle, it is possible to investigate the spectrum reconstruction employing "axial" response functions. In any case, since the instrument is designed to be irradiated laterally, this study was not performed.

5.1.4. Light W-PIE results

The L-WPIE with the addition of the polyethylene base was tested in the Laboratory room, as well as the L-WPIE without base in the horizontal configuration. The measurements for the L-WPIE without base in the vertical configuration were instead taken in the Secondary Standard Calibration Laboratory. The Secondary Standard Calibration Laboratory is part of the Quality Service of the Politecnico di Milano (LAT Calibration Center No. 104) and is used for photon dosimeters calibration. It is wider and better suited for neutron irradiations than the Laboratory room, but it was not available for this last test since it was being used for its original purpose (i.e., photon dosimeters calibration).

L-WPIE in the vertical configuration

Vertical L-WPIE Counts

section	counts	cps	σ_{cps}
HE	800	1.14765	0.0498
FAST	1667	2.7971	0.0685
EPITH	1146	1.9229	0.0568
TH	814	1.3658	0.0479

Table 5.3: Counts, counts per second and uncertainty after 10-minutes measurements

L-WPIE in the horizontal configuration

Horizontal L-WPIE Counts

section	counts	cps	σ_{cps}
HE	397	0.6661	0.0334
FAST	602	1.0101	0.0412
EPITH	684	1.1477	0.0439
TH	648	1.0873	0.0427

Table 5.4: Counts, counts per second and uncertainty after 10-minutes measurements

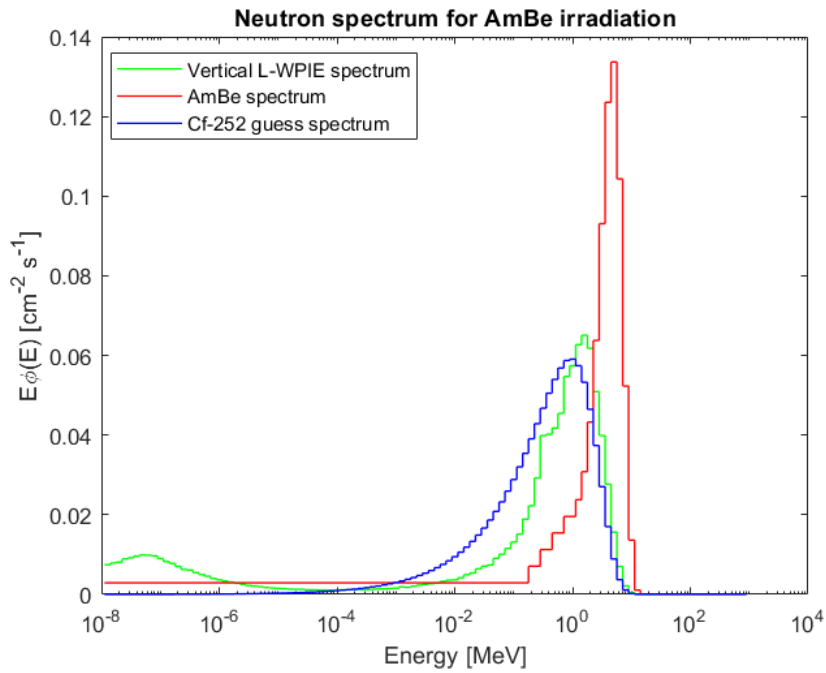
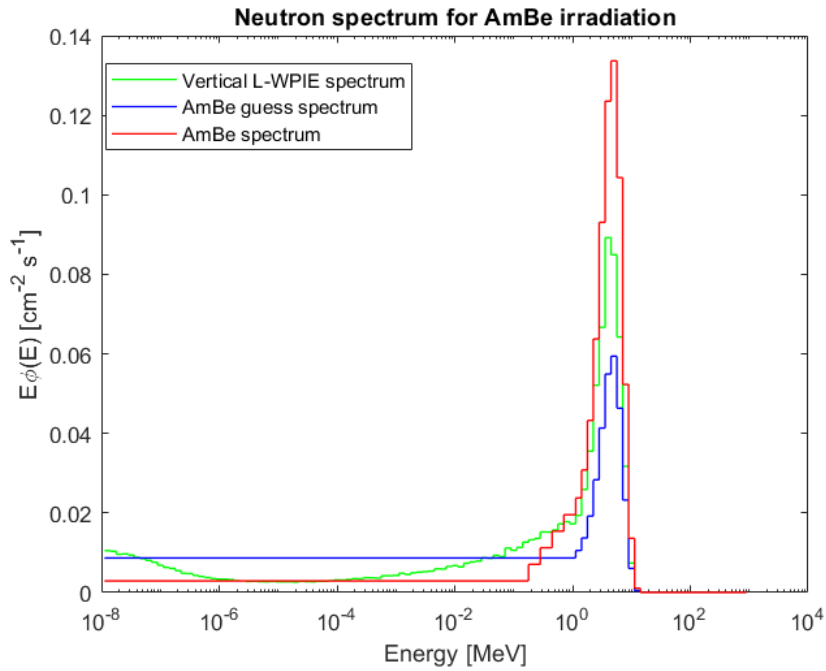


Figure 5.4: Reconstructed spectrum (green) and guess spectrum (blue) for AmBe irradiation of the L-WPIE in vertical configuration. Spectra are normalized for having unitary integral.

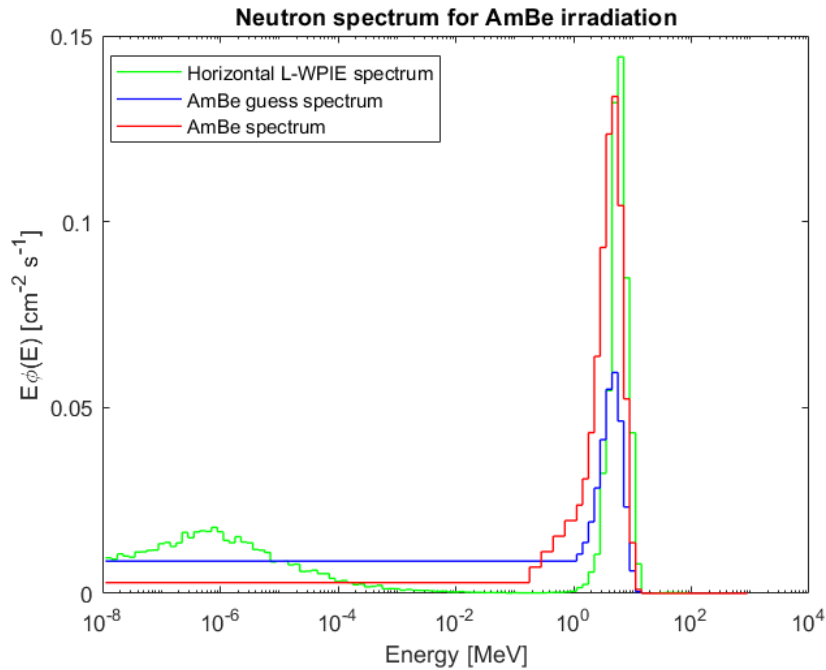


Figure 5.5: Reconstructed spectrum (green) and guess spectrum (blue) for AmBe irradiation of the L-WPIE in horizontal configuration. Spectra are normalized for having unitary integral.

L-WPIE in the vertical configuration without 3 cm polyethylene base

Vertical L-WPIE without 3 cm polyethylene base

section	counts	cps	σ_{cps}
HE	772	1.2953	0.0466
FAST	1680	2.8189	0.0688
EPITH	1291	2.1662	0.0603
TH	971	1.6292	0.0523

Table 5.5: Counts, counts per second and uncertainty after 10-minutes measurements

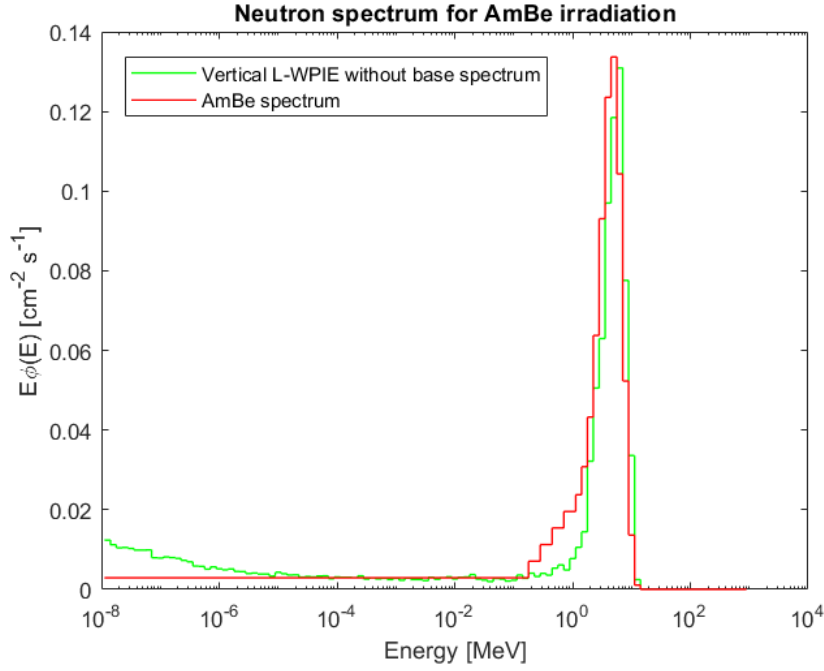


Figure 5.6: Reconstructed spectrum (green) and guess spectrum (blue) for AmBe irradiation of the L-WPIE in vertical configuration without 3 cm polyethylene base. Spectra are normalized for having unitary integral.

L-WPIE in the horizontal configuration without 3 cm polyethylene base

Horizontal L-WPIE without 3 cm polyethylene base

section	counts	cps	σ_{cps}
HE	563	0.9447	0.0398
FAST	735	1.2333	0.0455
EPITH	683	1.9547	0.0573
TH	641	1.1460	0.0425

Table 5.6: Counts, counts per second and uncertainty after 10-minutes measurements

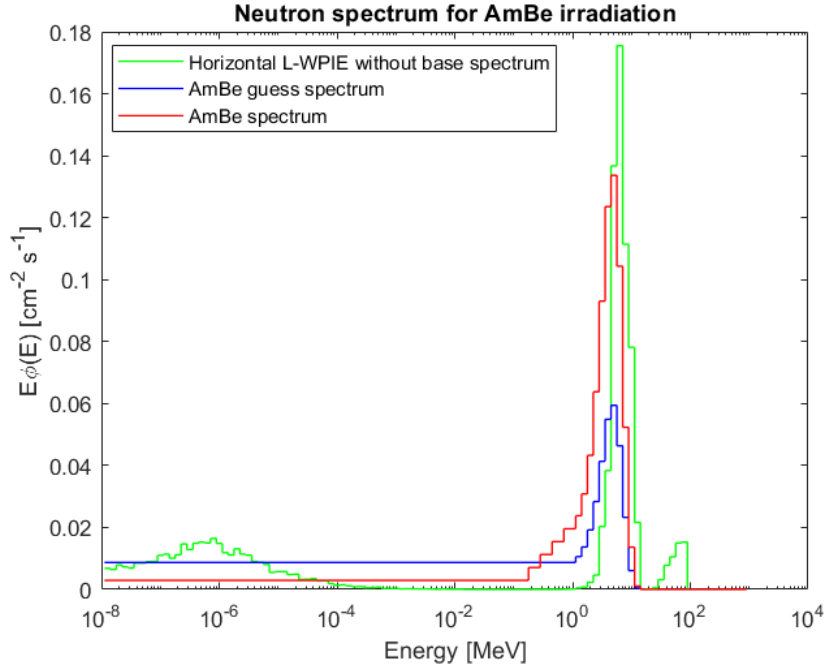


Figure 5.7: Reconstructed spectrum (green) and guess spectrum (blue) for AmBe irradiation of the L-WPIE in horizontal configuration **without 3 cm polyethylene basis**. Spectra are normalized for having unitary integral.

Comments on L-WPIE measurements, with and without the addition of the 3 cm polyethylene base

Comparing the counts for the L-WPIE, with and without the addition of the HPDE base, irradiated in vertical position, it is expected that the response should not be affected by the base addition, since the source is lateral. Indeed, the High Energy and Fast sections measured the same counts according to uncertainty. However, detected counts in Epithermal and Thermal sections show differences. This is due to the fact that the two measurements were performed in different rooms. Since the Epithermal and Thermal sections mainly detect lower energy neutrons, i.e. the scattered ones, the difference between the detected counts is reasonable.

Regarding the measurements performed in horizontal position, the addition of the 3 cm HPDE base introduces a further shielding for the source. For this reason, many less counts were detected by the L-WPIE with the base.

However, the addition of the base provides an improvement of the spectrum reconstruction, which doesn't show the unphysical High Energy peak. This behaviour was expected, since the response functions employed to unfold the spectrum are the radial ones. The addition of the base increases the lateral thickness, in this way the High Energy response in

horizontal configuration is more similar to the simulated one, and the unfolding algorithm generates a better spectrum.

5.1.5. Results discussion

The AmBe source neutron measurements performed with the different moderators in the vertical configuration of Figure 5.1a all resulted in a satisfactory spectrum reconstructions using a realistic guess spectrum. In particular, the peak energy is identified and it is slightly more accurate for the W-PIE reconstructed spectrum with respect to the L-WPIE and the L-WPIE without base ones. Moreover, the presence of the real thermal component, result of the fast component moderation in the room, even if not suggested by the guess spectrum, is correctly detected. This result is particularly important, since soil moisture measurement by cosmic neutron is based on the moderating power of soil.

The unfolding reconstructions performed with the Cf-252 guess spectrum demonstrate the algorithm capability to shift the peak towards the real energy of the emitted source and, again, to identify the thermal component. No relevant difference can be detected between the W-PIE and L-WPIE performance. Table 5.7 contains the measured fluxes computed, for each configuration, integrating the spectra unfolded using AmBe spectrum as guess spectrum. The flux measured by W-PIE and L-WPIE were performed in the same room, i.e. the Laboratory room above mentioned, and the results for the Fast and Epithermal component agree according to uncertainty. Thermal flux components results are only slightly different. The flux measured by the L-WPIE without adding the polyethylene base were performed in the Secondary Calibration Laboratory.

	$\phi_{L-WPIE}[cm^{-2}s^{-1}]$	$\phi_{W-PIE}[cm^{-2}s^{-1}]$	$\phi_{L-WPIE,w/o,base}[cm^{-2}s^{-1}]$
Fast	0.1887±0.0174	0.1891±0.0063	0.2323±0.0095
Epithermal	0.1331±0.0162	0.1224±0.0068	0.0745±0.0070
Thermal	0.0461±0.0015	0.0406±0.0022	0.0542±0.0026

Table 5.7: L-WPIE, W-PIE and L-WPIE without base measured AmBe flux. The L-WPIE and W-PIE results shows optimal agreement. The L-WPIE without base measurement is affected by the lower thickness of the base which induce an overestimation of the fast flux.

The flux measured by the L-WPIE without the addition of the polyethylene base shows a fast component, i.e. the one coming directly from the source, which is not in agreement

with the measurements of the other two instrument. The fast component may be overestimated because of a contribution of neutrons scattered by the floor, due to the smaller HPDE thickness. The simulations for the response functions calculation did not include this contribution because they assumed the detector was irradiated in the void.

Since the flux is a result of the Unfolding algorithm, its uncertainty evaluation is not trivial. Section 5.3 described the steps followed for its computation.

5.1.6. Ambient dose equivalent rate estimation

The ambient dose equivalent rate at 2 meters from the source was estimated in order to compare the L-WPIE and W-PIE results with the one obtained using the LUPIN counter manufactured by ElseNuclear, showing good capability of measuring the ambient dose equivalent rates [34], [35].

The Ambient dose equivalent rate was computed as:

$$H^*(10) = \int_0^{\infty} h_{\varphi}(E)\varphi(E)dE \quad (5.1)$$

where φ is the spectral fluence and h_{φ} are the fluence-to-ambient dose equivalent conversion coefficients. To turn the W-PIE and L-WPIE acquired spectra into Ambient dose equivalent rate, the ICRP 74 [36] coefficients expressed in [pSv cm^2] were fitted in correspondence to the energy intervals of interest and were then multiplied by the flux $\phi(E)$ integrated over the whole spectrum. Results of the various measurements are thus expressed in pSv/s, they quite agree and can be found in Table 5.8.

	distance [m]	H*(10) [pSv/s]
LUPIN	2	87.5
H-WPIE	2	85.5
WPIE	2	88.9

Table 5.8: Ambient dose equivalent rate estimated from the flux measured by the W-PIE and the L-WPIE, showing good agreement

In addition to the integral computation, the Neutron Flux-To-Dose Equivalent Rate Conversion Factor of the AmBe source was computed by dividing the estimated $H^*(10)$ in Table 5.8 by the direct flux emitted from the source. The direct flux was computed by integrating the energy spectrum measured by W-PIE and L-WPIE for $E > 0.1$ MeV, to

discard the scattered neutron flux. The values obtained for the two instruments, shown in Table 5.9, were compared to the value that would be get from the AmBe ISO spectrum and the ICRP74 $h^*(10)$ coefficients.

	Conversion Factor[pSv cm^2]
ICRP 74	391
W-PIE	395.2
L-WPIE	385.2

Table 5.9: Conversion factors computed from the three instrument flux measurements, showing good agreement

5.2. Parco Nord campaigns: Cosmic rays measurement

Three outdoor experimental activities were conducted with the three different versions of the W-PIE neutron spectrometer to test them with respect to the Soil Moisture measurement purpose by detection of Neutron Cosmic Rays radiation. In particular, cosmic neutrons flux can be used to investigate soil moisture on an intermediate scale (i.e, an area of hectares and depth of tens of centimeters), which is relevant for several applications, such as farming, irrigation and atmospheric models. For these reasons, measurements were carried out in a open field in the northern part of Milano, Italia, allowing to investigate the technique in a properly large area.

The three different instruments were tested in Laboratory with an AmBe source, as described in section 5.1, before the open field measurements. Moreover, previous studies [2] performed on the very first W-PIE assessed the spectrometer sensitivity to cosmic radiation and its spectrometric capabilities, giving to the unfolding algorithm a reasonable cosmic neutron spectrum. However, during the activities described in [2], the instrument was not tested in a truly open field. The instrument capabilities were thus validated in the first outdoor campaign described in this section, in which cosmic neutrons measurements with the W-PIE were performed. The W-PIE measurement was taken previous to this thesis work and is here analysed to make a comparison between the two systems.

The first version of the L-WPIE without the 3 cm polyethylene base was tested in the second campaign. However, the system didn't show a satisfactory reconstruction of the cosmic spectrum, as shown in Figure 5.8. This probably came from the High Energy

section dimension, which was altered from the initial optimized prototype. For this reason, a polyethylene base 3 cm thick was commissioned and added to perform the third outdoor measurement campaign.

Moreover, during the second campaign some water penetrated into the electronic head of the detector, preventing its operation. Due to the M800 fault, data were collected for very few days. For this reason, a soil moisture estimation could not be performed and data were investigated just to evaluate the spectrometric capabilities with respect to the natural irradiation.

Considering these issues, the second campaign results are not reported.

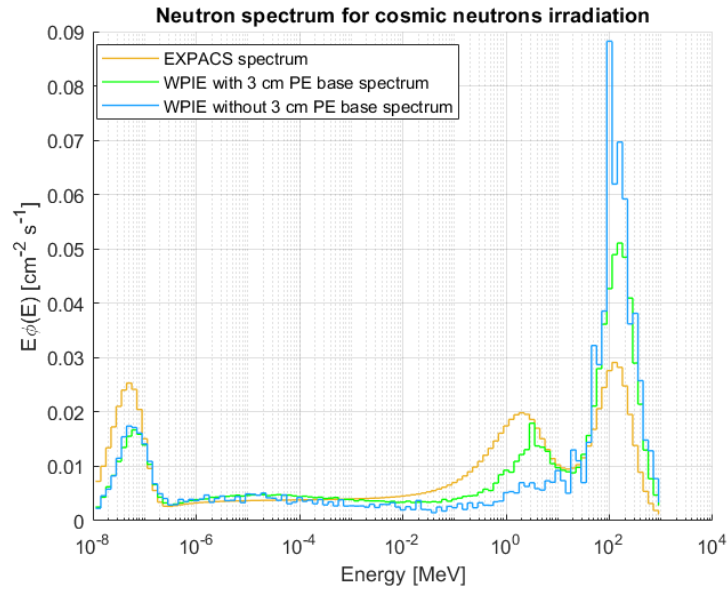


Figure 5.8: Reconstructed neutron spectra for the two versions of L-WPIE

The following sections first describe the setup installed in Parco Nord and how the measurement was conducted, which was equal for the three campaigns. Then results of the following activities are reported and commented:

- Measurements with the W-PIE performed from 22/07/2022 to 01/10/2022;
- Measurements with the last L-WPIE version, i.e. the one with the addition of the 3 cm polyethylene base performed from 15/02/2023 to 30/03/2023;

5.2.1. Parco Nord Installation, Setup and Measurements acquisition

The instrumentation for measuring Soil Moisture by means of the W-PIE neutron spectrometer was installed in Parco Nord, a park of more than 600 heactars in the northen part of Milano, Italia. Equipment, shown in Figure 5.9 , was made by:

- The neutron spectrometer, i.e. the M800 neutron detector coated with moderators;
- A weather station monitoring environmental parameters such as external temperature, air pressure and precipitations;
- Two soil moisture probe taking point measurement of water content in the soil;
- A field computer inside a robust plastic box, provided with a pad which can be easily interrogated remotely thanks to a small antenna;
- A solar panel powering each system;

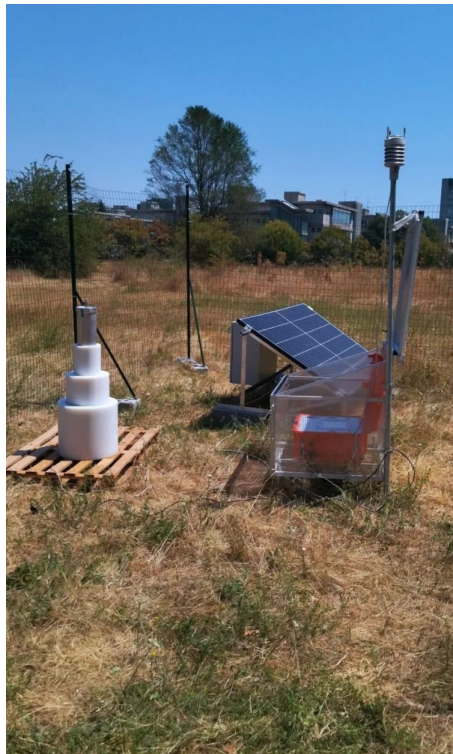


Figure 5.9: Installation of the WPIE in the Parco Nord site

The detector was connected to the computer by an Ethernet cable and controlled by a Python script allowing to set the measurements duration and number. For each measurement, a file containing the counts and the cps acquired in each section, named with date

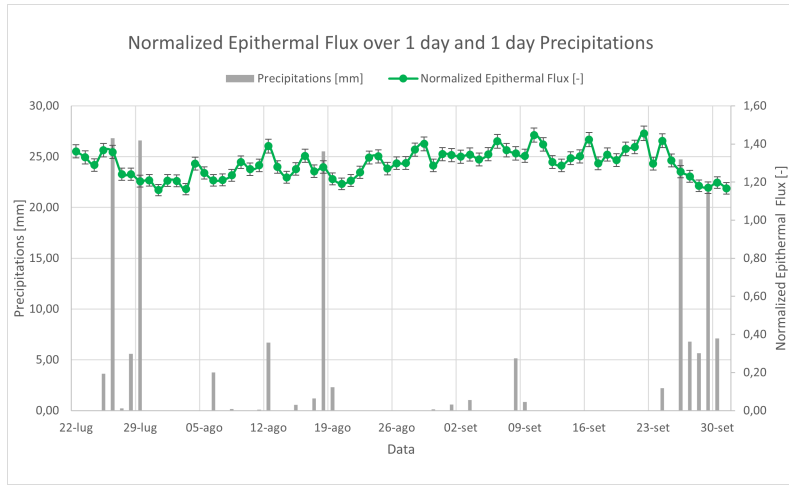
and time of the acquisition start up, is created by the script. After each counts measurement, the unfolding algorithm is performed providing in output the neutron spectrum. The flux values in the four energy regions (thermal, epithermal, fast and high energy) are then calculated from the spectrum and saved in a file.

The integration of the detector system with the weather station and the two soil moisture probes allowed to have remotely exportable information on: precipitation levels, air temperature and humidity, air pressure, wind speed and direction and finally soil moisture and temperature.

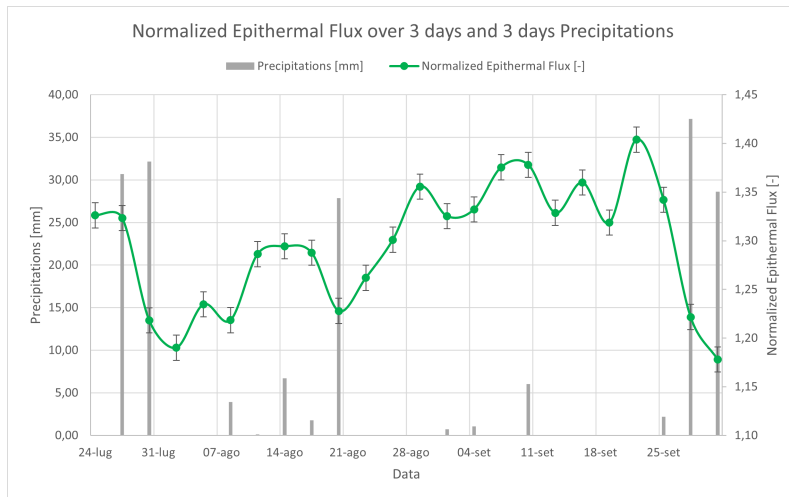
5.2.2. Results: Epithermal Flux variations

Soil Moisture estimation by means of the universal calibration function makes use of the Epithermal neutrons as a probe to investigate the water content in the intermediate area [23]. In this work, a normalized epithermal flux was defined as $\frac{\phi_{EPI}}{\phi_{HE}}$. This was done because the epithermal flux depends on the soil moisture, but is also affected by other factors such as pressure and solar activity. On the contrary, the high energy flux does not depend on soil moisture, yet it is affected by the environmental factors. Therefore the ratio between the two quantities is expected to depend just on the soil moisture. Before estimating Soil Moisture as described in Section 5.2.3, the normalized epithermal flux oscillations were investigated to analyse its trend with respect to precipitations. The trends considering the average daily normalized epithermal flux do not allow an easy identification of the precipitations effects on the flux variations, as can be seen in Figure 5.14, due to noise of flux fluctuations. However, considering the normalized epithermal flux averaged over three days the correlation is observable. In the following pictures, normalized epithermal flux results are shown together with precipitations, for the W-PIE measurements and the L-WPIE ones.

W-PIE normalized epithermal flux and precipitations trends



(a) 1 day



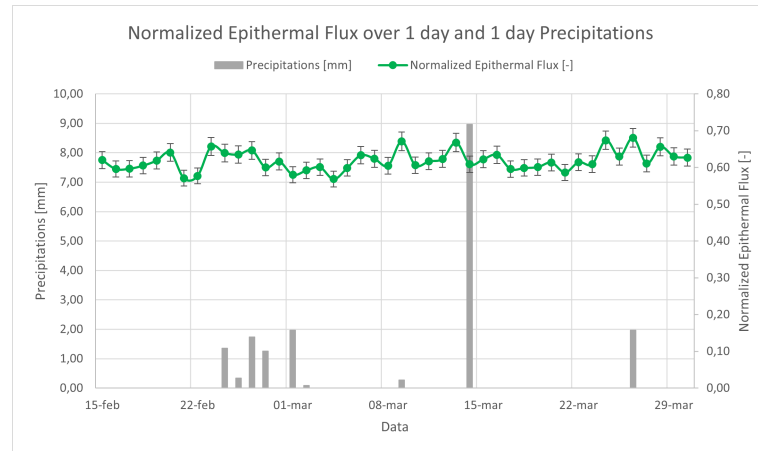
(b) 3 days

Figure 5.10: Normalized Epithermal flux measured by W-PIE, averaged over 1 day (a) and 3 days (b). The columns show the precipitations per day expressed in mm

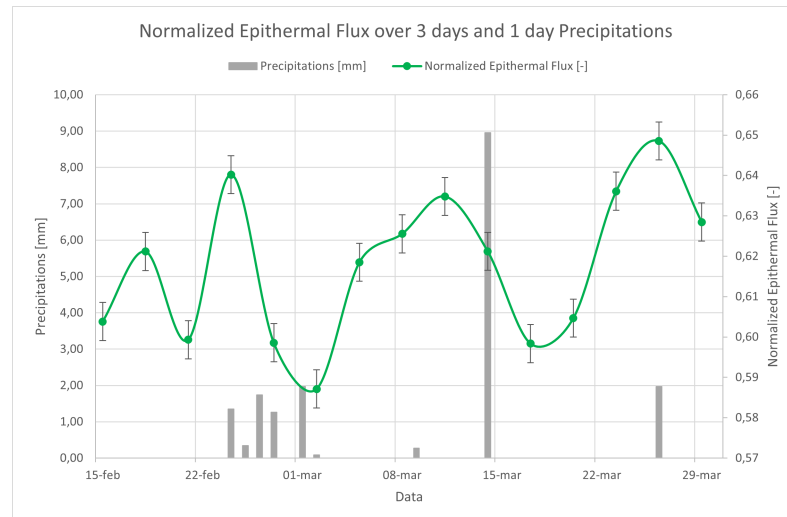
L-WPIE normalized epithermal flux and precipitations trends

The second outdoor campaign carried out between February and March 2023 is characterized by a quite poor dynamics with respect to precipitations as can be seen from the grey columns in Figure 5.10. Moreover, some fluctuations can be observed the first points in Figure 5.11b. This phenomenon may be due to Temperature compensation of the electronics of the detector, which may have been off for the first measuring days. According to this phenomenon, an increasing air temperature should result in an increase of the noise affecting the SiPMs signal. Part from the first three points, the trends of a decreasing

normalized epithermal flux is confirmed from the L-WPIE measurements



(a) 1 day



(b) 3 days

Figure 5.11: Normalized Epithermal flux measured by WPIE, averaged over 1 day (a) and 3 days (b). The columns show the precipitations per day expressed in mm

5.2.3. Soil Moisture Evaluation from the W-PIE and L-WPIE measured flux by means of the universal calibration function

The Soil Moisture content was estimated employing the universal calibration function discussed in Chapter 1, 1.4.3. Earth is constantly subjected to a flux of galactic charged particles, 90% of which are protons, interacting with the atmosphere generating neutrons that are detectable at the ground level. The neutrons of fast and epithermal region of the energy spectrum undergo scattering with surrounding nuclei. Being hydrogen the most

effective neutron scatterer, and being this element found in water for the greatest part, the intensity of the epithermal and fast neutron flux can be used as a probe for measuring changing level of water in soil.

Calibration of cosmic ray soil moisture probe is usually performed locally collecting soil samples. Being this kind of calibration impractical in most cases, the universal calibration equation was derived in previous studies [23] using MCNPx to cope with difficult calibration case. The equation is nearly invariant with soil chemistry and requires one simple calibration parameter determination. Further details on the calibration options can be found in Chapter 1, 1.4.3

Soil moisture mainly affects the epithermal-to-fast neutron intensity above the ground. Epithermal-to-fast neutrons are therefore the main particles used for assessing the water content in a field with the CRNS technique. Simulations were performed with the code URANOS [26] to find the correlation that best explains the relationship between neutron flux and water content in soil for the instrument employed. Results of Figure 5.12, taken from [26], showed that epithermal flux is more sensitive to change in water content.

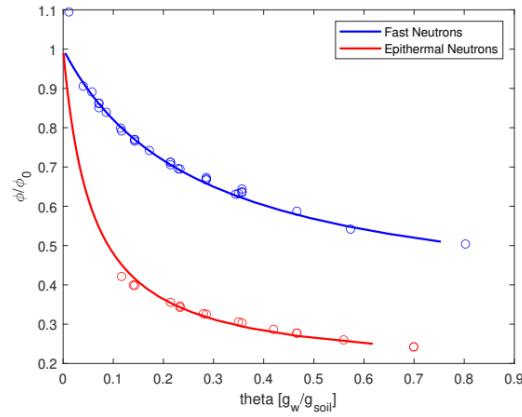


Figure 5.12: Relation between the epithermal and fast neutron flux as a function of the soil moisture. The figure is taken from [26]

The calibration function employed defines the relationship between the fast neutron intensity and soil moisture θ :

$$\theta - \theta_{off} = \frac{a_0}{\phi/\phi_0 - a_1} - a_2 \quad (5.2)$$

The soil moisture is the gravimetric soil moisture, i.e. $\frac{weight_{soil, wet}[g] - weight_{soil, dry}[g]}{weight_{soil, dry}[g]}$.

The flux ϕ of the equation employed was the epithermal flux normalized by the high

energy flux, whose behaviour is shown in section 5.2.2. The normalization by the High energy flux allows to take into account the solar activity. Solar activity directly influences the High energy neutron flux, i.e. the primary neutron flux. Epithermal neutron flux variations, being the result of higher energy neutron slowing down, may thus be affected by solar activity cyclic variation. Another environmental factor affecting the neutron flux above ground is the atmospheric pressure: the higher the pressure the higher the neutron flux is attenuated. High energy neutron flux, not affected by water content variation in soil, was then used to correct the flux with respect to changes due to these phenomenon.

The parameters a_0 , a_1 and a_2 were found by performing Montecarlo Simulations with the code URANOS [26]. In this sense, a spectrometer represents an advantage with respect to the usual counters employed in CRNS. Indeed, the computed coefficients mentioned above are absolute, since they relate the epithermal flux measure, in $cm^{-2}s^{-1}$, to the soil moisture. For the CRNS usual counters, instead, the coefficients may vary with different instruments, since the quantity measured is counts, which depend on the specific instrument response.

The calibration parameter ϕ_0 is the measured flux corresponding to a know value of θ . It should assessed by measuring θ in numerous soil samples, within the area of interest, by oven-drying. In this case, ϕ_0 was found by inverting equation 5.2:

$$\phi_0 = \bar{\phi} \frac{\bar{\theta} + a_2 + \theta_{off}}{a_0 + a_1\bar{\theta} + a_1a_2 + a_1\theta_{off}} \quad (5.3)$$

using as $\bar{\theta}$ the mean soil moisture measured by the two SM probes, the average values of normalized epithermal flux as $\bar{\phi}$, and θ_{off} as fitting parameter.

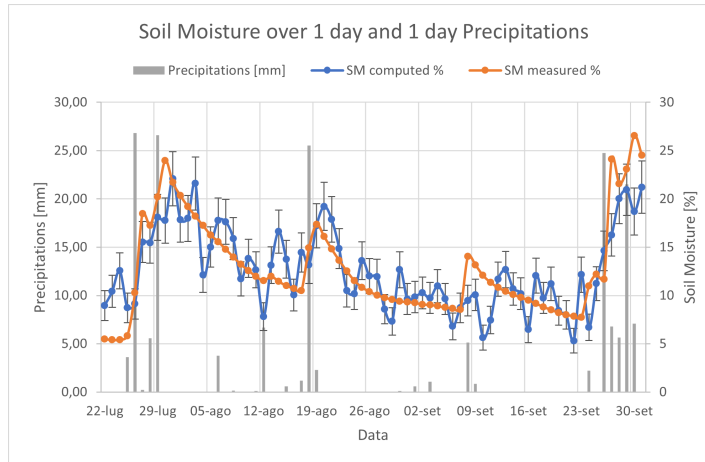
θ_{off} represents the offset contribution to neutron moderation, i.e. the contribution of stationary source such as lattice water and vegetation. It's evaluation is not trivial and requires detailed analysis of the soil and vegetation around the detector. In this case, it was evaluated fitting the obtained data. In particular, some training days were selected to minimize the statistical variable χ^2 :

$$\chi^2 = \sum_i \frac{(\theta_{estimated,i} - \theta_{measured,i})^2}{\theta_{estimated,i}} \quad (5.4)$$

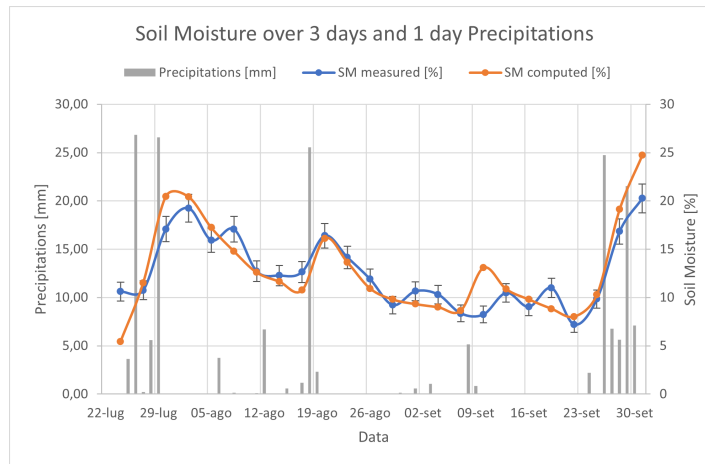
$\theta_{estimated}$ is the one obtained by equation 5.2 while $\theta_{measured}$ is the mean soil moisture measured by the two probes. The index i runs over the days over which the soil moisture is computed.

Soil Moisture results: W-PIE campaign measurements

Figure 5.13 shows the soil moisture estimation results for the W-PIE measurements. Soil moisture was estimated as average soil moisture per day and per three days. The value of θ_{off} found is approximately $0.15 \frac{g_{water}}{g_{soil}}$.



(a) 1 day



(b) 3 days

Figure 5.13: Soil Moisture estimation in shown together with the soil moisture measurements and precipitations, for 1 day (a) and 3 days (b) average. Error bars refer to 1σ .

One day soil moisture estimation shows some fluctuations, as well as epithermal flux. Error bars refers to 1σ uncertainty. Uncertainty was estimated propagating the normalized epithermal flux error:

$$\Delta\theta \approx \sqrt{\left(\frac{d\theta}{d\phi_{NE}} \Delta\phi_{NE}\right)^2} \quad (5.5)$$

where ϕ_{NE} is the normalized epithermal flux. The uncertainty relative to the parameters

θ_{off} , ϕ_0 , a_1 , a_2 , a_3 was neglected. $\Delta\phi_E$ and $\Delta\phi_{HE}$ relative to the epithermal and high energy fluxes, employed to compute $\Delta\phi_{NE}$ were derived from the procedure described in 5.3, and the result was 3% for one day decreasing to 1.76% for tree days.

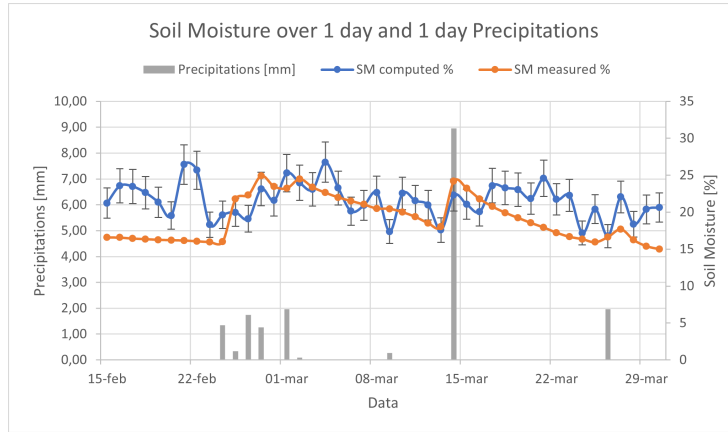
Soil moisture results: L-WPIE campaign measurements

The θ_{off} found by minimizing the χ^2 error was 0. This is not in agreement with the one found in the W-PIE campaign. Some considerations may explain the mismatch between soil moisture estimated by Universal calibration function and soil moisture measured by the probes.

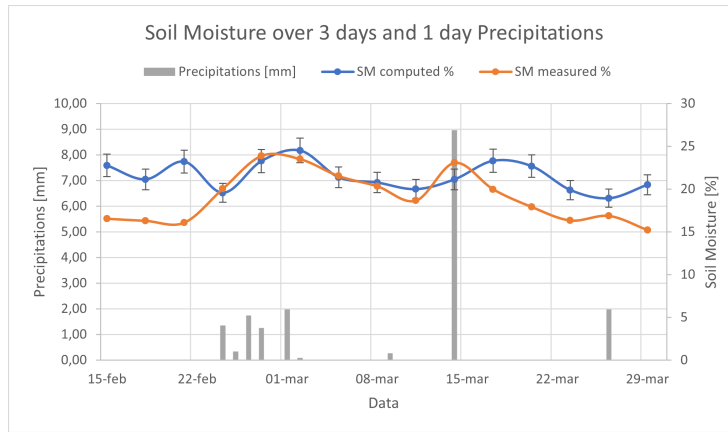
The first days values of the flux in 5.14 show some fluctuations which are not in agreement with the precipitations behaviour. This implies that these values probably are due to statistical fluctuations, and they are not representative of the soil moisture variations in the field.

In addition, soil moisture probes should be buried several cm under the ground to work properly. In this case, probably they were installed too on the surface. Indeed, a kind of time-shift is observable in data between days from the end of February to the 20th of March. This may be due to water permeation more deeply in the ground with respect to the soil probe position. In this way, the L-WPIE spectrometer measured an higher soil moisture than the one detectable by the soil moisture probes. Water on the surface evaporates much before the deeper one. For this reason, soil moisture on the surface tends to decrease very fast, while the soil more in-depth remains wet.

Comparing the results obtained with the L-WPIE (Figure 5.14 measurements with the ones obtained with the W-PIE, the L-WPIE was not able to accurately follow the soil moisture trend measured by the soil moisture probes. It has to be considered that in the W-PIE campaign started in July, precipitations were of about 25 mm/day on dry soil and the instrument resulted more sensible to soil moisture variations. The L-WPIE campaign of February was instead characterised by minimal precipitations (up to 9 mm/day) on a probably already moist ground. Actually, the L-WPIE measured an average soil moisture within a penetration depth bigger than the one reached by the moisture probe installed near the surface. Since the average moisture in depth changed very little, the L-WPIE sensitivity was not enough to detect such variations.



(a) 1 day



(b) 3 days

Figure 5.14: Soil Moisture estimation is shown together with the soil moisture measurements and precipitations, for 1 day (a) and 3 days (b) average. Error bars refer to 1σ .

5.3. Flux uncertainty evaluation procedure

The Soil Moisture evaluation was performed exploiting the universal calibration function [23]. In particular, the flux values employed for the Soil Moisture estimation were the result of the deconvolution of the counts measured by the W-PIE versions. Since this deconvolution is based on iterative procedures, the common approach of statistical error propagation cannot be easily used. For this reason, an accurate evaluation of the flux uncertainty was performed with the algorithm described in this section in order to propagate the error through the Soil Moisture measurement.

The procedure described below was also adopted to estimate the flux uncertainty for the AmBe flux measurements reported in Table 5.7. It consisted in the following steps:

1. The cps acquired, for Laboratory activities, or the mean cps averaged over measuring days, for outdoor measurements, were assumed to be the real interaction rate for each region of the detector
2. A counting time was chose, starting from 1 hour
3. The expected counts in each region were calculated as $\text{Counts} = \text{cps} \times \text{counting time}$ and each of them was considered Poisson distributed
4. Four new values of counts (one for each region) were randomly sampled from the four Poisson distributions of step 3
5. The unfolding was performed resulting in four values of neutron flux, one for each section
6. By repeating the previous steps for $N = 1000$ times, 1000 values of flux for each section are obtained
7. The distribution of these values can be fitted, and its spread can be associated to the flux uncertainty. The fitting function employed was a Gaussian function and from its parameter μ and σ the relative uncertainty is computed

counting time (h)	$\sigma\%$
1	8.6
24	1.76
72	0.99

Table 5.10: W-PIE cosmic neutron epithermal flux uncertainties

Figure 5.7 shows the flux uncertainty behaviour proportional to \sqrt{t} , where t is the counting time, as expected for the counts too. This uncertainty analysis was done for the epithermal and HE fluxes. Then, the error was propagated to the normalized epithermal flux $\frac{\phi_{EPI}}{\phi_{HE}}$ through the general formula:

$$\Delta f(x_1, x_2, \dots, x_n, \Delta x_1, \Delta x_2, \dots, \Delta x_n) = \sqrt{\sum_{i=1}^n \left(\frac{\partial f}{\partial x_i} \Delta x_i\right)^2} \quad (5.6)$$

where f is $\frac{\phi_{EPI}}{\phi_{HE}}$ and $x_i = \{\phi_{EPI}, \phi_{HE}\}$.

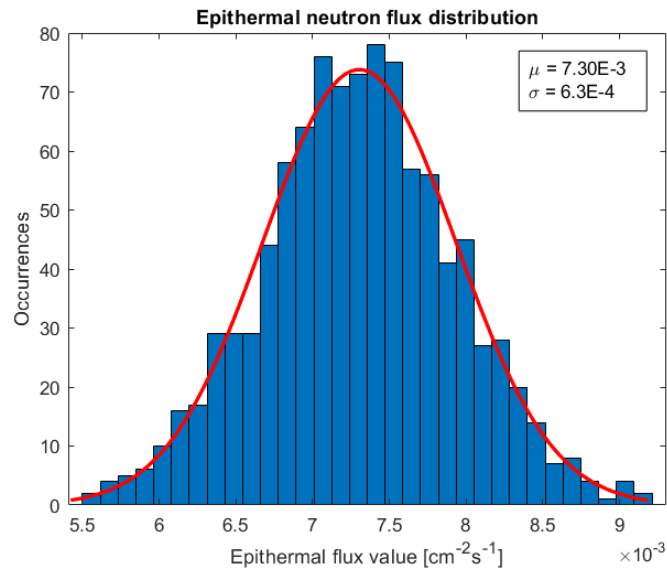


Figure 5.15: Distribution of the cosmic epithermal neutron flux values for 1 hour counts

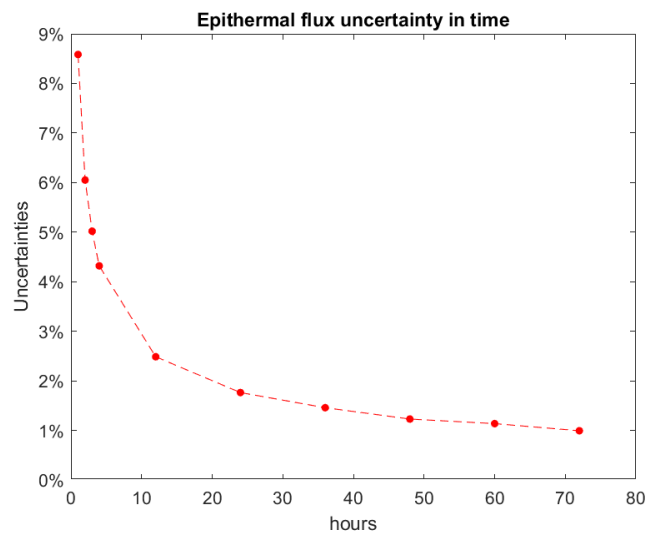


Figure 5.16: Uncertainty of the epithermal cosmic neutron flux time behaviour, scaling down approximately with the square root of the counting time.

6 | Conclusions

In this work, the light version of the W-PIE innovative cosmic neutron spectrometer developed at Politecnico di Milano was designed and tested.

The W-PIE is a spectrometer specifically aimed to measure the cosmic neutron energy distribution and relate the epithermal neutron flux to the water content in soil. It is made by a ^3He -free thermal detector divided in four sections and covered by four different moderating layers, each responding to a specific energy range of the cosmic neutron spectrum measurable at ground level. The spectrum reconstruction is performed thanks to an unfolding algorithm implemented in Python, allowing a real-time reconstruction of the neutron spectrum. The high energy section contains a layer of 2 cm of lead, necessary to detect the high energy neutrons exploiting spallation-fragmentation reaction, which makes the device quite heavy, difficult to be transported and to be managed during the outdoor installation procedures.

The W-PIE design was the starting point of the new optimization implemented to reduce the thicknesses of the various coatings with the aim to lighten the overall system. A multi-objective figure of merit was defined, taking into account the desired ideal properties of the spectrometer set of response functions, and including the low-weight objective. The four response functions were theoretically determined performing Monte Carlo simulations thanks to the MCNP code, a general-purpose code simulating many particles transport including neutrons.

An accurate MCNP model of the thermal detector was employed and the moderating structure were implemented. The figure of merit maximization lead to the identification of the optimal coating thicknesses. The final design reduced a lot the weight of the system, in particular, thanks to the reduction of the thickness of the layer of lead, which was reduced from 2 to 1 cm.

The L-WPIE moderators were commissioned and manufactured and the instrument was tested in several laboratory activities in Politecnico di Milano employing an AmBe neutron source. The spectrometric capabilities of the L-WPIE were tested showing satisfactory results. However, the measurements performed in the L-WPIE first outdoor campaign showed a fairly poor capability in reconstructing the cosmic spectrum. This was due to

the too small thickness of the HPDE base of the high energy section which induced the spectrometer to detect in that section a greater signal compare to what was expected and therefore implemented in the simulations determining the response functions. The radial thicknesses of the instrument were considered much more important since the greatest part of the signal was expected to impinge from the radial footprint. For this reason, a further HPDE layer 3.3 cm thick was commissioned and manufactured to be added to the device base.

The new version of the L-WPIE, i.e. the one with the addition of the HPDE base, was tested in laboratory activities and the results were compared with the ones obtained by the very first heavier W-PIE and the L-WPIE without base. Tests showed that the new L-WPIE successfully recognized the fast emission of the source even if the start guess spectrum of the unfolding algorithm was a different energy emission (Cf-252). In addition, the L-WPIE showed its sensitivity to the moderation of the source. This result was particularly important in view of the soil moisture measurement exploiting the water moderating power.

The L-WPIE was installed in a park in the northern part of Milano together with FDR soil probes and a weather station. An outdoor measurement campaign was carried out to acquire cosmic neutron flux data for soil moisture measurement with the Cosmic Ray Neutron Sensing method. The addition of the 3.3 cm polyethylene base to the L-WPIE improved the spectrum reconstruction which clearly represented the four energy regions. For 18 days across February and March 2023, neutron flux data were acquired together with soil moisture measurement performed by two probes and weather data to measure precipitations. The data of the epithermal flux were employed to perform soil moisture estimations by means of the universal calibration function. In particular, the variable chosen to correlate the flux measurements with the soil moisture was the epithermal flux normalized by the high energy flux. This was done to take into account the flux fluctuations related to the solar activity and air pressure changes. The flux variable is expected to decrease in correspondence of the occurrence of precipitations, i.e. of the increase of soil moisture.

Data of the epithermal flux averaged over one and three days were first investigated with respect to the precipitation trend. Results were compared to the W-PIE campaign carried out from July to October 2022. In this campaign, precipitations were of about 25 mm/day on dry soil and the instrument resulted more sensible to soil moisture variations. It has to be said that the L-WPIE campaign instead was characterised by minimal precipitations (up to 9 mm/day) on probably already moist ground. The first days flux measurements showed oscillations which could not be attributed to the occurrence of precipitations.

In the subsequent days, the flux actually showed a decrease when precipitations were revealed. This flux decrease is quite comparable to the decrease due to the statistical fluctuations of the first days. This means that probably the instrument is not able to discern the soil moisture changes from the background fluctuations in case of poor precipitations dynamic. The soil moisture estimation via the universal calibration function is affected by the previous considerations. In addition, the soil moisture probes were installed very near to the ground surface. This means that probably the flux measure and the soil probe measure are representative of soil moisture at different penetration depths. Water at the surface evaporates much faster than the water more in depth: this effect, together with the water permeation in the soil could explain the discrepancy between the soil moisture probes and L-WPIE estimations.

The future developments planned for this technology regards a further investigation of the L-WPIE behaviour with respect to its heavier counterpart, and a comparison of the W-PIE technologies with other traditional soil moisture measurements. In particular:

- the heavier W-PIE technology will be compared both with other conventional soil moisture measure (point scale measurement technologies and satellite remote sensing) and with CRNS, in a measurement campaign ongoing since April 2023 in Foggia, Italia.
- A new measurement campaign will start in July 2023 in Ferrara, during which the W-PIE and the L-WPIE will be exposed simultaneously to cosmic radiation. Even in this campaign there will be other soil moisture measurement technologies, both CRNS and traditional point-scale to make a comparison between the various methods.

Bibliography

- [1] M. Zreda, W. J. Shuttleworth, X. Zeng, C. Zweck, D. Desilets, T. Franz, and R. Rosolem. Cosmos: the cosmic-ray soil moisture observing system. *Hydrology and Earth System Sciences*, 16(11):4079–4099, 2012.
- [2] Andrea Cirillo, Ruggero Meucci, Michele Caresana, and Marco Caresana. An innovative neutron spectrometer for soil moisture measurements. *Eur. Phys. J. Plus*, 139, 985, 2021.
- [3] S.U.Susha Lekshmi, D.N. Singh, and Maryam Shojaei Baghini. A critical review of soil moisture measurement. *Measurements*, 54:92–105, 2014.
- [4] Pariva Dobriyal, Ashi Qureshi, Ruchi Badola, and Syed Ainul Hussain. A review of the methods available for estimating soil moisture and its implications for water resource management. *Journal of Hydrology*, 458-459:110–117, 2012.
- [5] Fedro S. Zazueta and Jiannong Xin. Soil moisture sensors. 1994.
- [6] N.A Nwogwu et al., editors. *A CONCISE REVIEW OF VARIOUS SOIL MOISTURE MEASUREMENT TECHNIQUES*, Department of Agricultural and Bioresources Engineering, Federal University of Technology, Owerri, P.M.B. 1526, Owerri, Imo State of Nigeria., 08 2018. PROCEEDINGS OF THE 3RD NIAE-SE REGIONAL CONFERENCE, UNIV. OF NIG., NSUKKA.
- [7] T.E Ochsner et al. State of the art in large-scale soil moisture monitoring. *Soil Science Society of America Journal*, 2013.
- [8] Dara Entekhabi, Eni G. Njoku, Peggy E. O’Neill, Kent H. Kellogg, Wade T. Crow, Wendy N. Edelstein, Jared K. Entin, Shawn D. Goodman, Thomas J. Jackson, Joel Johnson, John Kimball, Jeffrey R. Piepmeier, Randal D. Koster, Neil Martin, Kyle C. McDonald, Mahta Moghaddam, Susan Moran, Rolf Reichle, J. C. Shi, Michael W. Spencer, Samuel W. Thurman, Leung Tsang, and Jakob Van Zyl. The soil moisture active passive (smap) mission. *Proceedings of the IEEE*, 98(5):704–716, 2010.
- [9] Clarence J. Ehlers, Lymon C. Reese, and James N. Anagnos. The nuclear method

- of soil-moisture determination at depth. Technical Report 2, CENTER FOR HIGHWAY RESEARCH, THE UNIVERSITY OF TEXAS AT AUSTIN, 06 1969. Research Report Number 89-4.
- [10] Steven van der Veeke, Ronald Koomans, and Han Limburg. Using a gamma-ray spectrometer for soil moisture monitoring: development of the the gamma soil moisture sensor (gsms). In *2020 IEEE International Workshop on Metrology for Agriculture and Forestry (MetroAgriFor)*, pages 185–190, 2020.
- [11] Marica Baldoncini, Matteo Albéri, Carlo Bottardi, Enrico Chiarelli, Kassandra Giulia Cristina Raptis, Virginia Strati, and Fabio Mantovani. Investigating the potentialities of monte carlo simulation for assessing soil water content via proximal gamma-ray spectroscopy. *Journal of Environmental Radioactivity*, 192:105–116, 2018.
- [12] Robert L. Grasty. Radon emanation and soil moisture effects on airborne gamma-ray measurements. *Geophysics*, 62:1379, September 1997.
- [13] T.C. Feng, J.P. Cheng, M.Y. Jia, R. Wu, Y.J. Feng, C.Y. Su, and W. Chen. Relationship between soil bulk density and pvr of in situ spectra. *Nuclear Instruments and Methods in Physics Research Section A: Accelerators, Spectrometers, Detectors and Associated Equipment*, 608(1):92–98, 2009.
- [14] *Cosmic Ray Neutron Sensing: Use, Calibration and Validation for Soil Moisture Estimation*. Number 1809 in TECDOC Series. INTERNATIONAL ATOMIC ENERGY AGENCY, Vienna, 2017.
- [15] Peter K.F. Grieder. *COSMIC RAYS AT EARTH*. Library of Congress Cataloging-in-Publication Data, The address, 1 edition, 2001.
- [16] M. Köhli, M. Schrön, M. Zreda, U. Schmidt, et al. Footprint characteristics revised for field-scale soil moisture monitoring with cosmic-ray neutrons. *Water Resour. Res*, 2015.
- [17] Marco Barrantes, Jose Valdes, O Musalem, A Hurtado, Marcos Anzorena, Rocio Garcia, R Taylor, Yasushi Muraki, Yasuhiro Matsubara, Takashi Sako, Y Sasai, N Hinaro, N Tateiwa, H Tsujihara, L González, Ernesto Ortiz, Shoichi Shibata, K Watanabe, and Taku Sakai. Atmospheric corrections of the cosmic ray fluxes detected by the solar neutron telescope at the summit of the sierra negra volcano in mexico. *Geofísica Internacional*, 57:253–275, 10 2018.
- [18] Tatsuhiko Sato and Koji Niita. Analytical functions to predict cosmic-ray neutron spectra in the atmosphere. In *Radiation Research*, 2006.

- [19] Jannis Weimar, Markus Köhli, Christian Budach, and Ulrich Schmidt. Large-scale boron-lined neutron detection systems as a 3he alternative for cosmic ray neutron sensing. In *Frontiers in Water*, 2020.
- [20] Markus Köhli, Jannis Weimar, Martin Schrön, Roland Baatz, and Ulrich Schmidt. Soil moisture and air humidity dependence of the above-ground cosmic-ray neutron intensity. In *Frontiers in Water*, 2021.
- [21] Ruggero Meucci. Design of a neutron spectrometer for soil moisture monitoring starting from Arktis M800 thermal neutron detector. Master’s thesis, Politecnico di Milano, 2020-2021.
- [22] Darin Desilets, Marek Zreda, and Ty Ferré. Nature’s neutron probe: Land surface hydrology at an elusive scale with cosmic rays. *Water Resources Research - WATER RESOUR RES*, 46, 11 2010.
- [23] T. E. Franz, M. Zreda, R. Rosolem, and T. P. A. Ferre. A universal calibration function for determination of soil moisture with cosmic-ray neutrons. *Hydrology and Earth System Sciences*, 17(2):453–460, 2013.
- [24] R. Baatz, H.R. Bogaen, H.-J. Hendricks Franssen, J.A. Huisman, W. Qu, C. Montzka, and H. Vereecken. Calibration of a catchment scale cosmic-ray probe network: A comparison of three parameterization methods. *Journal of Hydrology*, 516:231–244, 2014. Determination of soil moisture: Measurements and theoretical approaches.
- [25] Marek Zreda, Darin Desilets, T. P. A. Ferré, and Russell L. Scott. Measuring soil moisture content non-invasively at intermediate spatial scale using cosmic-ray neutrons. *Geophysical Research Letters*, 35(21), 2008.
- [26] Andrea Cirillo, Ruggero Meucci, Marco Caresana, et al. Improving cosmic-ray neutron sensing with neutron spectrometry. *International Workshop on Metrology for Agriculture and Forestry (MetroAgriFor)*, 2022.
- [27] D.J Thomas and A.V Alevra. Bonner sphere spectrometers—a critical review. *Nuclear Instruments and Methods in Physics Research Section A: Accelerators, Spectrometers, Detectors and Associated Equipment*, 476(1):12–20, 2002. Int. Workshop on Neutron Field Spectrometry in Science, Technology and Radiation Protection.
- [28] Gordon Michel Stuart et al. Measurement of the flux and energy spectrum of cosmic-ray induced neutrons on the ground. *IEEE Transactions on Nuclear Science*, pages 3427–3434, 2004.

- [29] G. Zorloni, P. Tancioni, and M. Caresana. Feasibility study of a shielding-independent radiation portal monitor system for revealing ²⁴¹Am orphan.
- [30] Denise B. Pelowitz. *MCNPX USER'S MANUAL*, 2.6.0 edition, 04 2008.
- [31] Joel A. Kulesza, Terry R. Adams, et al. *MCNP Code Version 6.3.0 Theory User Manual*, rev. 1 edition, 09 2022.
- [32] Iso 8529-2, Part 2, Geneva, 2000.
- [33] M.Matzke. Unfolding procedures. *Radiat.Prot.Dosim*, pages 149–168, 2003.
- [34] M. Caresana, C. Cassell, M. Ferrarini, E. Hohmann, G. P. Manessi, S. Mayer, M. Silari, and V. Varoli. A new version of the lupin detector: Improvements and latest experimental verification. *Review of Scientific Instruments*, 85(6):065102, 2014.
- [35]
- [36] ICRP. Conversion coefficients for use in radiological protection against external radiation. *ICRP Publication 74*, 1996. Ann. ICRP 26 (3-4).

A | Appendix A

In this appendix the tables of the manufactured coatings are reported.

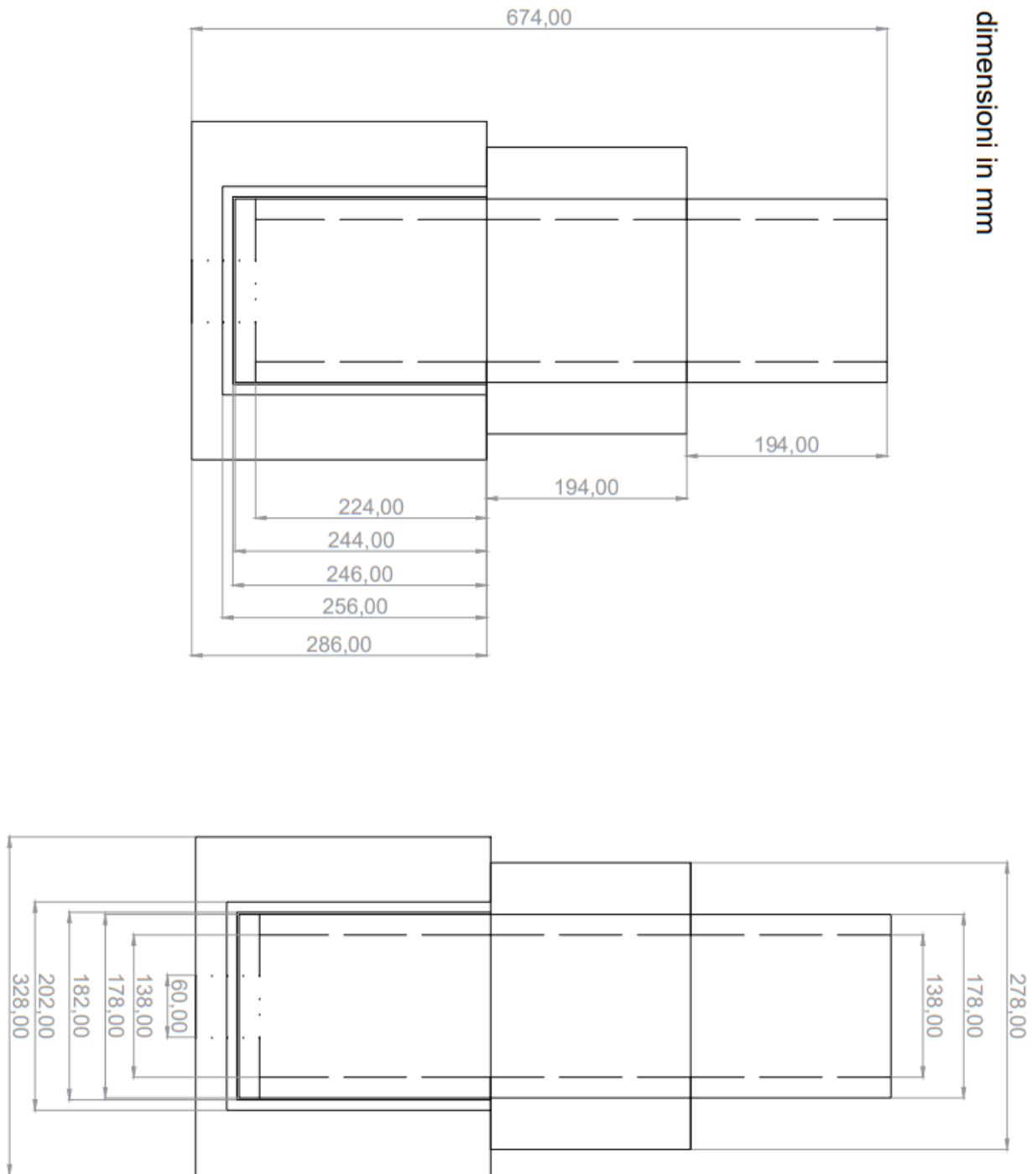


Figure A.1: Coatings orthogonal projections of the L-WPIE without base.

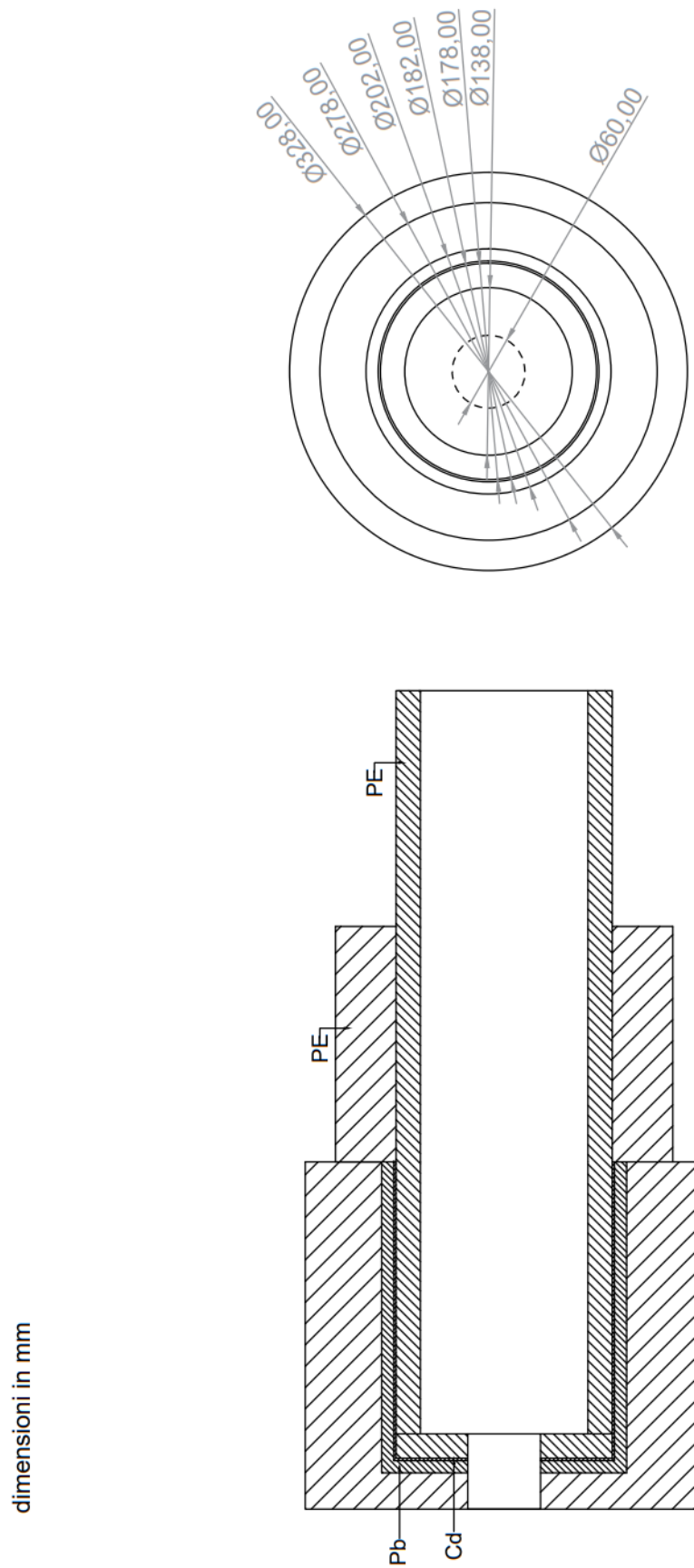


Figure A.2: Coatings orthogonal projections of the L-WPIE without base.

dimensioni in mm

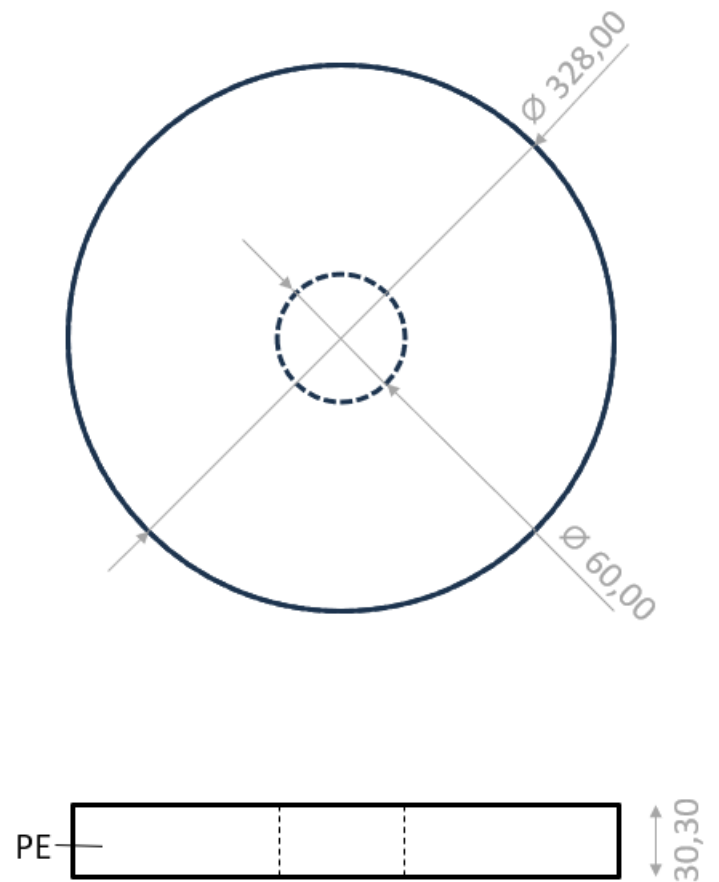


Figure A.3: Coatings orthogonal projections of the base to be added for the final L-WPIE design.

List of Figures

1.1	Schematic diagram of a tensiometer. Figure taken from [3]	7
1.2	Schematic representation of the remote sensing technique. Figure taken from [7]	10
1.3	Depth moisture probe. Figure taken from [9].	12
1.4	Depth neutron probe in working position. Figure taken from [].	13
1.5	Fundamental spectra obtained with Monte Carlo simulations referred to a dry soil with uniform radionuclide concentration. Figure taken from [11]	15
1.6	The three component of the cascade shower. Figure taken from [17]	18
1.7	Neutron spectrum simulated by EXPACS at ground level plotted as neutron fluence rate per energy bin	19
1.8	Comparison of elastic neutron cross sections of hydrogen (red), nitrogen (green), oxygen (blue), carbon (black), silicon (ocher), and aluminium (grey) for kinetic energies between 5 meV and 1 GeV. Figure taken from [16]	21
1.9	Cosmic-ray neutron spectrum above ground simulated by URANOS with a water content of 0.2 g out of 1 g of soil [21].	23
1.10	The effect of water content in soil (θ) on the cosmic neutrons energy spectrum [16]. Dry soils show greater fluxes in the epithermal ($10^{-6} - 10^{-1} MeV$) and fast ($10^{-1} - 20 MeV$) energy ranges.	23
1.11	Radial footprint and penetration depth	27
2.1	Processes inside a bonner sphere	31
2.2	Sphere response functions example	32
2.3	14-element Gordon Bonner sphere	33
2.4	W-PIE	34
2.5	M800 ARKTIS	34
2.6	Schematic representation of M800	35
2.7	Energy ranges in cosmic spectrum	37
3.1	Random walks examples in MCNP	40
3.2	MCNP Cards	41

4.1	MCNPX cuts of M800	45
4.2	Planar source configuration and description	46
4.3	W-PIE Response Functions and MCNP model	48
4.4	Comparison between starting Response functions vs weight optimized ones	52
4.5	Original optimized design	55
4.6	Original optimized design response functions	55
4.7	LW-PIE design manufactured by "Officina Finotti" company.	57
4.8	LW-PIE with the cut base response functions.	57
4.9	LW-PIE design manufactured by "Officina Finotti" company with the ad- joint of a 3.3 thick polyethylene base.	58
4.10	LW-PIE with the addition of a 3.3 thick polyethylene base. response func- tions.	59
5.1	AmBe irradiation experimental setup	63
5.2	W-PIE in vertical configuration spectra	65
5.3	W-PIE in horizontal configuration spectrum	66
5.4	L-WPIE in vertical configuration spectra	68
5.5	L-WPIE spectrum in horizontal configuration	69
5.6	L-WPIE in vertical configuration spectrum	70
5.7	L-WPIE spectrum in horizontal configuration without 3 cm polyethi- lene base	71
5.8	Reconstructed neutron spectra for the two versions of L-WPIE	75
5.9	WPIE in Parco Nord	76
5.10	Epithermal normalized flux for W-PIE	78
5.11	Epithermal normalized flux for L-WPIE	79
5.12	Epithermal and Fast flux sensitivity to water content	80
5.13	Soil Moisture estimation with W-PIE	82
5.14	Soil Moisture estimation with W-PIE	84
5.15	Epithermal Flux uncertainty	86
5.16	Uncertainty behaviour	86
A.1	Coatings ortogonal projections of the L-WPIE without base.	96
A.2	Coatings ortogonal projections of the L-WPIE without base.	97
A.3	Coatings ortogonal projections of the base to be added for the final L-WPIE design.	98

List of Tables

1.1	Slowing down of neutrons from 1 MeV to thermal energies by interaction with different isotopes.	21
4.1	Thicknesses of each coating layer for the starting W-PIE configuration. Thicknesses of the high energy section S1 refers both to lateral thicknesses and vertical thicknesses.	47
4.2	Optimization thicknesses dataset	50
4.3	Thicknesses of each coating layer for the weight-optimized W-PIE configuration obtained maximizing f.o.m. of eq. 4.3. Thicknesses of the high energy section S1 refers both to lateral thicknesses and vertical thicknesses.	51
4.4	Thicknesses of each coating layer for the weight-optimized W-PIE configuration obtained maximizing f.o.m. of eq. 4.3	52
4.5	Thicknesses of each coating layer for the weight-optimized W-PIE configuration obtained maximizing f.o.m. of eq. 4.4	53
4.6	Integrated response functions for $E > 100$ MeV	53
4.7	Comparison of the expected cps in each section of each design for a cosmic flux source given by EXPACS. Weight-optimized design results in a reduction of the High Energy cps detected.	54
5.1	Lab measurements: Vertical W-PIE Counts	64
5.2	Lab measurements: Horizontal W-PIE Counts	64
5.3	Lab measurements: Vertical L-WPIE Counts	67
5.4	Lab measurements: Horizontal L-WPIE Counts	67
5.5	Lab measurements: Vertical L-WPIE Counts without 3 cm polyethylene base	69
5.6	Lab measurements: Horizontal L-WPIE Counts without 3 cm polyethylene base	70

5.7	L-WPIE, W-PIE and L-WPIE without base measured AmBe flux. The L-WPIE and W-PIE results shows optimal agreement. The L-WPIE without base measurement is affected by the lower thickness of the base which induce an overestimation of the fast flux.	72
5.8	Ambient dose equivalent rate estimated from the flux measured by the W-PIE and the L-WPIE, showing good agreement	73
5.9	Conversion factors computed from the three instrument flux measurements, showing good agreement	74
5.10	W-PIE cosmic neutron epithermal flux uncertainties	85

Ringraziamenti

Ringrazio in modo particolare e con riconoscenza il Prof. Marco Caresana che mi ha permesso di effettuare questa ricerca, il Dott. Ing Andrea Cirillo che mi ha seguito con grande attenzione ed è stato fonte di ispirazione e guida. Infine, ringrazio la società Else Nuclear per avere supportato questo progetto.

